

AD-A092 365

COLD REGIONS RESEARCH AND ENGINEERING LAB HANOVER NH
MECHANICS OF CUTTING AND BORING. PART 5. DYNAMICS AND ENERGETIC--ETC(U)
SEP 80 M MELLOR
CRREL-80-21

F/6 13/9

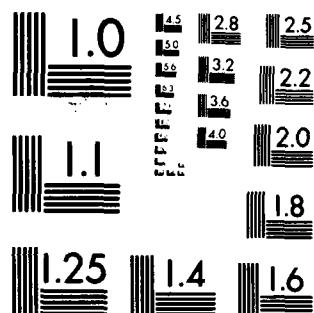
UNCLASSIFIED

NL

1 of 1
AL
AD-A092 365



END
DATE
FILMED
1 81
DTIC

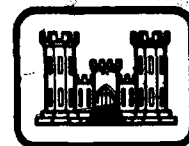


MICROCOPY RESOLUTION TEST CHART
NATIONAL BUREAU OF STANDARDS-1963-A

CRREL

REPORT 80-21

LEVEL

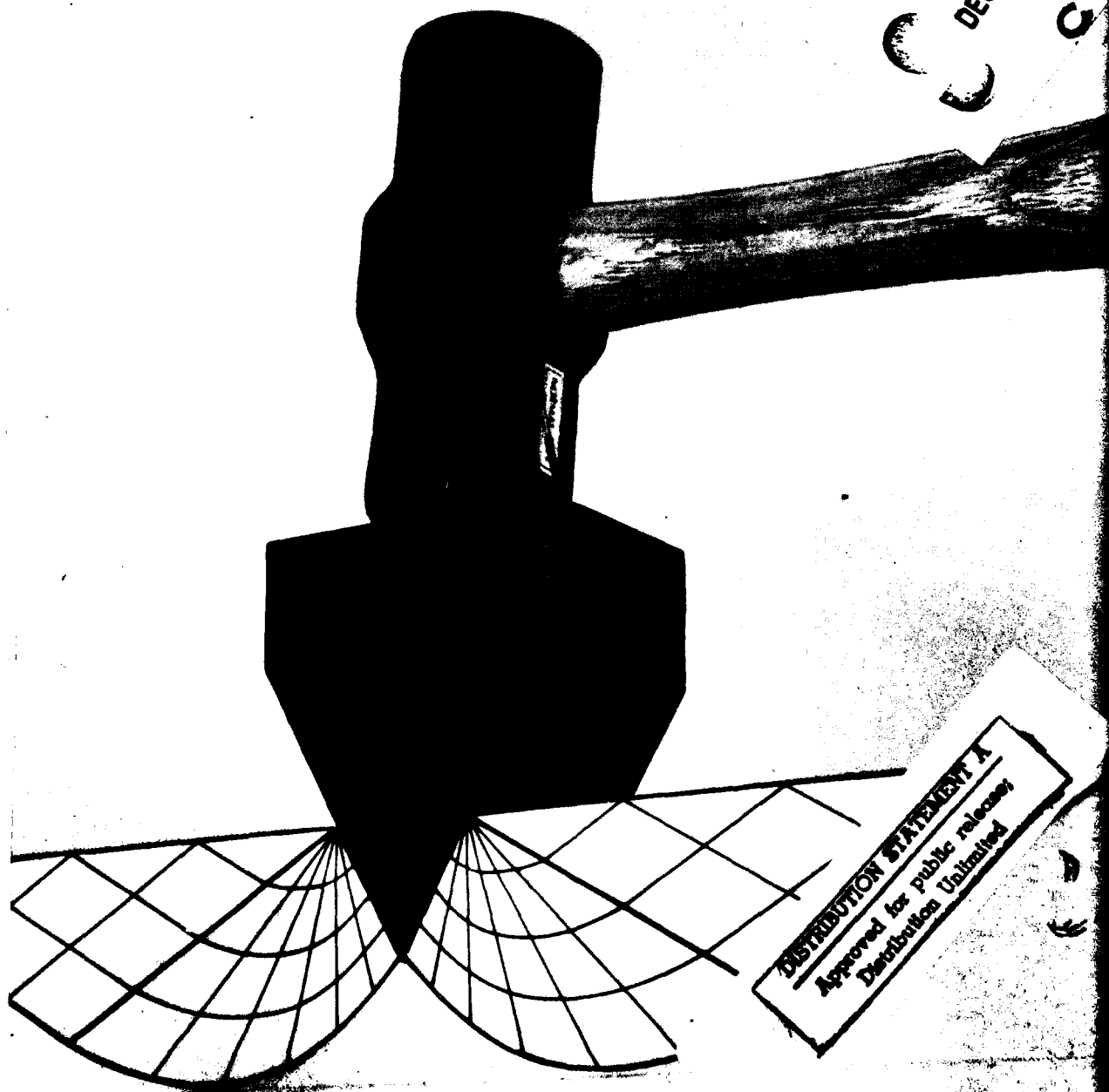


(12)
B.S.

Mechanics of cutting and boring
Part V: Dynamics and energetics of indentation tools

AD A092365

BDC FILE COPY



DISTRIBUTION STATEMENT A
Approved for public release;
Distribution Unlimited

80 1126 028

CRREL Report 80-21

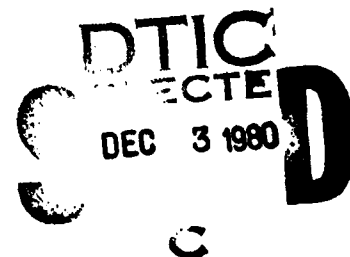
12



Mechanics of cutting and boring
Part V: Dynamics and energetics of indentation tools

Malcolm Mellor

September 1980



Prepared for
DIRECTORATE OF MILITARY PROGRAMS
OFFICE OF THE CHIEF OF ENGINEERS
By
UNITED STATES ARMY
CORPS OF ENGINEERS
COLD REGIONS RESEARCH AND ENGINEERING LABORATORY
HANOVER, NEW HAMPSHIRE, U.S.A.

Approved for public release, distribution unlimited.

Unclassified

SECURITY CLASSIFICATION OF THIS PAGE (When Data Entered)

REPORT DOCUMENTATION PAGE		READ INSTRUCTIONS BEFORE COMPLETING FORM
1. REPORT NUMBER 14 CRREL Report 86-21	2. GOVT ACCESSION NO. AD-A092365	3. RECIPIENT'S CATALOG NUMBER
4. TITLE (and Subtitle) MECHANICS OF CUTTING AND BORING Part 5: Dynamics and Energetics of Indentation Tools	5. TYPE OF REPORT & PERIOD COVERED	6. PERFORMING ORG. REPORT NUMBER
7. AUTHOR(s) 10 Malcolm Mellor	8. CONTRACT OR GRANT NUMBER(s)	9. PROGRAM ELEMENT, PROJECT, TASK AREA & WORK UNIT NUMBERS 16 DA Project 4A762730AT42 Technical Area A, Work Unit 002
11. CONTROLLING OFFICE NAME AND ADDRESS Directorate of Military Programs Office of the Chief of Engineers Washington, D.C. 20314	12. REPORT DATE 12 95	13. NUMBER OF PAGES 95
14. MONITORING AGENCY NAME & ADDRESS (if different from Controlling Office)	15. SECURITY CLASS. (of this report) Unclassified	15a. DECLASSIFICATION/DOWNGRADING SCHEDULE
16. DISTRIBUTION STATEMENT (of this Report) Approved for public release; distribution unlimited.		
17. DISTRIBUTION STATEMENT (of the abstract entered in Block 20, if different from Report)		
18. SUPPLEMENTARY NOTES		
19. KEY WORDS (Continue on reverse side if necessary and identify by block number) Boring machines Machine design Excavating machines Permafrost excavation Excavation Rock cutting Ice cutting		
20. ABSTRACT (Continue on reverse side if necessary and identify by block number) This report deals with the cutting of rock and other brittle materials by means of indentation tools. The principles of indentation cutters are dealt with at length, the coverage including elastic contact stresses for initial loading by various types of indenters, application of formal plasticity theory to penetration analysis, and a variety of theories and penetration analyses that are not based on plasticity theory. Practical indentation mechanisms are described, and theoretical analyses are given for the dynamics and energetics of various types of roller cutters. The final section reviews experimental investigations and results for rock-cutting discs, giving a systematic summary of available data.		

DD FORM 1 JAN 73 1473

EDITION OF 1 NOV 65 IS OBSOLETE

Unclassified

SECURITY CLASSIFICATION OF THIS PAGE (When Data Entered)

037100

50

PREFACE

This report was prepared by Dr. Malcolm Mellor, Physical Scientist, Experimental Engineering Division, U.S. Army Cold Regions Research and Engineering Laboratory. This work was funded by DA Project 4A762730AT42, *Design, Construction and Operations Technology for Cold Regions*, Technical Area A, *Combat Operations Support*, Work Unit 002, *Excavation in Frozen Ground*.

Technical review of the manuscript was provided by Paul V. Sellmann and Dr. Devinder S. Sodhi of CRREL.

The contents of this report are not to be used for advertising or promotional purposes. Citation of brand names does not constitute an official endorsement or approval of the use of such commercial products.

Accession For	
NTIS GRA&I	<input checked="checked" type="checkbox"/>
DTIC TAB	<input type="checkbox"/>
Unannounced	<input type="checkbox"/>
Justification	
By	
Distribution/	
Availability Codes	
Dist	Avail and/or Special
A	

CONTENTS

	Page
Abstract	i
Preface	ii
Foreword	viii
Introduction.....	1
Terminology.....	1
Principles of indentation cutters.....	2
Action of an indentation cutter	2
Initial stresses for idealized conditions	6
Failure criteria	18
Initiation of failure	19
Plastic yielding.....	19
Penetration analyses that are not based on plasticity theory.....	30
Interpretation of penetration data	35
Effects of indenter geometry on force-penetration relationships	40
Practical indentation mechanisms.....	46
Types of indenters.....	46
Dynamics of a simple disc cutter.....	46
Dynamics of a taper-edge disc cutter	49
Dynamics of a taper-edge disc with bearing friction.....	51
Action of a studded disc	53
Action of a toothed cutter.....	55
Forces on a studded disc.....	56
Forces on a wheel with wedge-shaped teeth.....	58
Energetics of disc cutters.....	59
Energetics of a studded disc.....	60
Energetics of a tooth cutter	62
Experimental data for disc cutters	63
Experimental investigations.....	63
Relationships between normal force and penetration	64
Relationships between tangential force and penetration	67
Relationship between force and penetration for tooth cutters	68
Effect of cutter radius on cutting forces	69
Effect of cutting speed on cutting forces.....	70
Influence of edge angle on cutting forces for a taper-edge disc	70
Shape of groove cross section	71
Force reduction by interaction between adjacent cutting tracks.....	73
Calculation of specific energy.....	74
Specific energy as a function of penetration depth	74
Effect of cutter radius on specific energy	77
Effect of edge angle on specific energy	77
Variation of specific energy with cutting speed.....	78
Effect of groove spacing on specific energy.....	78
Variation of specific energy with rock strength.....	81
Literature cited	81

ILLUSTRATIONS

Figure	Page
1. Indentation bits for percussive drilling	4
2. Roller cutters for drills, raise borers, and tunneling machines.....	5
3. The action of an indentation tool	7
4. System of coordinates for analysis of a knife-edge load or a point load	8
5. Stress components induced on a plane at depth $y = a$ when a knife-edge load is applied to the surface of an elastic half-space at $x = 0, y = 0$	8
6. System of coordinates for analysis of a knife-edge load	9
7. Stress components induced on a plane at depth $y = a$ when a knife-edge load inclined at 45° is applied to the surface of an elastic half-space at $x = 0, y = 0$	10
8. Uniformly distributed strip load	10
9. Pressure distribution at the interface between a rigid flat-face panel and an elastic half-space	11
10. Pressure distribution under a long semi-cylindrical indenter.....	11
11. Stress components induced along the y -axis in an elastic half-space when a semi-cylindrical indenter is applied at $x = 0, y = 0$	12
12. Pressure distribution under a flat-face indenter that has a smooth transition to rounded edges	13
13. Comparison of pressure distribution beneath various kinds of two-dimensional indenters.....	13
14. Radial variation of stress components on a plane at depth $z = Z$ when a point load is applied perpendicular to the surface of an elastic half-space at $r = 0, z = 0$	14
15. Distribution of stresses along the z -axis when a spherical indenter is pressed against the surface of an elastic half-space	16
16. Values of the dimensionless factors m and n	17
17. Slip line fields for incipient plastic yielding under a two-dimensional rigid frictionless punch on the plane surface of a semi-infinite medium	20
18. Slip lines and displacements produced in a plastic half-space by a two-dimensional symmetrical wedge	22
19. The full line shows $(1 + \psi)$ as a function of β according to Hill	22
20. Penetration of a plastic half-space by a rigid frictionless wedge with a flat tip	23
21. Penetration of a half-space by a semi-cylindrical indenter.....	23
22. Comparison of two approximate solutions for penetration of a von Mises half-space by a smooth semi-cylindrical indenter.....	25
23a. Slip line field for a strip load on weightless Mohr-Coulomb material	26
23b. Slip line field for a smooth wedge entering a Mohr-Coulomb half-space	26
24. Variation of nominal bearing pressure with wedge angle for a smooth wedge in linear Mohr-Coulomb material	27
25. Slip line field for a slender rough wedge entering a Mohr-Coulomb material	28
26. Variation of nominal bearing pressure with wedge angle for a slender rough wedge in linear Mohr-Coulomb material	29
27. Slip line field for a squat rough wedge that forms a false nose in Mohr-Coulomb material	30
28. Wedge penetration model for Evans' analysis	31
29. Effect of β on the dimensionless factor, assuming two different values for the interface friction coefficient.....	31

Figure	Page
30. Wedge penetration model for the analysis by Paul and Sikarskie	32
31. Effect of β on the dimensionless factor in eq 77 for two values of ϕ	33
32. Effect of β on the dimensionless factor of eq 78, taking two values of ϕ	33
33. Expected trends of force-penetration relations for indenters in complete contact with ductile material that does not strain-harden or strain-soften	36
34. Force/penetration relationship for a flat punch indenting an ice surface	36
35. Force/penetration relationships for a flat punch indenting frozen sand	36
36. Force/penetration relationship for a wedge indenting ice	36
37. Force/penetration relationship for a wedge indenting frozen sand	36
38. Relationship between force and projected area of the indentation for a 0.5-in.-diameter hemisphere pressed into Solenhofen limestone	37
39. Force/penetration relation for a hemispheric indenter pressed into Solenhofen limestone	38
40. Potential influence of compliance in the loading system	38
41. Impression of typical force/penetration characteristic for an actual experiment on rock	39
42. Effect of wedge angle β on the dimensionless "indenter factor" for Indiana limestone and Tennessee marble	41
43. Effect of β on the dimensionless "indenter factor" for Indiana limestone	41
44. Effect of β on the dimensionless "indenter factor" for ice and frozen sand	41
45. Effect of β on the dimensionless "indenter factor" for cones and pyramids	43
46. Effect of radius for a spherical indenter	43
47. Rolling disc of uniform thickness	47
48. Force components on the rim of a simple disc cutter	47
49. Variation of axle forces with penetration depth for a disc of uniform thickness	48
50. Variation of axle forces with disc radius for a disc of uniform thickness	48
51. Rolling disc with a tapered rim	49
52. Variation of axle forces with penetration for a taper-edge disc	51
53. Variation of axle forces with disc radius for a taper-edge disc	51
54. Taper-edge disc with bearing friction	52
55. Rolling disc with peripheral studs	53
56. Minimum penetration for positive operation of a studded disc	53
57. Geometry of a toothed cutter	55
58. Maximum penetration of a toothed cutter before "bottoming-out" occurs	56
59. Forces on a studded disc	56
60. Illustration of variation of axle forces on a studded disc when the action is limited to penetration of one stud at a time	57
61. Illustration of variation of axle forces on a cutter with wedge-shaped teeth when the action is limited to penetration of one tooth at a time	59
62. Force components as functions of penetration depth for a disc cutter operating in wet and dry sandstone	64
63. Force components as functions of penetration depth for disc cutters and a tooth cutter operating in wet and dry chalk	64
64. Penetration depth as a function of the normal force component for disc cutters operating in marble	65
65. Penetration depth as a function of the normal force component for a disc cutter operating on a variety of rock types	65
66. Penetration depth as a function of normal force component for a disc cutter operating in various types of hard rock	66

Figure	Page
67. Force components as a function of penetration depth for a disc cutter operating in different types of rock.....	66
68. Relationship between normal force and penetration depth for toothed cutters in sandstone.....	67
69. Relationship between tangential and normal force components for disc cutters operating in marble.....	67
70. Relationship between tangential and normal force components for a disc cutter operating in different types of rock.....	68
71. Relationship between tangential and normal force components for a disc cutter operating in various types of rock.....	68
72. Force components as functions of diameter for disc cutters operating in wet and dry sandstone.....	69
73. Force components as functions of diameter for disc cutters operating in various types of rock.....	69
74. Force components plotted against cutter speed for a disc operating in wet and dry sandstone	70
75. Force components as functions of edge angle for disc cutters operating in wet and dry sandstone.....	70
76. Force components as functions of edge angle for disc cutters operating in various types of rock.....	71
77. Relation between width and depth for grooves made in marble by disc cutters.....	72
78. Relation between width and depth for grooves excavated by a disc cutter in various types of hard rock.....	72
79. Relation between width and depth for grooves excavated by a disc cutter in various types of rock	72
80. Width of the groove excavated by a disc cutter plotted against uniaxial compressive strength for various rocks	72
81. Effect of lateral spacing between parallel cutting grooves.....	73
82. Variation of force components with groove spacing for disc cutters operating in wet and dry sandstone	74
83. Specific energy plotted against penetration depth for roller cutters working in chalk....	75
84. Specific energy as a function of penetration depth for a disc cutter operating in wet and dry sandstone.....	75
85. Specific energy as a function of penetration depth for disc cutters operating in different kinds of rocks.....	75
86. Volume of the excavated groove plotted against energy input for a disc cutter operating in marble	75
87. Groove volume as a function of input energy for a disc cutter operating in a variety of rock types	76
88. Groove volume as a function of input energy for a disc cutter operating in various types of rock.....	76
89. Specific energy plotted against diameter for disc cutters operating in wet and dry sandstone.....	77
90. Specific energy as a function of edge angle for disc cutters operating in wet and dry sandstone	77
91. Specific energy plotted against cutting speed for a disc operating in wet and dry sandstone.....	78

Figure	Page
92. Variations of specific energy with groove spacing for discs and toothed rollers operating in wet and dry chalk	79
93. Variation of specific energy with groove spacing for disc cutters operating in wet and dry sandstone	79
94. Specific energy as a function of uniaxial compressive strength for normal indentation devices.....	80

MECHANICS OF CUTTING AND BORING

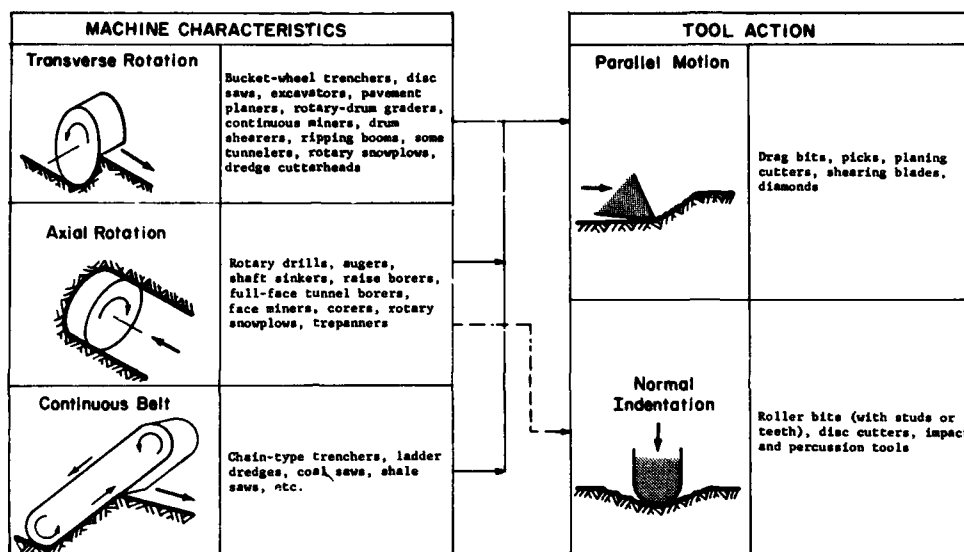
FOREWORD

There are a multitude of tasks that involve the cutting, drilling, or excavating of natural ground materials and massive structural materials. The required technology varies with the properties of the materials and with the scale of operations, but a broad distinction can be made on the basis of the strength, cohesion, and ductility of the material that is to be worked. In weak materials that have little cohesion (e.g. typical soils) the forces and energy levels required for separation and disaggregation are often small compared with the forces and energy levels required for acceleration and transport, and materials handling technology dominates the consideration. By contrast, in strong materials that exhibit brittle fracture characteristics (e.g. rock, concrete, ice, frozen ground) the forces and energy levels required for cutting and breaking are high compared with those required for handling the broken material, and the technical emphasis is on cutting and breaking processes.

CRREL has long been concerned with excavating and drilling in ice and frozen ground, and over the past decade systematic research has been directed to this technical area. The research has covered a wide range of established technologies and novel concepts but, for short term applications, interest has necessarily centered on special developments of proven concepts. In particular, there has been considerable concern with direct mechanical cutting applied to excavation, cutting, and drilling of frozen soils, glacier ice, floating ice, and dense snow. During the course of this work, numerous analyses and design exercises have been undertaken, and an attempt is now being made to develop a systematic analytical scheme that can be used to facilitate future work on the mechanics of cutting and boring machines.

In the industrial sector, rock-cutting machines are usually designed by applying standard engineering methods in conjunction with experience gained during evolution of successive generations of machines. This is a very sound approach for gradual progressive development, but it may not be appropriate when there are requirements for rapid development involving radical departures from established performance characteristics, or for operations in unusual and unfamiliar materials. A distinct alternative is to design more or less from first principles by means of theoretical or experimental methods, but this alternative may not be practically feasible in its more extreme form.

There are numerous difficulties in attempting a strict scientific approach to the design of rock-cutting machines. The relevant theoretical rock mechanics is likely to involve controversial fracture theories and failure criteria, and to call for detailed material properties that are not normally available to a machine designer. Direct experiments are costly and time-consuming, and experimental data culled from the literature may be unsuitable for extrapolation, especially when (as is sometimes the case) they are described by relationships that violate the basic physics of the problem. Comprehensive mechanical analyses for rock-cutting machines have not yet



Classification of machines and cutting tools for analytical purposes.

evolved, and while established design principles for metal-cutting machine tools may be helpful, they do not cover all pertinent aspects. For example, there are usually enormous differences in forces and power levels between machine tools and excavating machines, and force components that can be almost ignored in a relatively rigid machine tool may be crucial design factors for large mobile rock cutters that are highly compliant.

In dealing with cold regions problems where neither outright empiricism nor highly speculative theory seem appropriate, some compromise approaches have been adopted. While simple and practical, these methods have proved useful for analysis and design of cutting and boring machines working under a wide range of conditions in diverse materials, and it seems possible that they might form the basis for a general analytical scheme. The overall strategy is to examine the kinematics, dynamics and energetics for both the cutting tool and the complete machine according to a certain classification, adhering as far as possible to strict mechanical principles, but holding to a minimum the requirements for detailed information on the properties of the material to be cut.

Kinematics deals with the inherent relationships defined by the geometry and motion of the machine and its cutting tools, without much reference to the properties of the material being cut. *Dynamics* deals with forces acting on the machine and its cutting tools, taking into account machine characteristics, operating procedures, wear effects, and material properties. *Energetics* deals largely with specific energy relationships that are determined from power considerations involving forces and velocities in various parts of the system, taking into account properties of the materials that are being cut.

These mechanical principles are applied in accordance with a classification based on the characteristic motions of the major machine element and the actual cutting

tools, as illustrated above. Machines are classified as *transverse rotation*, *axial rotation*, or *continuous belt*, while the action of cutting tools is divided into *parallel motion* and *normal indentation*.

Transverse rotation devices turn about an axis that is perpendicular to the direction of advance, as in circular saws. The category includes such things as bucket-wheel trenchers and excavators, pavement planers, rotary-drum graders, large disc saws for rock and concrete, certain types of tunneling machines, drum shearers, continuous miners, ripping booms, some rotary snowplows, some dredge cutter-heads, and various special-purpose saws, millers and routers. *Axial rotation* devices turn about an axis that is parallel to the direction of advance, as in drills. The category includes such things as rotary drills, augers and shaft-sinking machines, raise borers, full-face tunnel boring machines, corers, trepanners, some face miners, and certain types of snowplows. *Continuous belt* machines represent a special form of transverse rotation device, in which the rotor has been changed to a linear element, as in a chain saw. The category includes "digger chain" trenchers, ladder dredges, coal saws, shale saws, and similar devices.

In tool action, *parallel motion* denotes an active stroke that is more or less parallel to the surface that is being advanced by the tool, i.e. a planing action. Tools working this way include drag bits for rotary drills and rock-cutting machines; picks for mining and tunneling machines; teeth for ditching and dredging buckets; trencher blades; shearing blades for rotary drills, surface planers, snowplows, etc.; diamond edges for drills and wheels; and other "abrasive" cutters. *Normal indentation* denotes an active stroke that is more or less normal to the surface that is being advanced, i.e. one which gives a pitting or cratering effect such as might be produced by a stone chisel driven perpendicular to the surface. Tools working this way include roller rock bits for drills, tunneling machines, raise borers, reamers, etc.; disc cutters for tunneling machines; and percussive bits for drills and impact breakers.

A few machines and operations do not fit neatly into this classification. For example, certain roadheaders and ripping booms used in mining sump-in by axial rotation and produce largely by transverse rotation, and there may be some question about the classification of tunnel reamers and tapered rock bits. However, the classification is very satisfactory for general mechanical analysis.

Complete treatment of the mechanics of cutting and boring is a lengthy task, and in order to expedite publication a series of reports dealing with various aspects of the problem will be printed as they are completed. The main topics to be covered in this series are:

1. Kinematics of transverse rotation machines (Special Report 226, May 1975)
2. Kinematics of axial rotation machines (CRREL Report 76-16, June 1976)
3. Kinematics of continuous belt machines (CRREL Report 76-17, June 1976)
4. Dynamics and energetics of parallel-motion tools (CRREL Report 77-7, April 1977)
5. Dynamics and energetics of indentation tools
6. Dynamics and energetics of transverse rotation machines (CRREL Report 77-19, August 1977)
7. Dynamics and energetics of axial rotation machines
8. Dynamics and energetics of continuous belt machines (CRREL Report 78-11, April 1978)

MECHANICS OF CUTTING AND BORING

Part 5: Dynamics and Energetics of Indentation Tools

Malcolm Mellor

INTRODUCTION

Indentation is a simple and effective method for cutting and drilling hard materials, especially rocks and concrete. A punch or chisel is thrust or driven perpendicularly against the surface of the material and, if that material is brittle, a pit or crater is formed. The average contact stress needed to indent a brittle material tends to be rather high, so that primitive applications of the technique relied entirely upon inertial loading, either by hand hammers and pick axes or by drop weights. In modern applications of indentation cutting, percussion and impact are still the most versatile loading methods. Pneumatic and hydraulic loading mechanisms tend to dominate the field, although there are many and varied devices employing drop weights, internal combustion, or even impact by free projectiles. However, indentation by quasi-static thrust against a reaction has become increasingly important, first in roller rock bits for rotary drilling and later in large diameter tunneling machines and raise borers for hard rocks.

The first part of this report deals with the general principles of indentation tools and with experimental data for indentation into rock. The second part concentrates on the mechanics of rolling cutters and on experimental data for disc cutters. It does not consider the mechanics of devices for driving inertially-loaded indenters.

TERMINOLOGY

An *indentation cutter*, or *indentation tool*, is a device that forms a pit, crater or groove in the surface of a material by penetrating in a direction more or less perpendicular to the surface. The indentation process may involve 1) brittle fracture, with formation of loose fragments, 2) ductile yielding, with displacement of material towards the free surface, 3) compaction of a readily compressible material.

A *roller cutter* is taken here to be any kind of device that indents a surface by means of a rolling action. Examples of such devices are wheel-type glass cutters, roller pastry cutters, roller rock bits for rotary drilling, disc cutters for rock-tunneling machines, free-rolling disc cutters for asphalt, rock-cutting disc cutters with studded rims, toothed-wheel roller rock cutters, studded roller drums for rock cutting, and so on.

The *penetration depth* of an indentation device is the distance from the starting surface to the tip of the indenter, measured normal to the surface.

The *cutting forces* of indentation devices are either resultant forces, or the components of resultant forces, at some specified stage of penetration. For simple indenters the cutting force is usually the direct thrust, more or less normal to the surface. For roller cutters, cutting forces are usually

measured at the axle of the roller, and defined in terms of orthogonal components parallel and normal to the surface (or travel direction of the roller).

Cutting speed, as applied to roller cutters, is the travel velocity of the axle parallel to the working surface. The term cutting speed is not often applied to simple indenters, although it may be used to describe the mean rate of penetration, e.g. when an indenter is thrust into a material by a laboratory testing machine.

Constant penetration operation of a roller cutter means that the normal distance between the axle and the (smooth) work surface remains constant as the roller travels, so that *penetration depth* does not vary. For constant penetration operation, the mountings of the roller must be stiff.

Constant thrust operation of a roller cutter is supposed to mean that the normal component of *cutting force* remains constant as the roller travels. In reality, constant thrust is virtually unattainable in brittle materials (the requirements are perfect compliance and zero inertia).

A *pit*, or *crater*, made by an indenter is usually taken to be the cavity that remains when the indenter is withdrawn and loose fragments are cleared away. In brittle material this cavity is usually bigger than the volume of the indenter that penetrated, partly because of "overbreak" to the sides, and partly because of crushing under the tip of the indenter.

A *groove*, or *kerf*, made by a roller cutter is the channel, often irregular, left after passage of the roller. As in the case of a crater, the cross-sectional area of a groove in brittle material is usually greater than the cross-sectional area of the part of the roller that penetrated.

Groove spacing is defined here as the center-to-center distance between parallel grooves.

The *specific energy* of an indentation tool is the work put into the indentation process per unit volume of material displaced. Alternatively, for a continuous uniform process it is the power input for indentation divided by the volumetric displacement rate. The dimensions of specific energy are energy per unit volume, which is the same as force per unit area, or stress (e.g. $\text{in.-lbf/in.}^3 \equiv \text{lbf/in.}^2$; $\text{J/m}^3 \equiv \text{N/m}^2$).

The *cutter radius* for a roller cutter is the radius to the extreme tip of the disc edge, the studs, or the teeth.

Studs, or *buttons*, are hard projections, usually of tungsten carbide, set into the rims of discs or the surfaces of roller drums.

The *stud radius* on a studded disc is taken as the radial distance between the tip of the stud and the disc perimeter in which it is set.

The *wedge angle*, or *cone angle*, of an indenter is the apex angle for the part of the tool that penetrates the work. In this report the half-angle is denoted by β , so that the total wedge angle is 2β .

The *edge angle* of a disc cutter is the apex angle of a cross section of the rim. In this report the half-angle is denoted by β , so that the total edge angle is 2β .

PRINCIPLES OF INDENTATION CUTTERS

Action of an indentation cutter

The distinguishing characteristic of an indentation cutter is that its active element penetrates in a direction more or less perpendicular to the surface that is being cut, in contrast to a parallel-motion tool, which travels parallel to the surface that is being cut. In its simplest form, the indentation tool is thrust into a surface normally, so that it either displaces material by some kind of plastic flow or compaction, or else forms a crater by brittle fracture. The cutting process progresses by stepping the tool forward to a fresh surface during the interval between successive working thrusts ("indexing"), so that a line of indentations or craters is formed. If the craters are very closely spaced a continuous groove, or kerf, is created.

Thrusting perpendicular to the surface is the action of a simple punch, a typical percussive rock drill (Fig. 1), or an impact breaker. There are other indentation cutters which penetrate in a direction that is not exactly perpendicular to the surface being cut. These are mainly the various types of free-rolling disc cutters and roller cutters (Fig. 2).

Indentation tools of the punch type can thrust into the work at an oblique angle, and under these circumstances there may be some confusion about the distinction between the "indentation" and "parallel-motion" classifications. For present purposes, a punch would be classed as an indentation tool if it were repeatedly withdrawn and then thrust back against a fresh surface, whereas it would be classed as a parallel-motion tool if it were held into the work and driven parallel to the surface by continuous thrust or repeated impulses (like a stone-mason's chisel).

When an indenter is brought into contact with a surface and force is applied, a stress field is set up in the work material and in the tool itself. The form of the stress field in the work material depends on the geometry of the contact area, the distribution of pressure within that area, and the stress/strain characteristics ("constitutive equations") of the material. In the present context it can be assumed that the work material will be elastic under moderate stresses, until plastic yielding occurs at some critical combination of stresses (or of stress invariants as defined by some failure criterion).

As increasing load is applied to an indenter, elastic stresses in the work material increase correspondingly, but the deformation is small (Fig. 3a). When the elastic limit is reached and plastic yielding begins, the indenter starts to penetrate the material, but the way in which it does so depends on a number of factors.

If the indenter is being loaded by a "soft" or compliant system, the release of strain energy which occurs at yielding will be accompanied by large displacements, and the indenter will tend to thrust abruptly into the material without completely unloading itself. By contrast, if the indenter is being loaded by a "stiff" or rigid system, stored strain energy can be released by a small displacement of the tool, which will thus tend to unload when the material yields abruptly.

The other major factor is the behavior of the work material, which is commonly characterized by the extent to which it displays ductile or brittle tendencies. In brittle material, where most of the deformation prior to failure is elastic, yielding occurs by cracking and a crater forms around the tip of the indenter (Fig. 3b). In ductile material, where there can be flow at high strain rates without cracking, the indenter can penetrate deeply by displacing material around itself (Fig. 3c). If the material is readily compressible, the indenter can penetrate by compressing or compacting its surroundings.

When indentation tools are used for cutting rock and similar materials, the usual expectation is that the bulk of the material will be brittle or friable at the prevailing strain rates. However, under high confining stresses, such as may exist in deep fluid-filled boreholes, rocks may exhibit a ductile response to penetration.

Indentation tools of the punch type are usually loaded inertially by repeated impulses. Impulsive loading can be produced by direct impact (e.g. cable tool drill, wrecker's ball, ballistic projectile, sand blasting) or by a drop weight (i.e. a hammer of any kind). Alternatively, percussion can be applied by hydraulic, pneumatic, explosive, or spring mechanisms (as in percussive drills, impact breakers, and modern pile drivers).

Indentation tools of the rotary type are usually loaded by static thrust against a reaction (e.g. rotary drills, raise borers, tunneling machines, asphalt disc cutters, glass cutters). In principle, rolling cutters can be operated with 1) constant thrust, so that penetration depth is not necessarily uniform or constant, and 2) constant displacement, or constant penetration depth, in which case the reaction force is not necessarily uniform or constant. When multiple cutters are fitted to a single machine, as on the boring head of a tunneling machine, the complete machine may operate at constant thrust while the individual cutters are operating effectively at constant depth. The kinematics of roller cutters has been treated in Part II of this series.

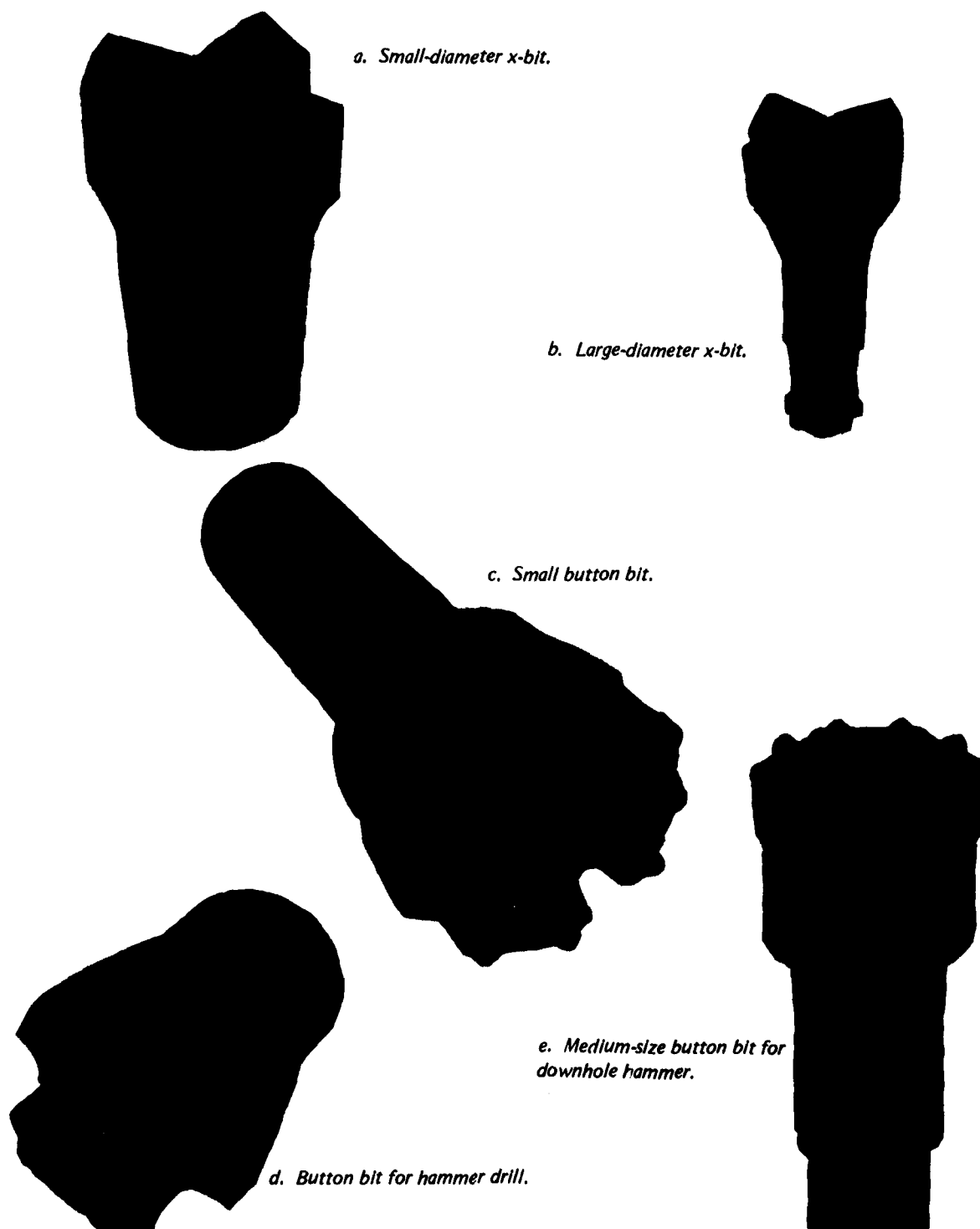
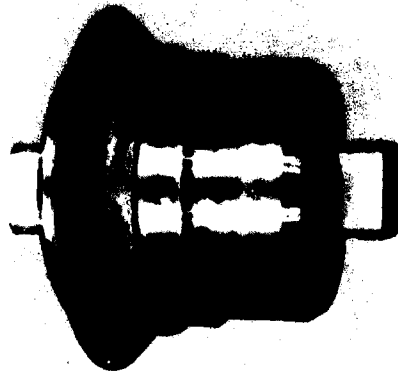
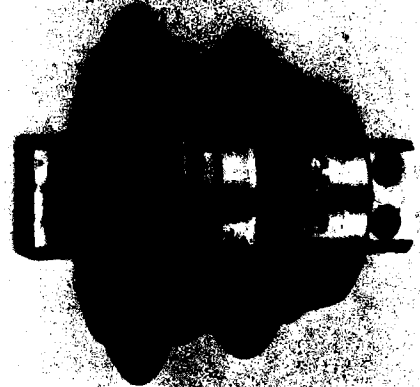


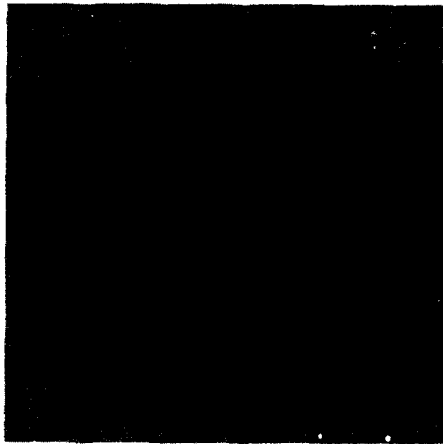
Figure 1. Indentation bits for percussive drilling. Photo credits: a, b and e—Kennametal Inc.; c and d—Baker Drill Inc.



a. Single taper-edge disc cutter.



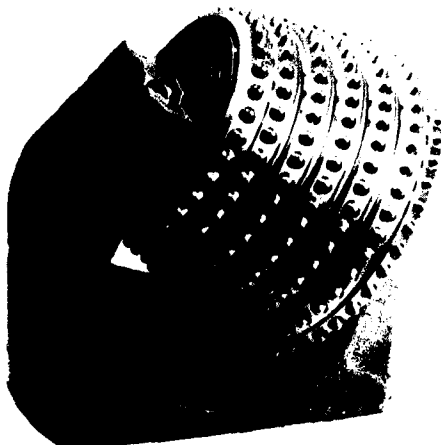
b. Double disc cutter.



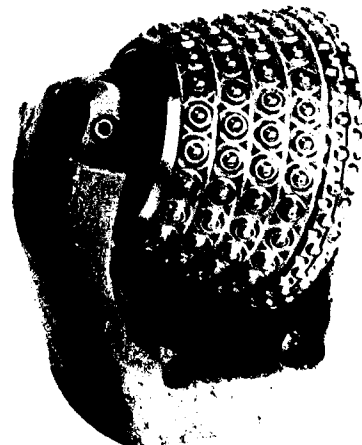
c. Four disc cutters on common axle.



d. Multiple disc cutter with hard inserts in the rims.

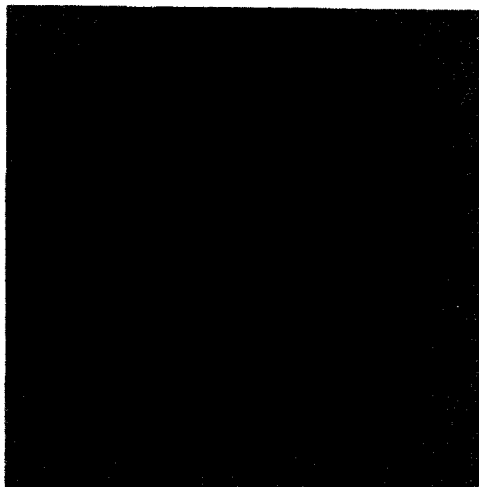


e. Roller cone with hard studs set around 7 discs.

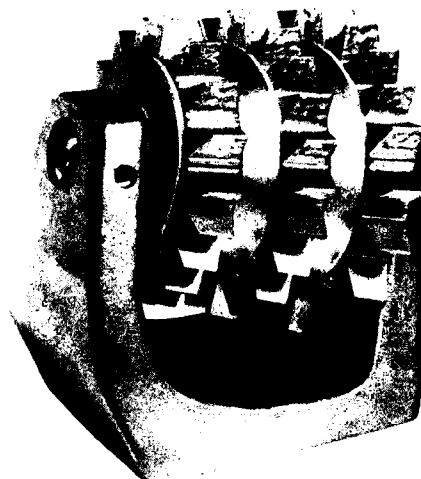


f. Studded roller cone with well supported buttons.

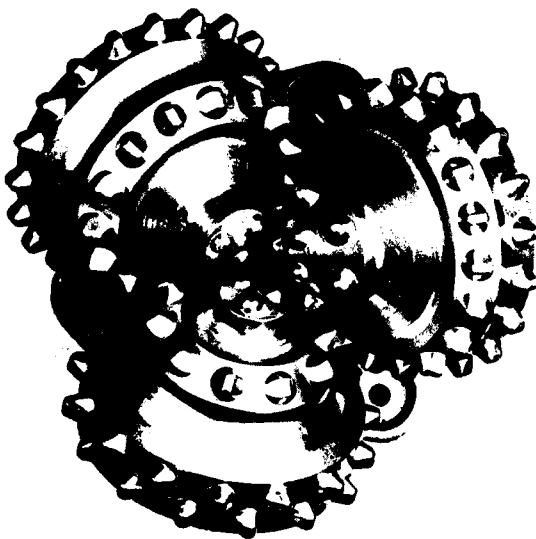
Figure 2. Roller cutters for drills, raise borers, and tunnelling machines. Photo credits: a and b—Alfred Wirth & Co.; c, g and h—Hughes Tool Company; d, e, f, i and j—Reed Tool Company.



g. Simple roller cone with staggered array of hard studs.



h. Three gear-tooth cutters on a common axle.



i. Tricone roller rock bit with hard indenter studs.



j. Toothed roller rock bit.

Figure 2 (cont'd). Roller cutters for drills, raise borers, and tunnelling machines.

Initial stresses for idealized conditions

In order to gain some insight into the stress fields that initiate an indentation process, it is helpful to first idealize the situation by considering the normal loading of a perfectly smooth plane surface that forms the boundary of an elastic semi-infinite medium. The aim is to examine the distribution of stress in the material loaded by the indenter, and in particular to consider the geometry and the stresses in the contact area between the indenter and the work material.

The two simplest idealizations for indenters are the knife-edge line load, representing a wide sharp wedge, and the point load, representing the tip of a sharp cone. These may seem to be unrealistic

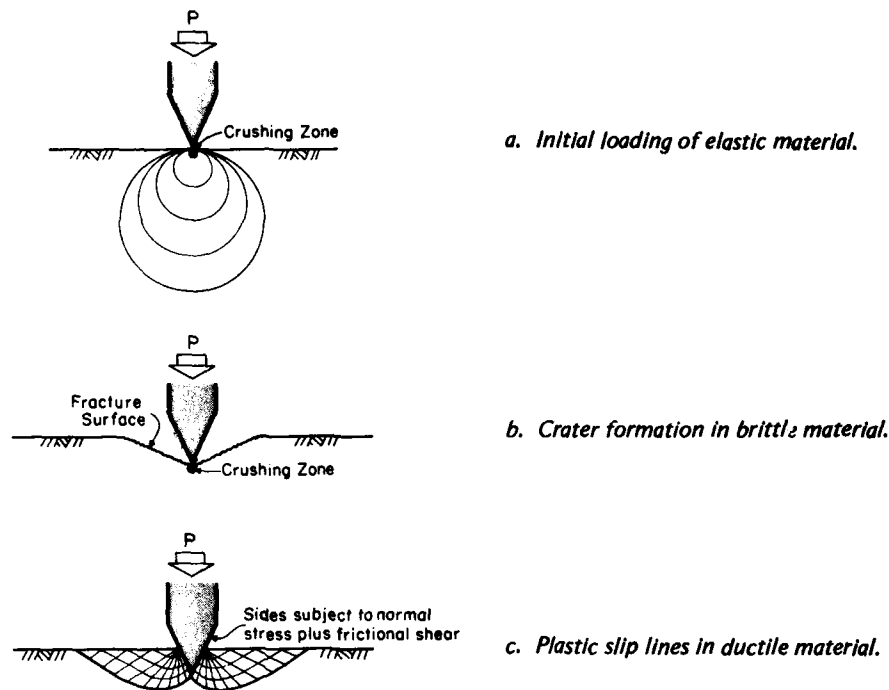


Figure 3. The action of an indentation tool.

oversimplifications. However, for the region outside of the immediate contact zone, the stress fields which they produce are virtually the same as those produced by more realistic distributed loads, by virtue of the Saint-Venant principle. To see the effects of more complicated distributed loads, some of the stresses on contact surfaces and along axes of symmetry can be obtained, leaving aside the more difficult problems of general stress distributions for these cases.*

Derivations for many of the required relationships for the simpler cases are given by Timoshenko and Goodier (1951), and solutions for more complicated cases are treated in the literature for linear elasticity. The results summarized here are arranged with two-dimensional solutions first, then axisymmetric three-dimensional solutions, and finally other three-dimensional cases. In all cases it is assumed that there is no friction between the punch and the material, and the usual assumptions of small-strain elastic theory apply.

Simple knife-edge loading

The first case for consideration is a simple knife-edge line load acting perpendicular to the plane surface of an elastic half-space. This two-dimensional problem relates to the action of a wide sharp wedge. The practical reality of finite contact area does not invalidate the theoretical results as long as it is understood that they do not apply very close to the contact.

When a knife-edge load of magnitude P' per unit length is applied perpendicular to the surface and a system of polar coordinates is taken (Fig. 4), the resulting stresses are

$$\sigma_r = -\frac{2P' \cos\theta}{\pi r} \quad (1)$$

*Results for more complicated cases are often illustrated by assuming that the indenter and the indented material have the same elastic constants. This assumption may not be realistic in rock-cutting problems.

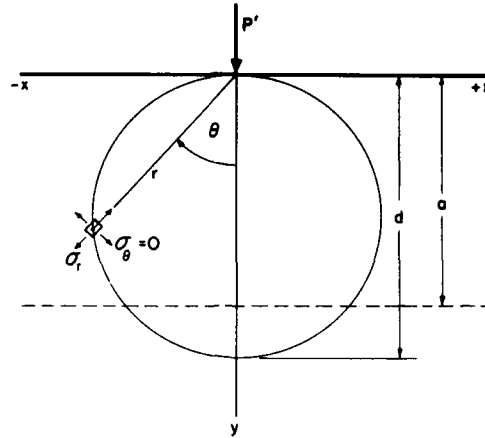


Figure 4. System of coordinates for analysis of a knife-edge load or a point load.

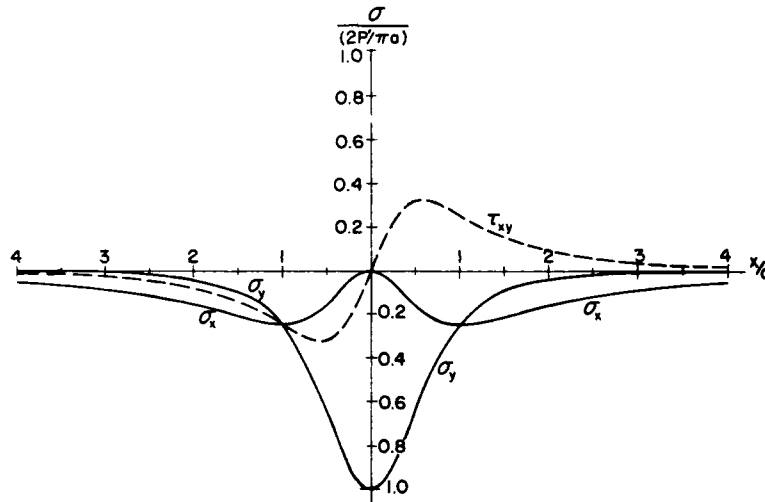


Figure 5. Stress components induced on a plane at depth $y = a$ when a knife-edge load is applied to the surface of an elastic half-space at $x = 0, y = 0$.

$$\sigma_{\theta} = 0 \quad (2)$$

$$\tau_{r\theta} = 0 \quad (3)$$

the negative sign denoting compressive stress. For any circle of diameter d drawn through the point of contact with center on the loading axis (Fig. 4), $d = r/\cos\theta$, and therefore all points on the circle have a constant radial stress of

$$\sigma_r = 2P'/\pi d. \quad (4)$$

In Cartesian coordinates (Fig. 4), the stress components are

$$\sigma_x = \sigma_r \sin^2\theta = -(2P'/\pi)(x^2 y)/(x^2 + y^2)^2 \quad (5)$$

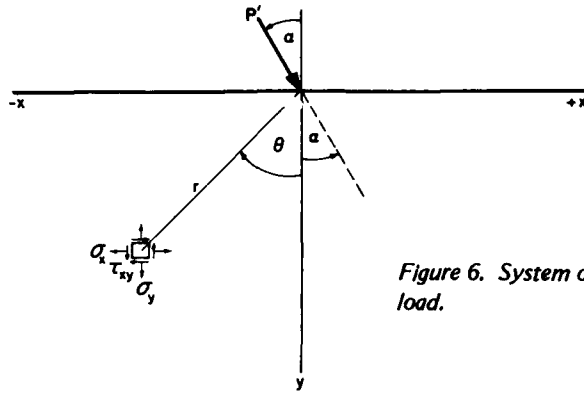


Figure 6. System of coordinates for analysis of a knife-edge load.

$$\sigma_y = \sigma_r \cos^2 \theta = -(2P'/\pi)(y^3)/(x^2 + y^2)^2 \quad (6)$$

$$\tau_{xy} = \sigma_r \sin \theta \cos \theta = (2P'/\pi)(xy^2)/(x^2 + y^2)^2. \quad (7)$$

On any plane that is parallel to the surface at depth $y = a$, the stress components vary with x as shown in Figure 5. The sign reversal for the shear stress τ_{xy} is simply a consequence of the sign convention; the stress field is completely symmetrical about the loading axis.

Inclined knife-edge loading

The solution for the normal knife-edge load can be modified to cover the case where the thrust line of the knife-edge load is inclined at an angle α from the normal direction. This case (Fig. 6) relates to the action of a wide sharp wedge or a wide chisel when it is pushed against the work at some arbitrary angle of inclination.

The stresses produced by the inclined load are given by eq 1-3 when the coordinate angle θ is replaced by $(\theta + \alpha)$, which is equivalent to measuring θ from the force direction:

$$\sigma_r = -(2P'/\pi r) \cos(\theta + \alpha) \quad (8)$$

$$\sigma_\theta = 0 \quad (9)$$

$$\tau_{r\theta} = 0. \quad (10)$$

The Cartesian stress components referred to axes that are parallel and normal to the material surface, respectively, then become:

$$\sigma_x = -(2P'/\pi r) \sin^2 \theta \cos(\theta + \alpha) \quad (11)$$

$$\sigma_y = -(2P'/\pi r) \cos^2 \theta \cos(\theta + \alpha) \quad (12)$$

$$\tau_{xy} = -(2P'/\pi r) \sin \theta \cos \theta \cos(\theta + \alpha) \quad (13)$$

where $r = (x^2 + y^2)^{1/2}$, $\sin \theta = -x/(x^2 + y^2)^{1/2}$, and $\cos \theta = y/(x^2 + y^2)^{1/2}$. Figure 7 shows the Cartesian stress components on a plane at depth $y = a$ when the knife-edge load is inclined at $\alpha = 45^\circ$. The diagram shows that in this case the normal stresses become tensile on one side of the normal through the loading line.

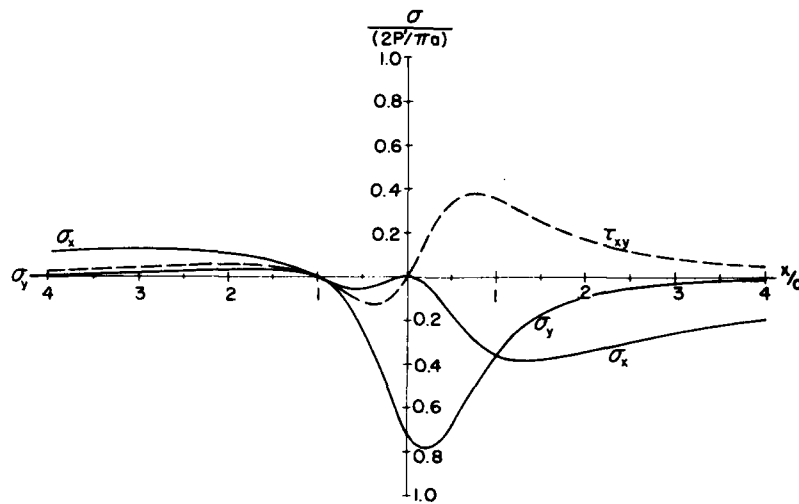


Figure 7. Stress components induced on a plane at depth $y = a$ when a knife-edge load inclined at 45° is applied to the surface of an elastic half-space at $x = 0, y = 0$.

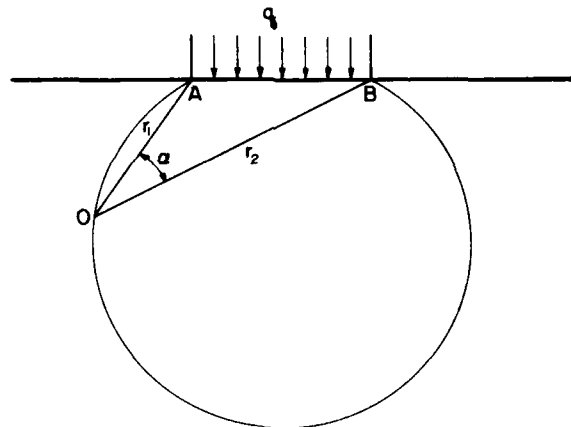


Figure 8. Uniformly distributed strip load.

Uniformly distributed strip load

The basic analysis for the knife-edge load can be used to obtain the stresses induced by a set of parallel knife-edge loads, or for an arbitrarily distributed two-dimensional strip load, by superposition. One case that might conceivably be of interest is a uniformly distributed normal pressure q (Fig. 8), although it should be recognized that this is *not* the loading that is applied by a flat-end rigid punch (see next item).

Referring to Figure 8, it is convenient to locate any arbitrary point O by the intersection of radii r_1 and r_2 drawn from points A and B at the outer limits of the load contact zone. If the included angle between OA and OB is α , the direction of one of the principal stresses at O is the bisector of $\angle AOB$ and the magnitudes of the principal stresses are

$$\sigma_1, \sigma_2 = -q\pi(\alpha \mp \sin\alpha). \quad (14)$$

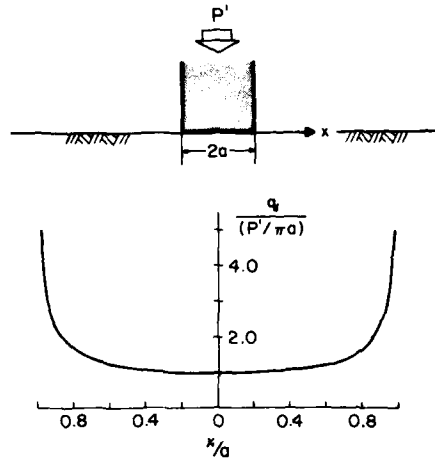


Figure 9. Pressure distribution at the interface between a rigid flat-face panel and an elastic half-space.

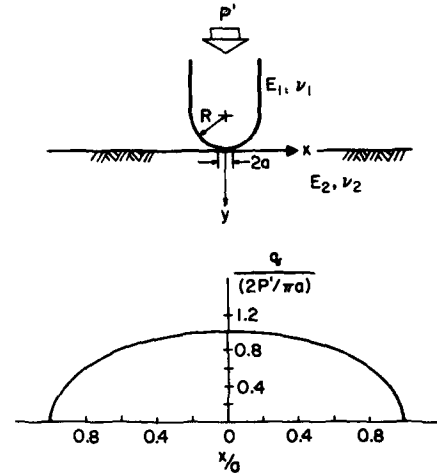


Figure 10. Pressure distribution under a long semi-cylindrical indenter.

For any circular arc drawn through A, B and O, with AB as chord, α is constant for all positions of O, so that the magnitudes of the principal stresses remain constant along the arc.

Pressure distribution beneath a flat-face punch

A flat-face rigid punch (Fig. 9) produces uniform deflection under the loaded area. The pressure distribution in the contact zone is given by

$$q = \frac{P}{\pi(a^2 - x^2)^{1/2}} = \frac{P'}{\pi a[1 - (x/a)^2]^{1/2}} \quad (15)$$

where P' is the normal force per unit length that is acting on the punch, and $2a$ is the width of the contact strip. Figure 9 shows this diagrammatically; note that theoretically q is infinite at $x = \pm a$.

Pressure from a long cylindrical indenter

When a long cylindrical surface is pressed against an elastic surface with force P' per unit length, the pressure distribution within the contact zone is elliptic, ranging from zero at the edges of the contact strip to a maximum pressure q_0 at the center of the strip. The maximum pressure q_0 is related to the applied force P' by

$$q_0 = 2P'/\pi a \quad (16)$$

where a is the half-width of the contact strip. The normal pressure q at the contact surface (σ_y at $y = 0$) is

$$q = q_0[1 - (x/a)^2]^{1/2} = (2P'/\pi a)[1 - (x/a)^2]^{1/2}. \quad (17)$$

Figure 10 shows the relation graphically.

The width of the contact strip $2a$ depends on the force P' , on the radius of the indenter edge R , and on the elastic moduli of both the indenter (E_1, ν_1) and the work material (E_2, ν_2):

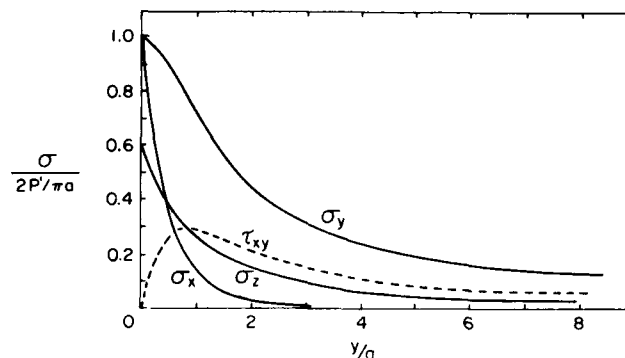


Figure 11. Stress components induced along the y -axis in an elastic half-space when a semi-cylindrical indenter is applied at $x = 0, y = 0$ for the case where $[(1-\nu_1^2)/E_1] = [(1-\nu_2^2)/E_2]$. (After Timoshenko and Goodier 1951.)

$$a = 2 \left[\frac{P'R}{\pi} \left(\frac{1-\nu_1^2}{E_1} + \frac{1-\nu_2^2}{E_2} \right) \right]^{1/2}. \quad (18)$$

Figure 11 gives the stress distribution in the material along the y -axis for the case where $[(1-\nu_1^2)/E_1] = [(1-\nu_2^2)/E_2]$.

Pressure from a flat-face indenter with rounded corners

On simple theory, the pressure under a flat-face indenter with square corners becomes infinite at the edges of the contact area (eq 15 and Fig. 7). By contrast, the pressure under a cylindrical indenter becomes zero at the edges of the contact area (eq 17 and Fig. 8). If a flat-face indenter has rounded corners, the pressure distribution has some of the characteristics shown by both the square-edge punch and the cylindrical punch.

If a flat-face indenter has its corners rounded off by smooth transition curves (no discontinuity in the curvature), then the distribution of normal pressure q on the surface of contact can be described by the relation

$$q = (4P'/3\pi a) [1 + 2(x/a)^2] [1 - (x/a)^2]^{1/2} \quad (19)$$

where x is distance from the punch centerline, $2a$ is the width of the contact area, and P' is the applied force per unit length.* Figure 12 shows this distribution; the pressure drops to zero at the edges of the contact area, and there are pressure maxima at $\pm(a/\sqrt{2})$.†

Comparison of pressure distributions for two-dimensional cases

In Figures 10 and 12 the pressure distributions were normalized with respect to the pressure on the centerline, but it is interesting to make a comparison of the various pressure distributions by normalizing with respect to the mean pressure $P'/2a$. Figure 13 shows the pressure distributions for: 1) uniformly distributed load, 2) the flat-face punch with square corners, 3) a circular cylinder, and 4) a flat-face punch with smoothly rounded corners.

* This relation for "a cylinder whose contour is a curve of the fourth degree" was derived by L.A. Galin. The English translation of Galin's book *Contact problems in the theory of elasticity* (I.N. Sneddon, Ed.) gives the equation incorrectly; the equation on p. 49 of the translation should have a^3 in the denominator instead of a^2 .

† The distribution under a pneumatic tire apparently has this general form, and the pressure maxima have been attributed to sidewall stiffness. In fact, the pressure distribution would be similar even under a solid tire.

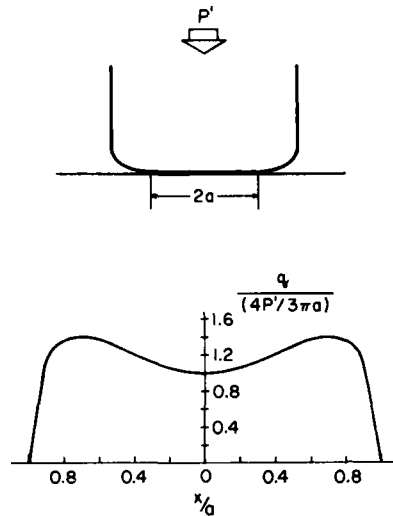


Figure 12. Pressure distribution under a flat-face indenter that has a smooth transition to rounded edges.

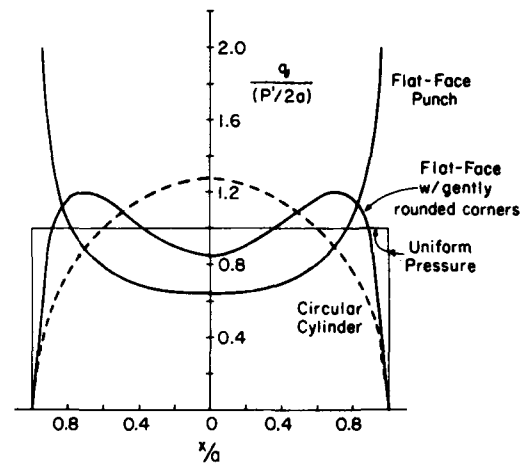


Figure 13. Comparison of pressure distribution beneath various kinds of two-dimensional indenters. Pressure q is normalized with respect to the mean bearing pressure $P'/2a$.

Simple point load

The obvious place to begin consideration of three-dimensional axisymmetric cases is the classic Boussinesq problem, which involves a point load P pressing normally on an elastic semi-infinite medium.* This is the three-dimensional equivalent of the knife-edge problem that was outlined at the beginning of this section. Taking cylindrical coordinates with the load point as origin and the load axis as the z -direction, the stress components are

$$\sigma_r = \frac{P}{2\pi r^2} \left\{ (1-2\nu) \left[1 - \frac{z}{(r^2+z^2)^{1/2}} \right] - \frac{3r^4 z}{(r^2+z^2)^{5/2}} \right\} \quad (20)$$

$$\sigma_\theta = -\frac{P}{2\pi r^2} (1-2\nu) \left[1 - \frac{z}{(r^2+z^2)^{1/2}} - \frac{r^2 z}{(r^2+z^2)^{3/2}} \right] \quad (21)$$

$$\sigma_z = -\frac{3P}{2\pi r^2} \frac{r^2 z^3}{(r^2+z^2)^{5/2}} \quad (22)$$

$$\tau_{rz} = -\frac{3P}{2\pi r^2} \frac{r^3 z^2}{(r^2+z^2)^{3/2}} \quad (23)$$

where ν is Poisson's ratio.

If a sphere is drawn through the loading point with its center on the loading axis, such that the surface plane is tangent to the sphere (three-dimensional equivalent of Fig. 4), there is a simple expression for the resultant stress on horizontal surfaces intersected by the sphere. The resultant stress

* Note that for the three-dimensional cases P is a force, whereas for the two-dimensional cases P' is a force per unit length.

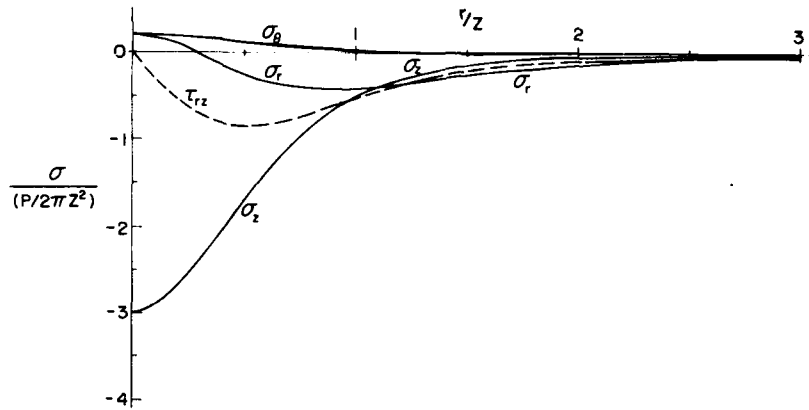


Figure 14. Radial variation of stress components on a plane at depth $z = Z$ when a point load is applied perpendicular to the surface of an elastic half-space at $r = 0$, $z = 0$ (for $\nu = 0.3$).

on any elementary horizontal surface is directed through the loading point, and its magnitude is $3P/2\pi d^2$, where d is the diameter of the sphere.

In Figure 14 the radial variation of stress components is shown for a plane at depth $z = Z$ with $\nu = 0.3$, following the convention that tensile normal stresses are positive.

Uniform pressure on a circular area

When a load is distributed over finite area, the resulting stresses can be obtained from the point load solution by superposition. A simple application of this principle gives the solution for uniform normal pressure q distributed over a circular area of radius a . Taking the z -axis for cylindrical coordinates as the normal direction through the center of the loaded area, with origin at the surface of contact, the stress components are:

$$\sigma_r = \sigma_\theta = -\frac{q}{2} \left[(1+2\nu) - \frac{2(1+\nu)z}{(a^2+z^2)^{1/2}} + \frac{z^3}{(a^2+z^2)^{3/2}} \right] \quad (24)$$

$$\sigma_z = -q \left[1 - \frac{z^3}{(a^2+z^2)^{3/2}} \right]. \quad (25)$$

For points on the z -axis, the maximum shear stress $(\sigma_\theta - \sigma_z)/2$ reaches its greatest value at a depth

$$z' = a \left[\frac{2(1+\nu)}{7-2\nu} \right]^{1/2} \quad (26)$$

at which depth it has the value

$$\tau_{\max} = \left(\frac{\sigma_\theta - \sigma_z}{2} \right)_{\max} = \frac{q}{2} \left[\frac{1-2\nu}{2} + \frac{2\sqrt{2}}{9} (1+\nu)^{3/2} \right]. \quad (27)$$

With $\nu = 0.3$,

$$z' = 0.638 a \quad \tau_{\max} = 0.33 q$$

i.e. the maximum shear stress, which is one-third of the applied pressure, occurs at a depth equal to about two-thirds of the radius of the load area.

Pressure under a circular rigid punch

For a flat-end rigid punch that has a circular loading area of radius a and an applied normal force P , the displacements under the punch are uniform and the distribution of pressure q with radius r is

$$q = \frac{P}{2\pi a^2 [1 - (r/a)^2]^{1/2}} \quad (28)$$

The pressure at the center, $P/2\pi a^2$, is half the average bearing pressure, and the pressure at the circumference is theoretically infinite.* The distribution of the dimensionless pressure $q/(P/2\pi a^2)$ with dimensionless radius r/a is exactly the same as the distribution shown in Figure 9.

Stresses under a spherical indenter

The case of a spherical surface pressing against the plane boundary of an elastic half-space is of considerable interest in the present context, since it relates to the action of the hemispheric studs or buttons that are used in many roller rock cutters and percussion tools. The significance of the particular geometry is restricted mainly to the zone immediately surrounding the contact, since the stress field outside this region is not much different from that produced by the point load (the Saint-Venant principle).

When a spherical surface is brought into contact with a plane under zero normal load there is, in theory, a point contact. As a force P is applied across the interface, a circular contact area develops, its radius a increasing as P increases. The radius of the contact area a is determined by the radius of the sphere R , the force P , and the elastic properties of the sphere and the material:

$$a = \left[\frac{3PR}{4} \left(\frac{1-\nu_s^2}{E_s} + \frac{1-\nu_m^2}{E_m} \right) \right]^{1/3} \quad (29)$$

where E_s and E_m are respectively Young's moduli for the sphere and the material, and ν_s and ν_m are Poisson's ratios for the sphere and the material.

The pressure distribution over the contact is ellipsoidal or hemispheric, with a maximum pressure q_0 at the center equal to 1.5 times the average pressure $P/\pi a^2$:

$$q = \frac{3P}{2\pi a^2} [1 - (r/a)^2]^{1/2} \quad (30)$$

$$q_0 = \frac{3P}{2\pi a^2} \quad (31)$$

The dimensionless pressure $q/(3P/2\pi a^2)$ varies with the dimensionless radius r/a in exactly the same way as is indicated in Figure 10.

* The infinite edge pressure also applies to the indenter itself. This is of interest in connection with the conventional uniaxial compression test, where a sharp-edged right circular cylinder is pressed between wide steel platens. The cylinder is quite likely to have its corners chipped or deformed plastically.

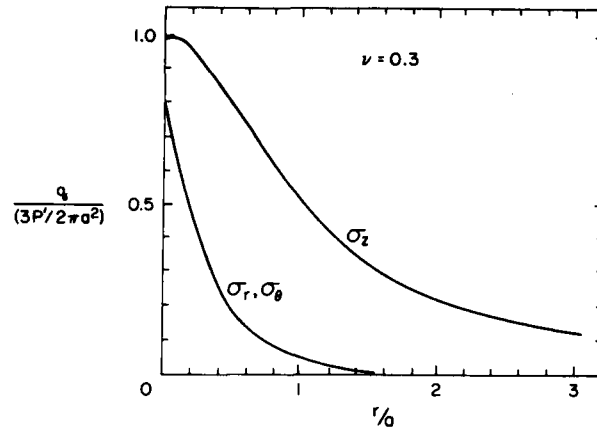


Figure 15. Distribution of stresses along the z -axis when a spherical indenter is pressed against the surface of an elastic half-space ($\nu = 0.3$). (After Timoshenko and Goodier 1951.)

Knowing the distribution of normal pressure and the size of the contact area, the stress field in the material immediately below the contact can be obtained by superposition from the point load solution if necessary. On the surface of the material there is no normal stress outside the contact area ($r > a$), but in the radial direction there is a maximum tensile stress at the edge of the contact zone ($r = a$). The value of this maximum tensile stress is

$$\sigma_r = \frac{(1-2\nu)}{3} q_0 = (1-2\nu) \frac{P}{2\pi a^2}. \quad (32)$$

The circumferential stress σ_θ at the same radius is a compressive stress of the same magnitude, i.e. $\sigma_\theta = -\sigma_r$. Since $\sigma_z = 0$, there is thus a state of pure shear at the boundary of the contact surface. The magnitude of this shear stress is $q_0(1-2\nu)/3$, which amounts to $0.133q_0$, or $0.2(P/\pi a^2)$, for $\nu = 0.3$.

The distribution of stress along the axis of symmetry is shown in Figure 15 for $\nu = 0.3$. The normal stresses are all compressive, and the maximum shear stress for $r = 0$ occurs at a depth equal to about 50% of the contact radius a (i.e. $z \approx a/2$). For $\nu = 0.3$, the value of this maximum shear stress is approximately $0.31 q_0$, or $0.47(P/\pi a^2)$.

Indenter with two-way curvature

For an indenter that has two principal radii of curvature, like the rim of a simple disc cutter, the contact area has an elliptical shape, and the distribution of pressure in the contact area is described by the ordinates of a semi-ellipsoid.

If the indenter has principal radii of curvature R and R' in orthogonal planes that are both normal to the surface of the medium, the lengths of the semi-axes of the elliptical contact zone a and b are given by

$$a = m \left[\frac{3P}{2} \frac{\left(\frac{1-\nu_1^2}{E_1} + \frac{1-\nu_2^2}{E_2} \right)}{\left(\frac{1}{R} + \frac{1}{R'} \right)} \right]^{1/2} \quad (33)$$

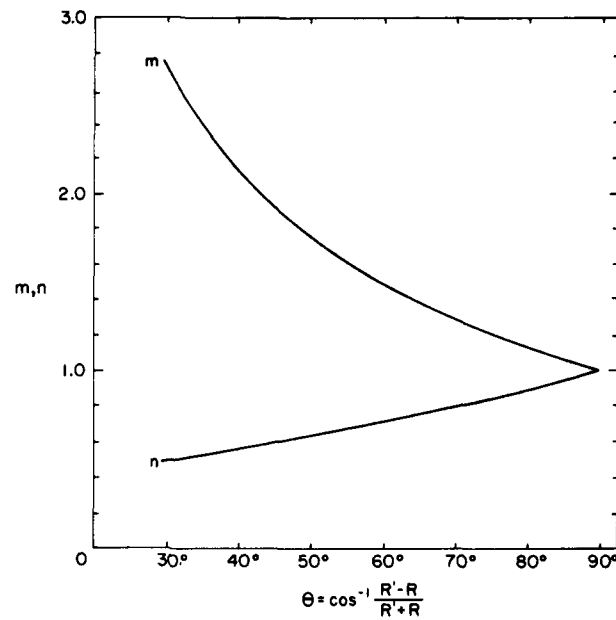


Figure 16. Values of the dimensionless factors m and n in eq 33 and 34. (Plotted from values quoted by Timoshenko and Goodier 1951, and credited to H.C. Whittemore and S.N. Petrenko 1921.)

$$b = n \left[\frac{3P}{2} \frac{\left(\frac{1-\nu_1^2}{E_1} + \frac{1-\nu_2^2}{E_2} \right)^{1/2}}{\left(\frac{1}{R} + \frac{1}{R'} \right)} \right] \quad (34)$$

where m and n are dimensionless numbers depending on R and R' . Values are reproduced by Timoshenko and Goodier (1951) and are given here in graphical form in Figure 16. The maximum pressure q_0 at the center of the contact area is

$$\sigma_z = -q_0 = -\frac{3P}{2\pi ab} \quad (35)$$

If x and y axes are taken from the center of the contact zone along the semi-axes a and b respectively, the principal stresses at the center are:

$$\sigma_x = -q_0 \left[2\nu + (1-2\nu) \frac{b}{a+b} \right] \quad (36)$$

$$\sigma_y = -q_0 \left[2\nu + (1-2\nu) \frac{a}{a+b} \right] \quad (37)$$

$$\sigma_z = -q_0 \quad (38)$$

At the ends of the axes of the ellipse, $\sigma_z = 0$, $\sigma_x = -\sigma_y$, and $\tau_{xy} = 0$; i.e. there is a state of pure shear, and the radial stress component is tensile. For the ends of the axes, the magnitudes of the shear stress and the principal stresses are as follows.

Major axis, $x = \pm a$, $y = 0$, $z = 0$:

$$\tau = \sigma_x = -\sigma_y = \frac{3P}{2\pi a^2} \frac{(1-2\nu)}{[1-(b/a)^2]} \left\{ \frac{1}{[1-(b/a)^2]^{1/2}} \tanh^{-1} [1-(b/a)^2]^{1/2} - 1 \right\}. \quad (39)$$

Minor axis, $x = 0$, $y = \pm b$, $z = 0$:

$$\tau = \sigma_x = -\sigma_y = \frac{3P}{2\pi a^2} \frac{(1-2\nu)}{[1-(b/a)^2]} \left\{ 1 - \frac{1}{[(a/b)^2 - 1]^{1/2}} \tan^{-1} [(a/b)^2 - 1]^{1/2} \right\} \quad (40)$$

The limits of the elliptic contact case are $a/b = 1$, which is the hemispheric indenter, and $a/b = \infty$, which is the long circular cylinder.

Failure criteria

Knowledge of the distribution of individual stress components, as derived from elastic analysis, does not immediately indicate where or when fracture or yielding of the target material will begin. For some materials, fracture may initiate when the maximum tensile stress reaches a critical level at some point. For other materials, yielding may begin when the shear stress reaches a critical level at some point in the material. In general, the stress conditions that produce onset of fracture or plastic yielding are described by a failure criterion.

A failure criterion is usually expressed as a critical combination of principal stresses that leads to failure. For some materials, notably metals subject to slow loading, yielding begins when the shear stress or deviatoric stress (given by the second invariant of the stress tensor) reaches a critical value, apparently irrespective of the bulk stress.* The Tresca criterion and the von Mises criterion are of this form. For other kinds of materials, such as brittle solids and granular media, the shear resistance increases significantly as the bulk stress increases, and the failure criterion has to take this into account. Probably the best known criterion with this more general form is the linear Mohr-Coulomb criterion, which assumes the shear strength of the material to be proportional to the confining pressure.

The simple Mohr-Coulomb criterion, like the Tresca criterion, is a two-dimensional relation in principal stress space; i.e. it is assumed that failure conditions are determined by the greatest and least principal stresses σ_1 and σ_3 , where $\sigma_1 > \sigma_2 > \sigma_3$. The relation is linear, and it can be expressed in terms of principal stresses as either

$$\frac{(\sigma_1 - \sigma_3)}{2} - \frac{(\sigma_1 + \sigma_3)}{2} \sin \phi = c \cos \phi \quad (41)$$

or

$$\sigma_1 [(\mu^2 + 1)^{1/2} - \mu] - \sigma_3 [(\mu^2 + 1)^{1/2} + \mu] = 2c \quad (42)$$

* Bulk stress here denotes the isotropic (or "hydrostatic") part of the stress tensor, as given by the first invariant. It is also referred to as the "mean normal stress" or "mean principal stress."

where the constants c and ϕ are identified with the intrinsic cohesion and the internal friction of the material, respectively. With ϕ taken as the angle of internal friction, μ is the corresponding coefficient of friction $\mu = \tan\phi$. It might be noted in passing that for relatively high pressure the McClintock-Walsh criterion (a derivative of Griffith theory applied to rocks) is identical in form to the Mohr-Coulomb criterion, with a substitution of $c = 2T$, where T is the uniaxial tensile strength of the material.

Actually there are indications that the linear Mohr-Coulomb criterion may be a good approximation only when the failure is "brittle," i.e. preceded by straining that is largely reversible. Under conditions that favor creep and ductile failure (i.e. high bulk stress, low strain rate and high temperature), the Mohr envelope seems to be nonlinear, with the critical shear stress tending to a limit for high confining pressures. A parabolic Mohr envelope has been assumed for some analyses of indentation cutting in rock (Cheatham 1964, Pariseau and Fairhurst 1967, Cheatham and Gnirk 1967). Adoption of a nonlinear criterion may be important for indentation studies even when there are no externally imposed pressures (as in deep drilling in fluid-filled holes), since the indenter itself can sometimes create high bulk stresses in the target material.

Initiation of failure

By combining the elastic stress distribution for an indenter with a suitable failure criterion, it ought to be possible to predict where failure will begin, and at what load level on the punch. For example, a set of Cartesian stress components expressed as functions of applied load, load area dimensions, and space coordinates can be combined to give the principal stresses as functions of the same variables by applying standard identities. The expressions for the principal stresses can then be combined in accordance with an appropriate failure criterion, e.g. eq 41 or 42. Finally, a distribution of "stress severity" corresponding to the chosen failure criterion can be obtained, and critical locations in the stress field can be identified. This is a laborious procedure that may or may not be illuminating. An example of results from such a procedure is provided by an analysis of failure initiation in the conventional uniaxial compression test made by Hawkes and Mellor (1970).

For present purposes it is probably not worth the effort to try to predict where failure will initiate, since local failure at a single point does not necessarily permit a complete failure of the system or structure. In order for an indenter to penetrate, either by chipping out a crater or by causing the material to flow, critical conditions have to develop over complete areas so that displacement surfaces can form. This is the kind of problem that is dealt with in plasticity theory.

Plastic yielding

In the present context, plastic yielding is considered to be the condition which allows an indenter to penetrate, but it does not necessarily imply that the material flows like toothpaste. The point is that failure conditions in the material have to spread through a finite zone before the indenter can penetrate.

After brief mention of the line load, which does not have finite contact area, we start with a consideration of the behavior of flat-face indenters, which have constant contact area and a characteristic plastic yield zone that develops at a fixed force level. Following this, other types of indenters, such as cylinders, wedges, spheres, cones and pyramids, are discussed. In the latter cases, the contact area increases as penetration increases, and there is progressive yielding under increasing force levels. For the whole of this part of the discussion it is assumed that the material follows the von Mises criterion, and that the indenter makes frictionless contact. In the second part of the discussion the Mohr-Coulomb criterion is introduced, and interfacial friction is considered.

Yielding under a knife-edge load

It is observed that, in materials which fail by shear, the flow or fracture develops along characteristic paths, or *sliplines*. Very often, these paths appear to develop in such a way that they maintain constant orientation with respect to the directions of principal stress. In the case of a knife-edge load, the principal directions are the radials from the loading point and the concentric semicircles that cross these radials orthogonally, since σ_r and σ_θ are principal stresses (see eq 1-3). Taking the usual polar coordinates r and θ , the curves that intersect the principal directions at constant angle μ are two orthogonal sets of logarithmic spirals described by

$$r = r_0 \exp(\pm \cot \mu \theta) \quad (43)$$

where r_0 is a constant. The initial elastic shear stress along each trajectory and the corresponding normal stress can be obtained by combining eq 1-3 with eq 43, together with standard resolution of stress components. This gives stresses which vary with θ , but in fact the failure cannot progress until the critical yield stress is reached over the complete length of a sufficient range of *sliplines*. Thus the elastic stresses are not directly useful in predicting failure loads for deep indentation. The alternative procedure adopted in plastic analysis is to deduce a *slipline* field that satisfies the yield criterion and the boundary conditions at the free surface and indenter surface, to obtain the stresses on the interface, and finally to calculate the applied force as a function of penetration by resolution of forces.

Two-dimensional flat-face punch

Consider a two-dimensional flat-face indenter, as shown in Figure 9 and Figure 17. The elastic stress solution shows that infinite pressure develops at the corners as soon as load is applied (eq 15 and Figure 9), which implies that there will be immediate local failure of the material under these corners. However, this local incipient failure serves only to relieve the stress concentrations there, and the indenter will penetrate by only a very small distance in accordance with the conditions of elastic equilibrium. As the force on the punch increases, the zone that is subject to the critical yield stress will spread, until eventually it develops a shape that permits the punch to displace material and penetrate, either by flow or by fracture.

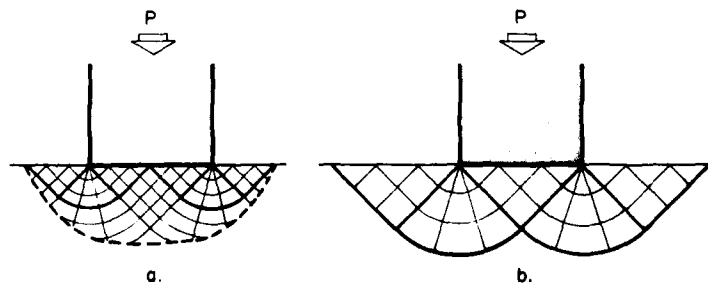


Figure 17. *Slipline fields for incipient plastic yielding under a two-dimensional rigid frictionless punch on the plane surface of a semi-infinite medium.*

In elementary plasticity theory (see Hill 1950, Prager and Hodge 1951), the incipient plastic yielding of material under a two-dimensional flat-face punch is treated by assuming a frictionless contact and no deformation of the surface outside the punch prior to yielding. The von Mises failure criterion is usually taken (this criterion is identical to the Tresca criterion for plane deformation), and for plane strain it is

$$\left(\frac{\sigma_x - \sigma_y}{2}\right)^2 + \tau_{xy}^2 = k^2 \quad (44)$$

where k is the yield stress for direct shear. From a Mohr circle construction an angle θ , which gives a shear direction, is defined as

$$\theta = \frac{1}{2} \tan^{-1} \left[\frac{2\tau_{xy}}{\sigma_x - \sigma_y} \right] \pm \frac{\pi}{4} \quad (45)$$

For the free surface immediately adjacent to the punch, $\sigma_y = 0$, $\tau_{xy} = 0$ and, from eq 44, $\sigma_x = -2k$. From eq 45 it is found that the shear directions, or slip lines, intersect the surface at 45° in this region. If the contact surface of the punch is frictionless, then $\tau_{xy} = 0$ in this area also, so that again the shear directions intersect the contact surface at 45° . With shear directions meeting the surface at 45° throughout the plastic region, a complete slip field can be constructed by taking 45° fan lines from the corners of the punch and crossing them with orthogonal curves, as shown in Figure 17. The outside limits of the plasticized zone remain undetermined, and historically there have been different interpretations. However, in all cases the predicted critical load on the punch P' is the same, i.e.

$$\sigma_y = -\frac{P'}{2a} = -2k(1+\pi/2) = -5.14k \quad (46)$$

or

$$P' = 4ak(1+\pi/2). \quad (47)$$

Equation 46 indicates that penetration will occur when the bearing pressure of the punch reaches about five times the direct shear strength of the material. Practical rules-of-thumb for penetration are often stated in terms of the uniaxial compressive strength of the target material. For example, there is a widely held view that an indenter will penetrate rock when the nominal bearing pressure reaches about 10 times the uniaxial compressive strength. In terms of the uniaxial test, k might be taken as octahedral shear stress at failure, i.e. the axial stress divided by $\sqrt{2}/3$. Thus eq 26 could be rewritten in terms of the uniaxial strength σ_c as

$$\sigma_y = 5.14(\sigma_c \sqrt{2}/3) = 2.42\sigma_c. \quad (48a)$$

Alternatively, k might be taken as $\sigma_c/2$, in which case

$$\sigma_y = 2.57\sigma_c. \quad (48b)$$

Flat-face cylindrical punch

A solution that has been obtained for the flat-face cylindrical indenter (see Hill 1950) gives a yield-point loading of

$$\sigma_y = 2.85Y = 4.94k \quad (49)$$

where Y and k are yield stresses in uniaxial tension and shear respectively for a material following the Mises criterion. If we take $\sigma_c = Y = k\sqrt{2}/3$ for this kind of material, the result is not much different from that obtained in the corresponding two-dimensional case (eq 46-48), since

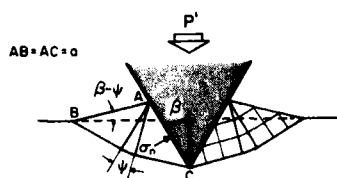


Figure 18. Slip lines and displacements produced in a plastic half-space by a two-dimensional symmetrical wedge.

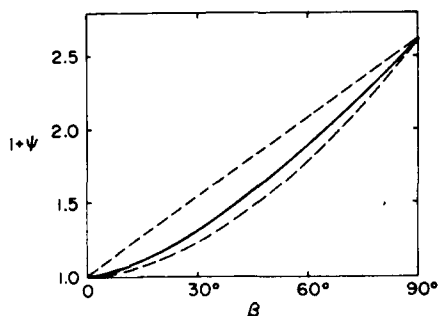


Figure 19. The full line shows $(1+\psi)$ as a function of β according to Hill (1950). The broken straight line represents the relation used by Cheatham (1958). The broken curve is the approximation given by eq 59, and taken for ease of integration in eq 60.

$$\sigma_y = 2.33 \sigma_c. \quad (50a)$$

If the alternative of $k = \sigma_c/2$ is taken,

$$\sigma_y = 2.47 \sigma_c. \quad (50b)$$

For most practical purposes, eq 48 and 50 say the same thing.

Two-dimensional wedge

When a two-dimensional wedge of uniform cross section is thrust normally into an incompressible semi-infinite medium, displacement can take place according to the system of slip lines shown in Figure 18. If there is no friction between the wedge and the material, the surfaces AC are subject only to a uniform normal pressure σ_n . If the "fan angle" of the slip field is ψ (Fig. 18) and the yield stress in direct shear for the Mises criterion is k , then the normal pressure on the wedge is

$$\sigma_n = 2k(1+\psi). \quad (51)$$

If the dimensions AB and AC in Figure 18 are a , then the normal load per unit length P' that corresponds to this amount of indentation is given by

$$P' = 2\sigma_n a \sin\beta = 4ka(1+\psi) \sin\beta \quad (52)$$

in which ψ is a function of β :

$$\cos(2\beta - \psi) = \frac{\cos\psi}{1 + \sin\psi} = \tan\left(\frac{\pi}{4} - \frac{\psi}{2}\right). \quad (53)$$

Figure 19 gives the relation between $(1+\psi)$ and β . Taking $k = \sigma_c\sqrt{2}/3$ as before, the nominal bearing pressure on the horizontally projected area of the wedge is

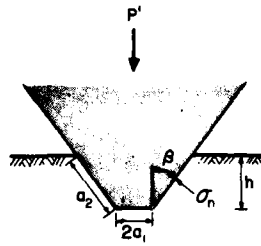
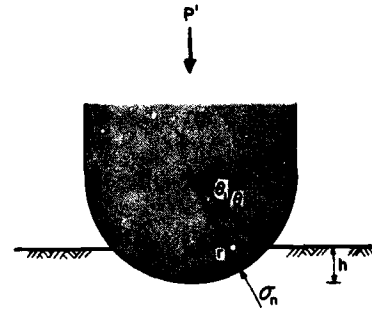


Figure 20. Penetration of a plastic half-space by a rigid frictionless wedge with a flat tip.

Figure 21. Penetration of a half-space by a semi-cylindrical indenter.



$$\frac{P'}{2a \sin \beta} = \frac{P' \psi}{2h \tan \beta} = \sigma_n = \frac{2\sqrt{2}}{3} \sigma_c (1 + \psi) = 0.94 (1 + \psi) \sigma_c \quad (54a)$$

or, for $k = \sigma_c/2$,

$$\sigma_n = (1 + \psi) \sigma_c \quad (54b)$$

where $(1 + \psi)$ ranges from 1.0 for an infinitely sharp wedge to $(1 + \pi/2)$, or 2.57, for a flat indenter.* The latter limit (i.e. $\sigma_n = 2.42 \sigma_c$ or $\sigma_n = 2.57 \sigma_c$) agrees with the result obtained directly for the flat-face two-dimensional punch (eq 48).

Two-dimensional wedge with flat tip

For a flat-tipped wedge making frictionless penetration of a von Mises material, as shown in Figure 20, the penetration resistance P' might be taken as equal to the resolved resultants of the normal pressures acting on the flat end and the sloping sides of the wedge, as proposed by Cheatham (1958). Thus, referring to the symbols of Figure 20,

$$P' = 2a_1 \sigma_{n1} + 2a_2 \sin \beta \sigma_{n2} = 2(a_1 \sigma_{n1} + h \tan \beta \sigma_{n2}). \quad (55)$$

From eq 48, or alternatively from eq 54 and Figure 19 with $\beta = 90^\circ$, the normal pressure on the flat tip σ_{n1} can be expressed as $2.42 \sigma_c$, or $2.57 \sigma_c$, as in Cheatham (1958). From eq 54, the normal pressure on the sloping faces σ_{n2} can be expressed as $0.94(1 + \psi) \sigma_c$, or $(1 + \psi) \sigma_c$, where $(1 + \psi)$ is given by Figure 19 for any specified value of β .

Two-dimensional semicylindrical indenter.

For a smooth semicylindrical indenter (Fig. 21), the penetration resistance P' is equal to the sum of the resolved incremental normal pressures that act on the interface:

$$P' = 2 \int_{\theta_1}^{\pi/2} \sigma_n \sin \theta r d\theta \quad (56)$$

in which σ_n is a function of θ .

* Cheatham (1958) gives $\sigma_n = (1 + \beta) \sigma_c$, attributing the result to Hill (1950). In fact, Hill's analysis gives eq 54 above.

Cheatham (1958) assumes that σ_n can be taken as the normal pressure which would act on a smooth wedge of half-angle θ . For a material following the von Mises criterion, he takes σ_n as $(1+\theta)\sigma_n$, apparently following the misinterpretation of Hill's wedge analysis that was mentioned earlier. As a practical matter, there may not be much objection to Cheatham's treatment, since it makes eq 56 readily integrable, and $(1+\theta)$ is not much different from $(1+\psi)$, as shown in Figure 19.

Cheatham's expression for σ_n implies, in terms of the shear yield stress k , a normal pressure of $2k(1+\theta)$. According to Hill (1950), this is the normal pressure required to expand a semicylindrical cavity in the surface of a plastic material. The semicylinder expansion is not the same case as indentation by a semicylindrical indenter, since geometric similarity is maintained in the former case, but not in the latter.

If we accept the approximation $(1+\psi) \approx (1+\beta)$, then eq 54 gives σ_n as

$$\sigma_n \approx 0.94(1+\beta)\sigma_c \quad \text{or} \quad \sigma_n \approx (1+\beta)\sigma_c$$

or, alternatively

(57)

$$\sigma_n \approx 0.94(1+\theta)\sigma_c \quad \text{or} \quad \sigma_n \approx (1+\theta)\sigma_c.$$

Equation 54 can then be integrated to give

$$P' = 1.89[1 - \sin\theta_1 + (1+\theta_1) \cos\theta_1] r \sigma_c \quad (58a)$$

or

$$P' = 2[1 - \sin\theta_1 + (1+\theta_1) \cos\theta_1] r \sigma_c \quad (58b)$$

in which $\theta_1 = \sin^{-1}(1-h/r)$. This is essentially the same as Cheatham's (1958) result. A somewhat closer approximation can be obtained by expressing the relationship of eq 53 and Figure 19 as

$$\psi = \frac{\pi}{2} (1 - \cos\beta). \quad (59)$$

This permits eq 56 to be written as

$$\begin{aligned} P' &= 2\sigma_c \int_{\theta_1}^{\pi/2} 0.94 \left[1 + \frac{\pi}{2} (1 - \cos\theta) \right] \sin\theta r d\theta \\ &= 1.89 \left[\left(1 + \frac{\pi}{2} \right) \cos\theta_1 - \frac{\pi}{4} \cos^2\theta_1 \right] r \sigma_c \end{aligned} \quad (60a)$$

or, alternatively,

$$P' = 2 \left[\left(1 + \frac{\pi}{2} \right) \cos\theta_1 - \frac{\pi}{4} \cos^2\theta_1 \right] r \sigma_c. \quad (60b)$$

Figure 22 compares the solutions given by eq 58 and eq 60.

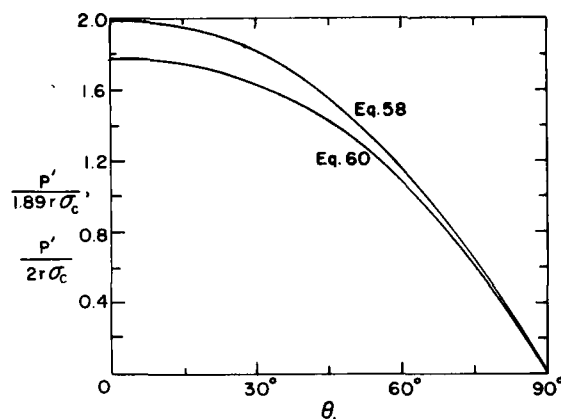


Figure 22. Comparison of two approximate solutions for penetration of a von Mises half-space by a smooth semi-cylindrical indenter.

Three-dimensional indenters

The most general cases are those involving three-dimensional indenters whose horizontal cross sections are non-uniform, such that the potential bearing area increases as penetration proceeds. Indenters of this kind include short wedges, pyramids, cones, and spheres.

According to Hill (1950), the nominal bearing pressure on the horizontally projected area is proportional to the uniaxial yield stress in these cases, provided that the material does not work harden. Thus,

$$\sigma_n = C \sigma_c. \quad (61)$$

The constant C depends on factors such as the shape of the indenter, the friction coefficient between indenter and material, and other properties of the material. However, C does not seem to vary much for well lubricated penetration of materials that follow a von Mises criterion. For squat cones ($\beta > 60^\circ$), C apparently lies between 2.5 and 3, which is not much different from the corresponding proportionality constants for long two-dimensional wedges (see eq 54 and Fig. 19). For spheres, C is said to be also about 3.

Standard hardness tests depend on indentation by a three-dimensional punch. In the Brinell test the indenter is a sphere, in the Vickers test it is a square pyramid, in the Rockwell test it is a sphere, cone or spherical-tipped cone, and in the Knoop test an elongated pyramid. Brinell and Vickers hardness values have the dimensions of stress, and are obtained by dividing the applied force by the surface area of the indentation pit. This is not quite the same thing as σ_n , which is the force divided by the *projected* area for lubricated contact. According to Tabor (1970), σ_n is equal to 3.2 times the yield stress (or flow stress) for a wide range of materials, and Tabor equates this shear yield stress to the uniaxial tensile strength.

Penetration of a Mohr-Coulomb material by a smooth wedge

The previous discussion assumes that the penetrated material conforms to a von Mises failure criterion; i.e. its shear resistance does not vary with confining pressure, or bulk stress. When rocks and similar materials are subjected to rapid penetration under typical environmental conditions, this assumption is unrealistic. The assumption of a linear Mohr-Coulomb failure criterion (eq 41 and 42) is probably a better approximation, provided that high bulk stresses are not created either by the geometry of the indenter or by the external environment.

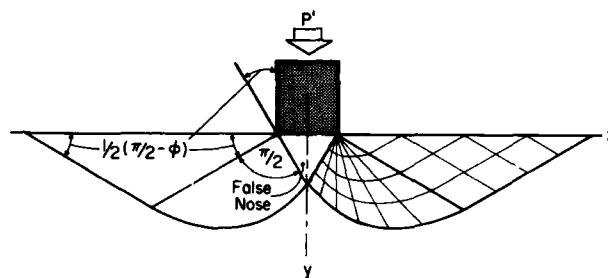


Figure 23a. Slipline field for a strip load on weightless Mohr-Coulomb material.

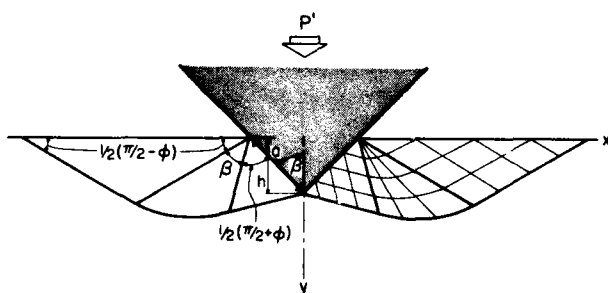


Figure 23b. Slipline field for a smooth wedge entering a Mohr-Coulomb half-space. (After Cheatham 1958, Pariseau and Fairhurst 1967).

When a *line load*, or *knife-edge load*, bears onto a Mohr-Coulomb half-space, the potential failure surfaces are defined by two sets of logarithmic spirals, as was the case for a line load on a von Mises material (eq 43). However, in this case the spirals intersect the free boundary not at 45° but at $(45^\circ \pm \phi/2)$, where ϕ is the "angle of internal friction" (or angle of shear resistance) for the Mohr-Coulomb material.

When the line load is extended to finite width, so that it becomes a *strip load*, the slip lines have to be smooth and continuous, and the most plausible pattern is one which forms a "dead wedge," or "false nose," under the strip load, together with zones of plastic displacement on both sides (Fig. 23a). The penetration force per unit length (P') for a flat strip of width $2a$ is given by Prandtl's theory, which is the basis for standard soil mechanics equations giving the bearing capacity of shallow strip footings on weightless soil:

$$\frac{P'}{2a} = \left[\frac{\exp(\pi \tan \phi) - \tan^2 \mu}{2 \tan \phi \tan \mu} \right] \sigma_c \quad (62a)$$

where $\tan \mu = (1 - \sin \phi) / \cos \phi$ and σ_c is the uniaxial compressive strength of the material [for a c - ϕ material, $\sigma_c = 2c \cos \phi / (1 - \sin \phi)$].

Cheatham (1958) and Pariseau and Fairhurst (1967) treated the penetration of a half-space by two-dimensional wedges, assuming a linear Mohr-Coulomb failure criterion and following the general lines of Prandtl theory. The wedge was allowed to penetrate without displacing the surface of the half-space, slipline fields were deduced for both smooth and rough wedges, and force-penetration relations were derived.

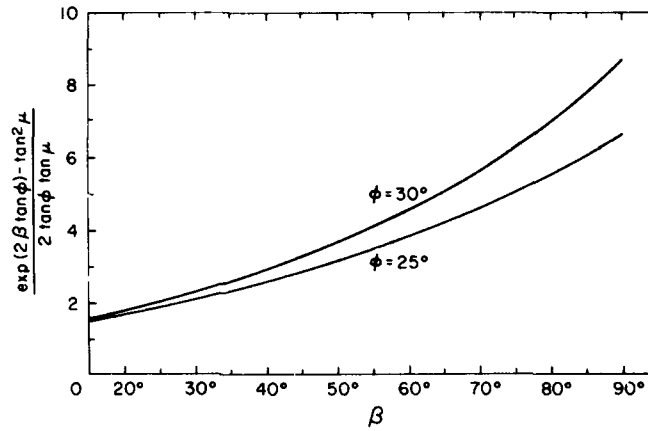


Figure 24. Variation of nominal bearing pressure with wedge angle for a smooth wedge in linear Mohr-Coulomb material.

Figure 23b gives the slipline field for a smooth wedge according to Cheatham (1958) and Fairhurst and Pariseau (1967). From the corresponding equilibrium conditions a force-penetration relation is obtained, and the results of Cheatham and of Fairhurst and Pariseau can be rewritten in conformance with the foregoing terminology as

$$\frac{P'}{2a \sin \beta} = \frac{P'}{2h \tan \beta} = \left[\frac{\exp(2\beta \tan \phi) - \tan^2 \mu}{2 \tan \phi \tan \mu} \right] \sigma_c \quad (62b)$$

where h is the penetration depth (Fig. 23b), ϕ is the "angle of internal friction," and μ is $\frac{1}{2}[(\pi/2) - \phi]$, such that

$$\tan \mu = \frac{1 - \sin \phi}{\cos \phi} \quad (63)$$

As before, the average bearing pressure on the horizontally projected area of the active part of the wedge is proportional to the uniaxial compressive strength of the material. The proportionality constant depends on the wedge angle β and the internal friction angle ϕ . For a given wedge in a given material, the penetration depth h is proportional to the applied force.

In Figure 24, the function that gives the proportionality constant between the nominal bearing pressure and the uniaxial compressive strength is shown graphically as a function of the wedge half-angle β for two values of ϕ . These factors are a good deal higher than the corresponding factors for the smooth wedge penetrating a von Mises material (i.e. the factors of Fig. 19 multiplied by 1.15).

Penetration of a Mohr-Coulomb material by a slender rough wedge

A solution for a "rough" wedge can be obtained by letting the interface coincide with a failure surface in the fan region, as in Figure 25. This maximizes the interfacial shear stress, and it is not necessary to specify an interfacial friction coefficient. The force-penetration relation obtained by Cheatham (1958) and Pariseau and Fairhurst (1967) can be written as

$$\frac{P'}{2a \sin \beta} = \frac{P'}{2h \tan \beta} = A_1 \sigma_c \quad (64)$$

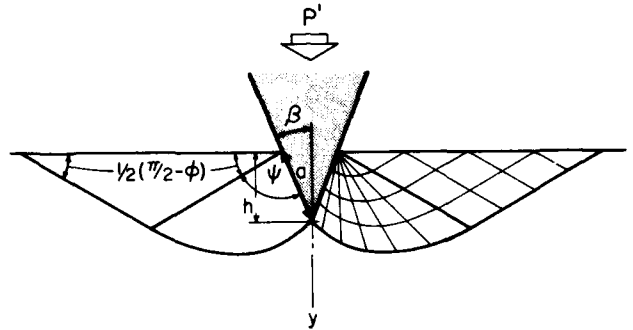


Figure 25. Slipline field for a slender rough wedge entering a Mohr-Coulomb material. (After Cheatham 1958, Pariseau and Fairhurst 1967.)

where

$$A_1 = \frac{[1 + \sin \phi (\cot \beta \tan \mu - 1)] \exp(2\psi \tan \phi) - \tan^2 \mu}{2 \tan \phi \tan \mu} \quad (65)$$

$$\mu = \frac{1}{2} \left(\frac{\pi}{2} - \phi \right) \quad (66)$$

$$\psi = \frac{\pi}{2} - \mu + \beta = \frac{1}{2} \left(\frac{\pi}{2} + \phi \right) + \beta. \quad (67)$$

For this case there is a restriction:

$$0 < \beta < \mu$$

i.e.

$$0 < 2\beta < \left(\frac{\pi}{2} - \phi \right). \quad (68)$$

Since ϕ is typically about 30° or somewhat less, the solution is valid for wedges whose included angle 2β is less than about 60° .

Figure 26 gives values of the function A_1 for two values of ϕ and a range of applicable wedge angles. The value of A_1 is the proportionality constant relating the nominal wedge pressure and the uniaxial compressive strength of the material. By comparing Figure 26 with Figure 24, it can be seen that friction dominates the penetration resistance in the case of a rough wedge.

Penetration of a Mohr-Coulomb material by a broad rough wedge

If the half-angle of the wedge β exceeds the limit set by eq 67, i.e. $\beta > \mu$, the face of the wedge can no longer coincide with a slipline, since the maximum fan angle is $\psi = \pi/2$ (see Fig. 27). Because the "rough" condition prohibits the interfacial slip that can occur with a "smooth" wedge (as in Fig. 23), a false nose of dead material forms between the limiting fan lines (Fig. 27). The force-penetration relation for this case (Pariseau and Fairhurst 1967) is

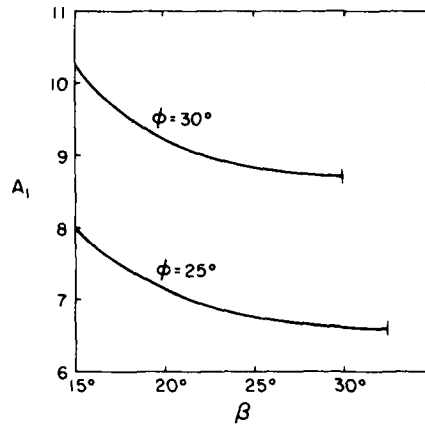


Figure 26. Variation of nominal bearing pressure with wedge angle for a slender rough wedge in linear Mohr-Coulomb material.

$$\begin{aligned} \frac{P'}{2a \sin \beta} &= \frac{P'}{2h \tan \beta} = \frac{\exp(2\psi \tan \phi) - \tan^2 \mu}{2 \tan \phi \tan \mu} \cdot \sigma_c \\ &= \frac{\exp(\pi \tan \phi) - \tan^2 \mu}{2 \tan \phi \tan \mu} \cdot \sigma_c \end{aligned} \quad (69)$$

where

$$\mu < \beta < \pi/2$$

or

$$\pi > 2\beta > (\pi/2 - \phi). \quad (70)$$

Since ϕ is likely to be about 30° or less, this means that eq 69 applies only to rough wedges that have a total included angle greater than 60° or so.

Once the wedge angle is big enough for a false nose to form, the proportionality constant linking the nominal bearing pressure with the uniaxial compressive strength becomes independent of the wedge angle β . For $\phi = 30^\circ$ the value of the constant is 8.7, and for $\phi = 25^\circ$ it is 6.6, i.e. the limit values shown in Figure 26.

Wedge penetration with nonlinear failure criteria and with finite interfacial friction

In general, the Mohr envelope for the failure criterion is nonlinear, and wedge indentation in accordance with a parabolic envelope has been considered by Cheatham (1964), Pariseau and Fairhurst (1967), Cheatham and Gnirk (1967), and Smith and Cheatham (1975). This criterion is written in terms of shear stress τ and normal stress σ :

$$\tau^2 = A\sigma + B. \quad (71)$$

Pariseau and Fairhurst take τ as the maximum shear stress, i.e. $\frac{1}{2}(\sigma_1 - \sigma_3)$, and σ as the mean normal stress, i.e. $\frac{1}{2}(\sigma_1 + \sigma_3)$. Cheatham and Gnirk take τ as $\tau_{r\theta}$ and σ as σ_θ in a system of polar coordinates.

The results of analyses for the nonlinear criterion are more suitable for direct application in numerical examples than for brief summarizing in general form, and they will not be discussed further here. However, it might be mentioned that the nonlinear envelopes which have been established

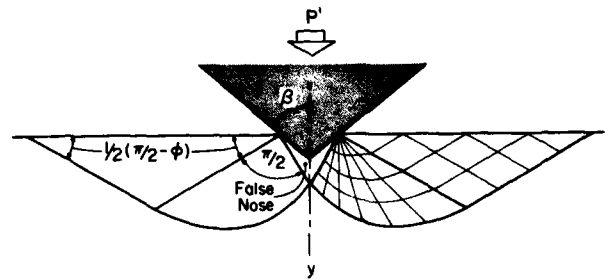


Figure 27. Slipline field for a squat rough wedge that forms a false nose in Mohr-Coulomb material.

experimentally tend to a limiting shear stress that is insensitive to changes in bulk stress; this is quite similar to the behavior described by the von Mises criterion. Thus the simple analyses for the linear Mohr-Coulomb criterion and the von Mises criterion provide acceptable approximations for the extremes of the external pressure range. The real need for a nonlinear criterion is brought about by large variations of bulk stress in the stress field imposed by the indenter itself.

Variation of the interfacial friction coefficient has the effect of modifying the ratio of tangential shear stress to normal stress on the interface. Thus it affects the direction of the major principal stress relative to the interface. If θ is the angle between the y -axis (of Fig. 23, 25 and 27) and the direction of the major principal stress, the values of θ in a linear Mohr-Coulomb material are $(\pi/2 - \beta)$ for the smooth wedge (Fig. 23), $(\mu - \beta)$ for the slender rough wedge (Fig. 25), and zero for the rough wedge with a false nose (Fig. 27). If θ is arbitrary, the penetration relationship, following Pariseau and Fairhurst (1967), is

$$\frac{P'}{2a \sin \beta} = \frac{P'}{2h \tan \beta} = A_2 \sigma_c \quad (72)$$

where

$$A_2 = \frac{1}{2 \tan \phi \tan \mu} \left\{ \left[\frac{1 + \cos 2\theta (1 + \cot \beta \tan 2\theta) \sin \phi}{(1 + \sin \phi)} \right] \exp(2\psi \tan \phi) - \tan^2 \mu \right\}. \quad (73)$$

Since θ is related to the interface friction angle ϕ' , eq 72 in effect describes the influence of ϕ' on the force-penetration relation. Pariseau and Fairhurst (1967) show how θ and ϕ' are related by Mohr circle constructions. They point out that if the normal stress along the face of the wedge is assumed constant, as in the preceding analyses, then specification of ϕ' is equivalent to specification of θ for eq 72. However, since θ varies also with the mean stress, this cannot really be justified, and other approaches may be required.

For present purposes it is not profitable to pursue these complications further.

Penetration analyses that are not based on plasticity theory

The ideas that were outlined in the previous section are all based on plasticity theory and formal failure criteria, and they are applicable to a fairly wide range of materials. By contrast, there are some other approaches that have been developed specifically for analysis of penetration into rock, using ad hoc assumptions.

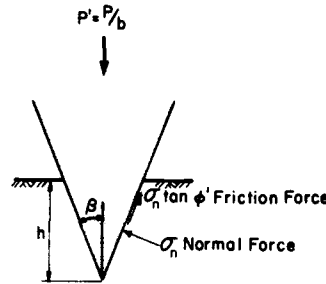


Figure 28. Wedge penetration model for Evans' analysis.

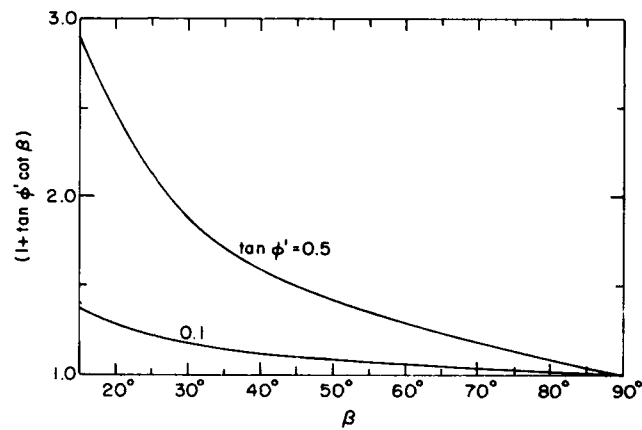


Figure 29. Effect of β on the dimensionless factor of eq 75, assuming two different values for the interface friction coefficient.

Penetration of wedges into coal, according to Evans

The penetration of wedges into coal was studied by Evans and others, and findings have been summarized by Evans and Pomeroy (1973). In the first instance, penetration resistance is assumed to be proportional to the projected bearing area $2hb \tan \beta$, where b is the uniform width of the wedge. It is further assumed that the critical normal stress exerted by the face of a smooth wedge is approximately equal to the uniaxial compressive strength of the coal. Thus, for a smooth wedge,

$$\frac{P}{2hb \tan \beta} = \sigma_c \quad (74)$$

The next step in the argument takes into account interfacial friction by assuming that the bearing surfaces are acted upon by uniform normal stress σ_n and uniform tangential stress $\sigma_n \tan \phi'$, where $\tan \phi'$ is the interface friction coefficient (Fig. 28). Resolving these stresses in the vertical direction, equating to P , and assuming (somewhat questionably) that $\sigma_n = \sigma_c$ gives

$$\frac{P}{2hb \tan \beta} = (1 + \tan \phi' \cot \beta) \sigma_c \quad (75)$$

Equation 74 implies that the nominal bearing pressure $P/(2hb \tan \beta)$ for penetration of a smooth wedge will not vary with the wedge angle β , which differs from the results that are obtained in formal plasticity theory.

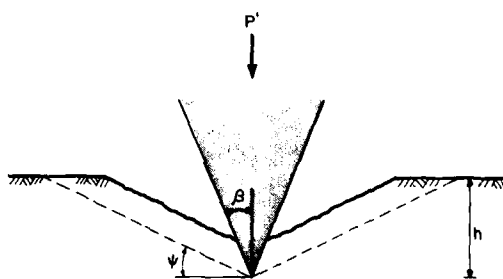


Figure 30. Wedge penetration model for the analysis by Paul and Sikarskie.

Introduction of interfacial friction according to eq 75 creates a finite dependence of bearing pressure on β , as shown in Figure 29. The upper curve in Figure 29 is drawn for $\tan \phi' = 0.5$, since measured values of the interfacial friction coefficient for steel against rock or coal are about 0.5 to 0.55 (Pariseau and Fairhurst 1967, Evans and Pomeroy 1973). However, Evans found that the best agreement with experimental penetration data was obtained by assuming $\tan \phi' = 0.1$, and the weaker angle dependence corresponding to this assumption is also shown in Figure 29.

*Wedge penetration into brittle material,
according to Paul and Sikarskie*

In a much quoted study of two-dimensional wedge penetration into brittle material, Paul and Sikarskie (1965) assumed that chips form repeatedly by fracture along planes that have constant inclination ψ (Fig. 30), where

$$\psi = \frac{1}{2} \left[\left(\frac{\pi}{2} \right) - \left(\frac{\beta + \phi}{2} \right) \right]. \quad (76)$$

Taking a linear envelope for the force-penetration characteristic, the relationship derived from these postulates, in the standard form adopted for this report, is

$$\frac{P'}{2h \tan \beta} = \cos \beta \frac{(1 - \sin \phi)}{1 - \sin(\beta + \phi)} \cdot \sigma_c. \quad (77)$$

Interfacial friction is not included in the relationship.

Figure 31 shows the dimensionless function on the right-hand side of the equation plotted against the wedge half-angle β for two values of ϕ . The apparent implication of the graph is that the contact pressure becomes infinitely large when $(\beta + \phi) = (\pi/2)$. The authors of the theory interpret this limit as a boundary between two modes of behavior: with $(\beta + \phi) < \pi/2$, the rock fails by both chipping and crushing, while with $(\beta + \phi) > \pi/2$, it fails only by crushing. Paul and Sikarskie (1965) also found that the best agreement between theory and experimental data was obtained by assuming small values of ϕ ($< 10^\circ$) and values of σ_c lower than the measured value.

*Cone penetration according to Miller and Sikarskie
and to Lundberg*

Miller and Sikarskie (1968) extended the two-dimensional wedge analysis of Paul and Sikarskie (1965) to cover three-dimensional indenters, notably cones and pyramids. For the cone penetrating brittle rock, the assumed situation is the rotationally symmetric version of the two-dimensional case illustrated in Figure 30. The envelope of the force-penetration characteristic is taken as parabolic; i.e. P is proportional to h^2 .

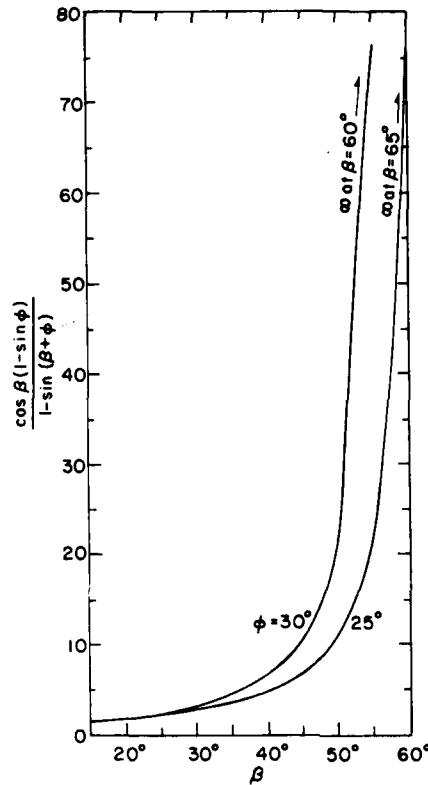


Figure 31. Effect of β on the dimensionless factor in eq 77 for two values of ϕ .

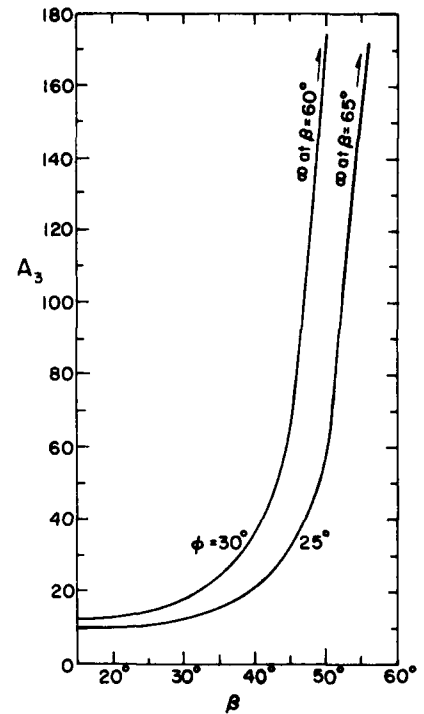


Figure 32. Effect of β on the dimensionless factor of eq 78, taking two values of ϕ .

By suitable manipulation, the results of Miller and Sikarskie yield the relationship:

$$\frac{P}{\pi h^2 \tan^2 \beta} = \frac{\sin \beta \cos \psi (1 - \sin \phi)}{2 \tan^2 \beta \sin^2 \psi \cos(\beta + \psi + \phi)} \cdot \sigma_c = A_3 \sigma_c. \quad (78)$$

In this case the failure angle ψ bears a rather complicated relationship to β and ϕ overall, and the original authors provided a graphical presentation of the relation. However, for practical values of β and ϕ , say $(\beta + \phi) > 20^\circ$, the relationship for a cone is close to linear.

Figure 32 shows how the function A_3 varies with the half-angle β for a cone, taking two assumed representative values for ϕ . The implication is that the contact pressure increases with β , becoming infinitely large when $(\beta + \phi) = (\pi/2)$.

Lundberg (1974) followed the same line of argument as Miller and Sikarskie, but his analysis included interfacial friction between the indenter and the rock. Designating the interfacial friction angle as ϕ' and arranging the results to correspond as closely as possible with eq 78, Lundberg's force/penetration relation is

$$\frac{P}{\pi h^2 \tan^2 \beta} = \frac{\sin(\beta + \phi') \cos \psi (1 - \sin \phi)}{2 \tan^2 \beta \sin^2 \psi \cos(\beta + \phi' + \phi + \psi)} \cdot \sigma_c = A_4 \sigma_c. \quad (79)$$

One of the problems with this equation is that A_4 becomes infinite at quite small values of β when seemingly realistic values of ϕ and ϕ' are inserted. For example, taking $\phi = 30^\circ$ and $\phi' = 28^\circ$ (i.e. an

interfacial friction coefficient of about 0.55), the bearing pressure goes to infinity when β reaches 32° . Lundberg obtained the best agreement between theory and experiment by assuming $\phi = 0$, $\phi' = 6^\circ$, and σ_c about 50% below the measured value. This is not much different from assuming frictionless contact and a von Mises failure criterion.

Penetration of rounded-edge wedges according to Dalziel and Davies

Recognizing that indenting tools have finite curvature on the cutting edge, Dalziel and Davies (1964) studied the penetration of coal by rounded-edge wedges. The experimental results indicated that penetration resistance P is approximately proportional to the square root of edge radius r :

$$P = k r^n \quad (80)$$

where k is a constant and $n \approx 1/2$. This was explained (see also Evans and Pomeroy 1973) in terms of an elastic stress field and a maximum tensile stress failure criterion; the tip radius effect is similar to the effect of crack tip radius in Griffith theory.

It might be noted that, for plastic indentation by a frictionless cylindrical edge, the uniform interfacial normal stress σ_n (which is equal to the penetration resistance divided by the projected bearing area) is

$$\sigma_n = \frac{P'}{2h[(2r/h)-1]^{1/2}} \quad (81)$$

where P' is the force per unit length and h is the depth of indentation. If the material were to fail at some critical value of σ_n , this would suggest proportionality between P and \sqrt{r} only when $(2r/h) \gg 1$, i.e. for indentation depths that are small compared to the edge radius.

Penetration of wedges and cones into brittle rock, according to Dutta

Dutta (1972) analyzed the penetration of broad wedges into brittle rock by assuming the formation of a false nose, as in Figure 27, but taking inclined fracture planes from the tip of the false nose in the way that Paul and Sikarskie took fracture planes from the tip of the wedge in Figure 30. However, whereas the angle of the fracture plane deduced by Paul and Sikarskie was the value given in eq 76, Dutta's value* was

$$\psi = \frac{1}{2} \left(\frac{\pi}{4} - \theta_f - \frac{\phi}{2} \right)$$

where θ_f is an angle of friction between crushed rock and intact rock, assumed to have small values, from 0° to 5° . From consideration of forces acting on the boundaries of the wedge and the displaced rock, and by implicitly assuming that the false nose has a half-angle of $(45^\circ - \phi/2)$, as in conventional plasticity theory, a relation for the first chipping stage was obtained, with corresponding relations of the same form for subsequent chipping stages. This can be written as

$$\frac{P'}{2h \tan \beta} = \frac{\cos \phi \sin \left[\left(\frac{\pi}{4} - \frac{\phi}{2} \right) + \theta_f \right]}{1 - \sin \left[\left(\frac{\pi}{4} + \frac{\phi}{2} \right) + \theta_f \right]} \cdot \sigma_c.$$

* The original paper has a number of misprints.

Since Dutta assumed values of ϕ from 20° to 30° , and values of θ_f from 0° to 5° , it would seem that θ_f is of rather little significance to either the force/penetration relation or the expression for the fracture angle. Neglecting θ_f , the function representing $P'/2h\sigma_c \tan\beta$ has the values 2.98, 3.11 and 3.23 for $\phi = 20^\circ, 25^\circ, 30^\circ$, respectively, and there is no dependence on β (in contradiction to Dutta's experimental data shown in Fig. 42).

A similar analysis for penetration of a cone led to the relation

$$\frac{P}{\pi h^2 \tan^2 \beta} = \frac{(1 - \sin \phi) \sin \theta' \cot^2 \left(\frac{\pi}{4} - \frac{\phi}{2} \right)}{2f(\theta', \phi)} \cdot \sigma_c$$

in which $f(\theta', \phi) = \sin \psi \tan \psi \cos(\psi + \theta' + \phi)$, ψ is as given above, and θ' is $[(\pi/4) - (\phi/2) + \theta_f]$.

Interpretation of penetration data

The foregoing theory provides some guidance for both the design of penetration tests and the interpretation of experimental data. However, it is first necessary to establish the common trends of the various theories, and also to resolve some apparent conflicts. It is convenient to start off by discussing the force/depth relationship for continuous penetration of a simple ductile material, leaving consideration of brittle material and discontinuous chipping until a little later.

Force-depth relationships for simple ductile materials

An indenter thrusting into ductile material maintains intimate contact with the material, so that the contact area either remains constant or increases continuously, depending on the geometry of the indenter. If the material does not strain-harden or strain-soften, it will flow steadily under the action of the indenter, and the force will be a smooth function of penetration depth, provided that the indenter penetrates at a steady rate. Given these conditions, all the theories are in agreement that force should be proportional to the *projection* of the bearing area on the original surface of the half-space when material type and indenter geometry are constants.

For a *flat-face indenter* of uniform cross-section, either a cylindrical punch or a strip punch, the simple expectation is that the force will remain constant as penetration proceeds. For an ideal rigid-plastic material, this behavior would be represented by the line A in Figure 33. For an ideal elastic-plastic material, there would be an initial linear increase of force with displacement until the plastic yield stress was reached, as indicated by the lines A' and A in Figure 33. For real materials, the expected response for an ideal elastic-plastic material is likely to be modified by strain-hardening, and possible also by strain-softening. Figures 34 and 35 give the results of a set of experiments in which Smith and Cheatham (1975) pressed flat punches into ice and frozen sand at relatively low rates. There was some brittle fracture which probably disturbed the force-penetration records, but overall the trend is more or less as might be expected. Force increases with penetration up to some limit, and thereafter remains constant or drops somewhat.

For a *two-dimensional wedge*, either a "long" wedge or a wedge with uniform finite length, the projected bearing area is directly proportional to penetration depth. If the wedge is pushed steadily into a simple material, it would therefore be reasonable to expect force to increase linearly with penetration, as indicated by line B in Figure 33. However, if the wedge were to be pushed into real ductile material in a series of finite steps, a more complicated force-penetration record could result. With penetration depth held constant in a viscous material, the force necessary to maintain that depth would tend to relax with time. With force held constant in a viscous material, there would be a tendency for the wedge to sink deeper due to creep, but this would be offset to some extent by the increase in bearing area, especially in nonlinear viscous material. Figures 36 and 37 give results

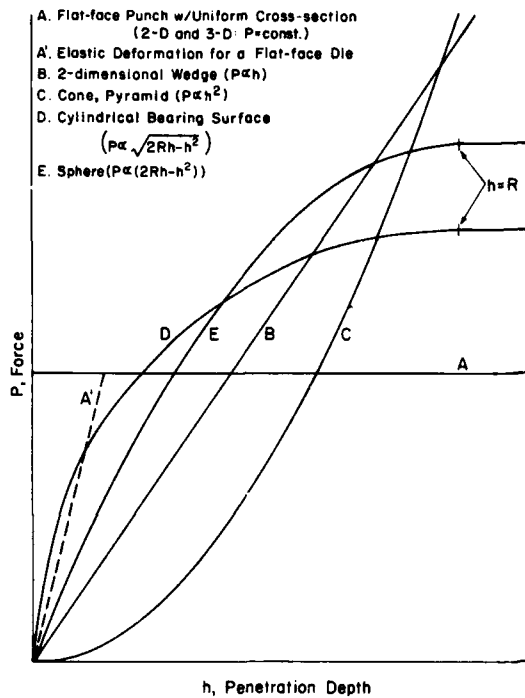


Figure 33. Expected trends of force-penetration relations for indenters in complete contact with ductile material that does not strain-harden or strain-soften.

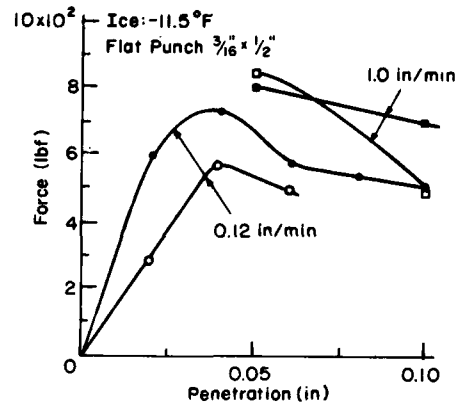


Figure 34. Force/penetration relationship for a flat punch indenting an ice surface (Smith and Cheatham 1975).

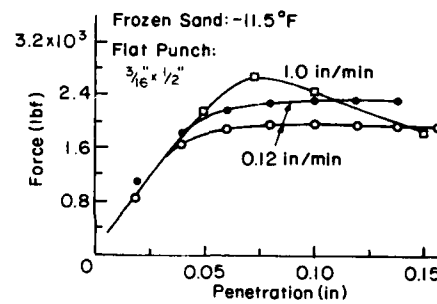


Figure 35. Force/penetration relationships for a flat punch indenting frozen sand (Smith and Cheatham 1975).

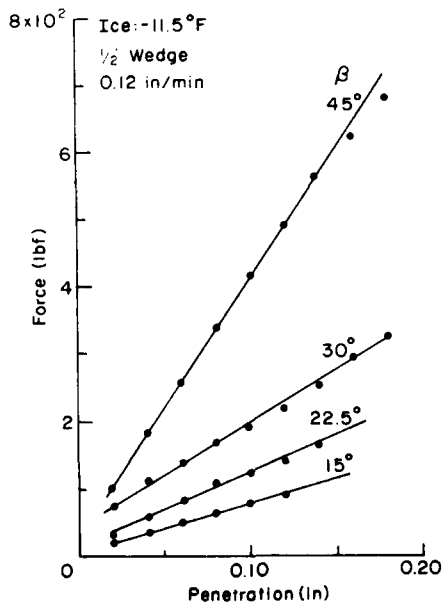


Figure 36. Force/penetration relationship for a wedge indenting ice (Smith and Cheatham 1975).

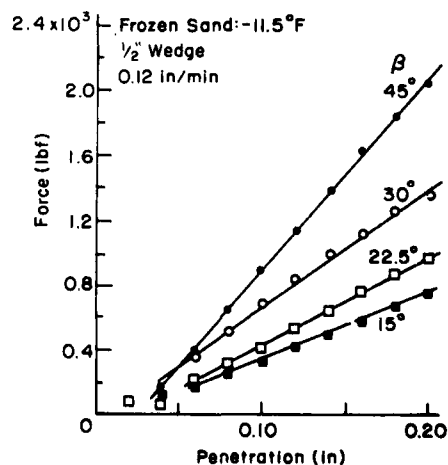


Figure 37. Force/penetration relationship for a wedge indenting frozen sand (Smith and Cheatham 1975).

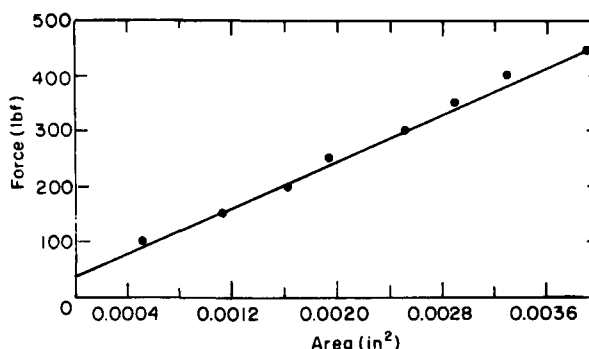


Figure 38. Relationship between force and projected area of the indentation for a 0.5-in.-diameter hemisphere pressed into Solenhofen limestone (Paone and Tananand 1966).

from experiments by Smith and Cheatham (1975), who forced wedges into ice and frozen sand at relatively low rates. The force-penetration relation is close to linear in both materials for a wide range of wedge angles.

A *conical indenter* has a projected bearing area that is proportional to the square of the penetration depth. Thus the force would be expected to increase with the square of the penetration depth when a cone is pushed steadily into a simple material, as indicated by curve C in Figure 33. The same situation exists for an indenter that is a *regular pyramid*, since the projected bearing area is also proportional to the square of the penetration depth.

An indenter that has a *cylindrical bearing surface* gives a projected bearing area per unit length of $2(2Rh - h^2)^{1/2}$, where R is the radius of the cylinder and h is the penetration depth. When $h \ll 2R$, force can be expected to be proportional to the square root of h , but in general the relationship is of the form indicated by curve D in Figure 33. The limit of force is reached when $h = R$.

A *spherical indenter* has a projected bearing area of $\pi(2Rh - h^2)$, where R is the sphere radius and h is the penetration depth. When $h \ll 2R$, force might be expected to be proportional to h . In general, the form of the relationship for simple materials is that indicated by curve E in Figure 33. The limiting force is reached when $h = R$. Paone and Tandanand (1966) pressed a sphere to small depths in Solenhofen limestone, producing permanent deformation but no chipping. They found that force was proportional to the projected area of the permanent indentation (Fig. 38), as might be expected from simple theory, and also that force was proportional to the irreversible penetration (Fig. 39), which is the approximation expected from simple theory. In both cases there was a force intercept; when this was divided by the calculated (Hertzian) bearing area, it was equivalent to an average pressure of 6.1 kbar, which is well above the uniaxial compressive strength of the limestone.

Force-depth relationships for brittle materials

With high penetration rates, low external confining pressures, and temperatures far below the melting point, the target material under an indenter will usually exhibit some brittle response if it is a nonmetallic substance. At typical penetration rates for cutting and drilling tools, brittle fracture will usually be produced in rocks, minerals, concrete and similar materials. As the force increases and the indenter penetrates, there is likely to be a series of more or less abrupt fractures that produce chips and develop a crater by a discontinuous process.

With discontinuous penetration of this kind, the general pattern of the force-penetration graph depends partly on the properties of the material and partly on the compliance of the loading system. The potential influence of compliance in the loading system is shown schematically in Figure 40.

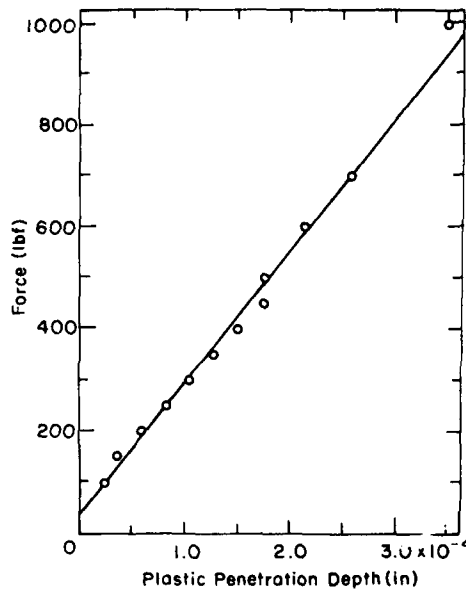


Figure 39. Force/penetration relation for a hemispheric indenter (0.5-in.-diameter) pressed into Solenhofen limestone (Paone and Tandan and 1966).

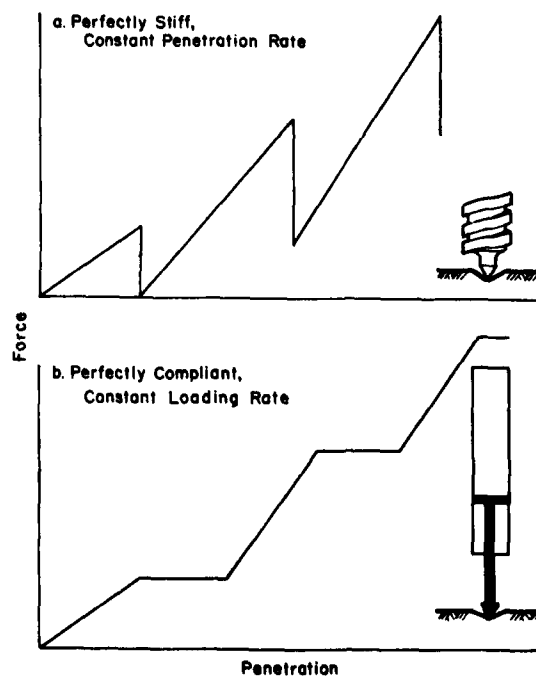


Figure 40. Potential influence of compliance in the loading system.

In Figure 40a, it is supposed that the loading system is perfectly stiff (e.g. a massive screw jack), so that it cannot jerk ahead to "take up the slack" when the material under the indenter yields abruptly. Such a system is capable of applying constant penetration rate. If there is not much confinement of the broken material, as might be the case when a very sharp wedge makes a shallow surface crater, then the penetration could drop abruptly almost to zero. By contrast, if some of the crushed material under the tip of the indenter remains trapped under stress when the large chips break free (say under a broad wedge or in a deep crater), then the penetration resistance will drop abruptly, but not all the way to zero.

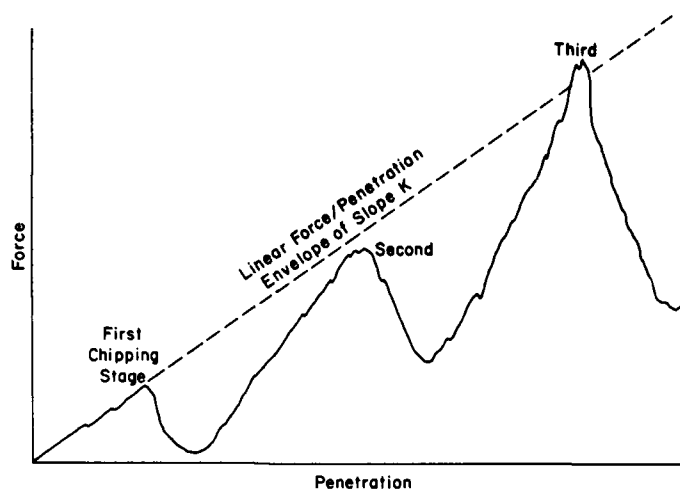


Figure 41. Impression of typical force/penetration characteristic for an actual experiment on rock.

In Figure 40b, it is supposed that the loading system is perfectly compliant (e.g. a large-volume gas actuator) and has zero inertia. With this kind of system, release of strain energy will give large displacements, and the loading system will tend to jerk forward without dropping load when the material yields abruptly. Such a system is capable of applying constant loading rate.

With real loading systems, the observed behavior is somewhere between the extremes indicated in Figure 40, and Figure 41 gives an impression of the kind of trace that might be obtained from an experiment on rock. With typical apparatus, the indenter might be pushed into rock by a hydraulic actuator, while the applied force is measured by a load cell. This is a fairly "soft" arrangement, and normally it will give some forward surging after each yield, or "chipping stage," as shown in Figure 41. However, in some experiments neither the rate of penetration nor the rate of loading are properly controlled, and consequently some odd features can be produced in test records. For example, some records show reversal of penetration after each yield, probably because the indenter is backed off each time, or because displacements are not being measured directly between the indenter and the target material. Whatever the procedure, in the final step a line is drawn through the major peaks of the test record, and this is taken as the equivalent of the continuous force-penetration curve that would be obtained in a ductile material.

The force-penetration envelope drawn through the peaks of a brittle indentation record perhaps ought to show similar trends to the force-penetration curves for ductile material. However, records of the kind depicted in Figure 41 are often too erratic or too limited in range to permit anything other than a straight line to be drawn. Furthermore, the increment of penetration that represents chip formation may not be related directly to force at all.

Linear force-penetration envelopes have been accepted as good approximations for a number of materials subjected to both ductile and brittle penetration by wedges and spheres. These materials include Indiana limestone (Pariseau and Fairhurst 1967, Benjumea and Sikarskie 1969, Hustrulid and Fairhurst 1971), Berea sandstone and Carthage marble (Gnirk 1966, Cheatham and Gnirk 1967), Solenhofen limestone (Paone and Tandanand 1966), Tennessee marble (Pariseau and Fairhurst 1967), ice and frozen sand (Smith and Cheatham 1975), sand/cement mortar (Vanzant 1963), and wide variety of other rocks (Dollinger 1977).

Nonlinear force-penetration envelopes have been recorded for brittle penetration of cones into granite and limestone by Miller and Sikarskie (1968), and into granite by Lundberg (1974). In both cases, analysis led to the expectation that force would be proportional to the square of penetration depth, and test results were in reasonable agreement with this expectation.

The slope of a linear force-penetration envelope is sometimes called a "penetration index"; it is usually designated by the symbol K , and has dimensions force/length. When K is determined for a particular type of rock and a particular type of indenter, such as the tungsten carbide stud of a roller cutter, it can be used directly in appropriate formulae for predicting boring rate. Dollinger (1977) has given data for 22 different rock boring projects that show a 1:1 correlation between actual and predicted boring rates, using the assumption that studs on an operating cutter penetrate to the same depth as studs tested in the laboratory when the load is the same in both cases.

When a parabolic relation between force P and penetration h is accepted for conical or pyramidal indenters, the proportionality constant K' that is given by P/h^2 is the equivalent of the penetration index K , although the dimensions of K' are force divided by length squared. For empirical predictions of boring rate, the penetration of a sharp conical stud on a roller cutter would be estimated as $\sqrt{P/K'}$.

Effects of indenter geometry on force-penetration relationships

All the theoretical relationships can be expressed in such a way that penetration resistance is proportional to the projected area of the bearing surface. The proportionality constant typically consists of the uniaxial strength of the material σ_c multiplied by a dimensionless function that is controlled by the yield properties of the material, the geometric properties of the indenter, and the interfacial friction coefficient. Thus the geometric factors that govern the projected bearing area can probably be accounted for in a straightforward way, leaving the residual geometric effects on the dimensionless function to be explored in the light of experimental evidence.

Effects of wedge angle

For a symmetrical wedge of half-angle β , the projected bearing area for a given penetration depth h is directly proportional to $\tan\beta$, and thus there is every reason to believe that the relationship between penetration resistance P and wedge angle β will include the factor $\tan\beta$. It therefore seems reasonable to separate out this rather obvious effect and examine the residual effect of β .

Following this line of reasoning, we look for the effect of β on the nominal bearing pressure $P/(2hb \tan\beta)$, where

$$\frac{P}{2hb \tan\beta} = f_1(\beta, \phi, \phi') \cdot \sigma_c. \quad (82)$$

Various formulations of $f_1(\beta, \phi, \phi')$ are given by the preceding theoretical results. The value of the function *increases* with β for: 1) a frictionless wedge in an ideal plastic material conforming to the von Mises criterion (i.e. $\phi = 0$, $\phi' = 0$), 2) a smooth wedge in a linear Mohr-Coulomb material (i.e. ϕ is finite and $\phi' = 0$), and 3) a smooth wedge penetrating Mohr-Coulomb material according to the theory of Paul and Sikarskie (i.e. ϕ is finite, $\phi' = 0$ and $\beta + \phi < \pi/2$). The value of the function *decreases* with β for: 1) a slender rough wedge in a linear Mohr-Coulomb material (i.e. ϕ is finite, ϕ is big enough to prevent interfacial slip, $\beta < \pi/4 - \phi/2$), and 2) penetration of Mohr-Coulomb material by a frictional wedge according to the theory of Evans (i.e. ϕ is finite, ϕ' is finite). The value of the function is *independent* of β for a broad rough wedge that forms a false nose when penetrating Mohr-Coulomb material (i.e. ϕ is finite, ϕ' is big enough to prevent interfacial slip, $\beta > \pi/4 - \phi/2$). There is clearly no simple trend, even in a qualitative sense, although the increasing trend seems to be associated with smooth wedges and the decreasing trend with rough wedges.

Before looking at experimental data, it might be well to recall that most of the theoretical results are for "long" wedges, while tests are made with wedges of finite length b . If $b \gg h$ there is probably not much of a problem, but if this condition is not met, as seems to be the case in some experiments, then the test data may be complicated by end effects.

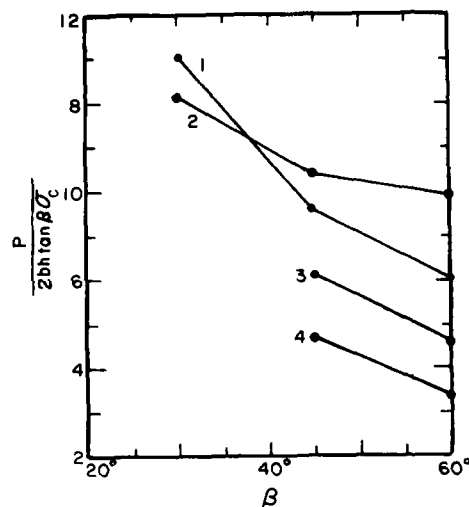


Figure 42. Effect of wedge angle β on the dimensionless "indenter factor." 1) Indiana limestone (Pariseau and Fairhurst 1967). 2) Tennessee marble (Pariseau and Fairhurst 1967). 3) Marble (Dutta 1972). 4) Darley Dale sandstone (Dutta 1972).

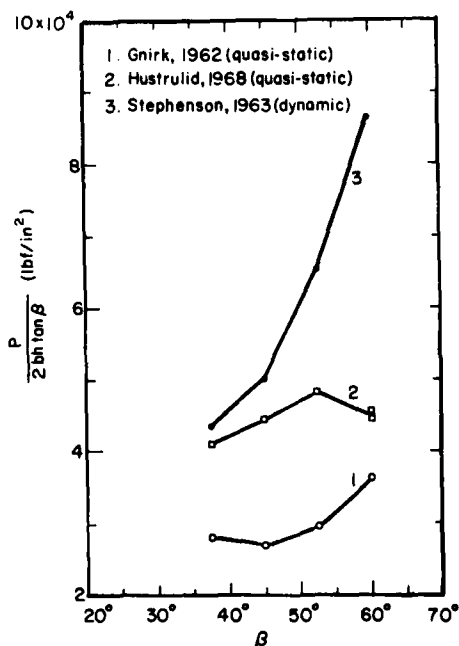


Figure 43. Effect of β on the dimensionless "indenter factor" for Indiana limestone according to data from various sources.

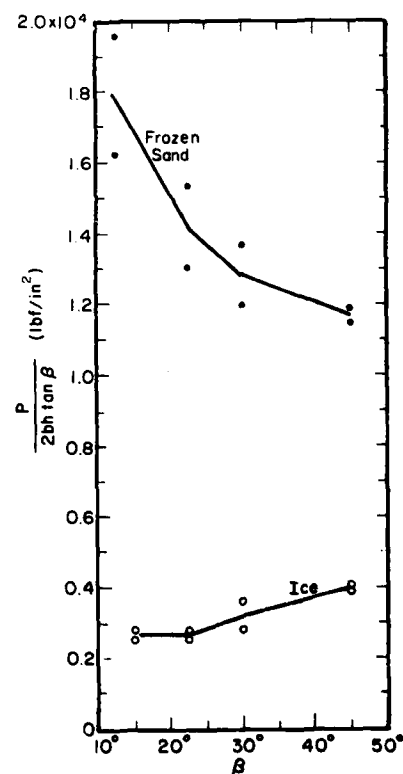


Figure 44. Effect of β on the dimensionless "indenter factor" for Ice and frozen sand (data from Smith and Cheatham 1975).

Figures 42-44 give some experimental data that have been taken from the literature and rearranged in accordance with eq 82 so as to show the form of $f_1(\beta, \phi, \phi')$. At first sight the apparent trends are just as confusing as those given by the various theories, since the function increases with β in some tests, even for the same material. Comparing the data for ice and frozen sand, there is a temptation to attribute the different trends to differences in interfacial friction, regarding a wedge in ice as a "smooth" wedge and one in frozen sand as a "rough" wedge. The data of Figure 42, which show a decreasing trend, were obtained with wedges that had a measured interfacial friction coefficient of about 0.55, so that these results might be considered reasonable in the light of theory. In Figure 43, the results of Gnirk (1962) and of Hustrulid (1968), obtained for quasi-static indentation, show only weak dependence on β , and taken together they show hardly any trend. However, the dynamic results of Stephenson (1963) show a very substantial increase of the function with β .

Effects of cone angle or pyramid angle

For symmetrical penetration by a right cone or a regular pyramid, the projected bearing area is proportional to the square of $\tan \beta$, where β is the half-angle of the cone or the half-angle between opposite faces at the apex of a pyramid. Continuing the argument that penetration ought to proceed at a definite value of the nominal bearing pressure, the angle effects for a cone can be separated out in accordance with the relation

$$\frac{P}{\pi h^2 \tan^2 \beta} = f_2(\beta, \phi, \phi') \cdot \sigma_c. \quad (83)$$

For a pyramid, the corresponding relation is

$$\frac{P}{4h^2 \tan^2 \beta} = f_3(\beta, \phi, \phi') \cdot \sigma_c. \quad (84)$$

Miller and Sikarskie (1968) showed experimentally that the nominal bearing pressure for cones, pyramids and spheres was independent of h , which provides some support for the idea that yielding occurs at a fixed value of the nominal bearing pressure.

In Figure 45 the experimental results of Miller and Sikarskie (1968) and of Lundberg (1974) are plotted in accordance with eq 83 and 84. The general impression is that $f_2(\beta, \phi, \phi')$ increases with β , but the evidence is inconclusive.

Effects of sphere radius

For a spherical indenter of radius R , the projected bearing area for a given penetration depth h is $\pi(2Rh - h^2)$. In contrast to the situation for wedges, cones and pyramids, geometric similarity is *not* maintained as the spherical indenter penetrates, and it is to be expected that sphere radius will have both a direct effect on the bearing area and an indirect effect connected with the ratio h/r . A relationship for any given penetration h can be written as

$$\frac{P}{\pi(2Rh - h^2)} = f_4(R, \phi, \phi') \cdot \sigma_c. \quad (85)$$

The straightforward way to explore the variation of $f_4(R, \phi, \phi')$ with R is to let R vary while comparing values for a given h in a given type of material. Such data do not seem to be available, but Miller and Sikarskie (1968) give the nominal bearing pressure when the first chip forms for two sizes of sphere (h is not reported). These results are shown in Figure 46, and for both types of rock there is a downward trend of the function as R increases. If the penetration depth is similar for both

1. Cone, Bohus Granite (Lundberg 1974)
2. Cone, Indiana Limestone (Miller and Sikarskie 1968)
3. Cone, Barre Granite (Miller and Sikarskie 1968)
4. Pyramid, Indiana Limestone (Miller and Sikarskie 1968)
5. Pyramid, Barre Granite (Miller and Sikarskie 1968)
6. Cone, Granite (Dutta 1972)
7. Cone, Marble (Dutta 1972)
8. Cone, Sandstone (Dutta 1972)

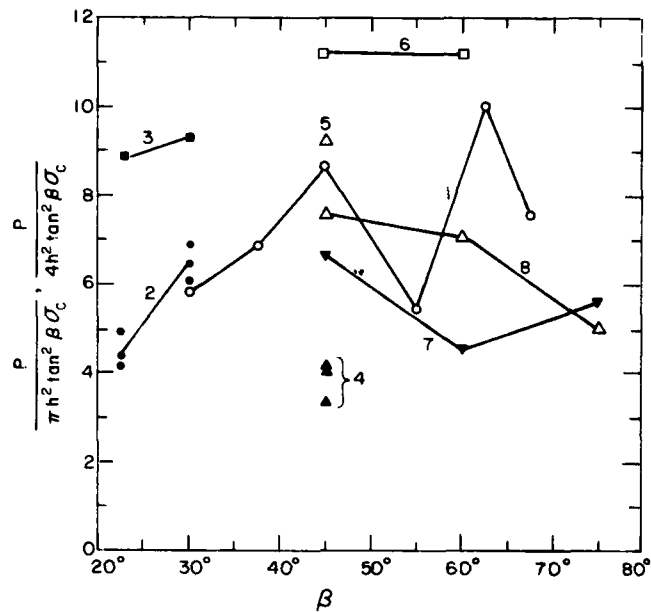


Figure 45. Effect of β on the dimensionless "indenter factor" for cones and pyramids.

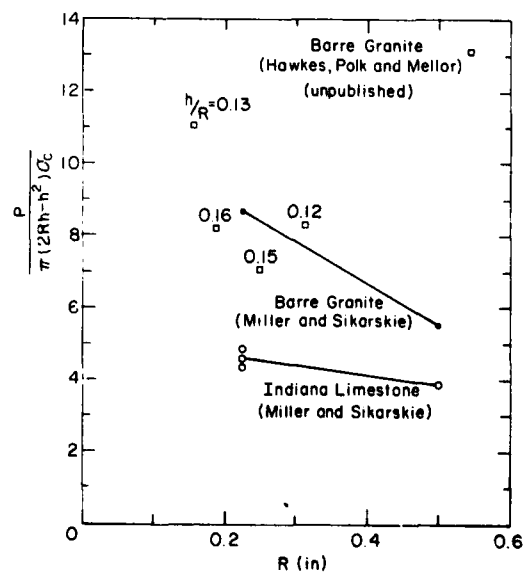


Figure 46. Effect of radius for a spherical indenter.

spheres, this trend is perhaps a little surprising; one might speculate that maybe it represents an effect of stressed volume (rock strength tends to decrease with increase of stressed volume). Figure 46 also gives some unpublished data by Hawkes, Polk and Mellor. Each plotted point represents a mean for 10 tests; values are for the first chipping stage, and the mean value of h/R is given. While these results do not of themselves define a definite trend, they tend to support the idea that the function decreases with R for a fixed value of h , and possibly also decreases with increase of h/R for a fixed value of R .

Effects of loading rate on penetration

Many indenter experiments are made under quasi-static conditions, with load and penetration increasing rather slowly. By contrast, most indentation tools complete their penetration very rapidly, say in 0.1 seconds or less, and there can be wide variations in penetration rate among different kinds of tools. Thus there is a question of how slow laboratory tests relate to typical tool operations, and how tool operations are affected by variations in penetration rate.

In principle there are a number of ways that loading rate or strain rate can influence the force-penetration relationship for an indenter. First of all, the strength of a material in a defined stress field shows an inherent rate dependence that might be loosely identified with thermally-activated processes; in general, strength increases as strain rate increases at any given temperature (it also increases as temperature decreases at any given strain rate). Secondly, constitutive relations and failure criteria can change as strain rate varies, and consequently the form of a stress field and the mode of failure may be rate-dependent. An extreme example is the transition from ductile to brittle behavior as strain rate increases. Finally, there are inertial effects and shock phenomena that become important at very high rates of loading.

Effect of strain rate or loading rate on material strength

To discuss the inherent rate-dependence of material strength, it is useful to first specify that the stress field imposed by the test should be controlled solely by the loading apparatus and the specimen geometry, without any dependence on the material properties. Uniaxial compression and uniaxial tension tests meet this specification, while beam tests and disc tests do not. Given such conditions, the peak strength of a material, or the maximum deformation resistance, will increase as the strain rate or the loading rate increases. The extent to which this effect shows up is related directly to the ductility displayed by the material under the prevailing conditions. Ductile behavior is favored by low strain rate, high temperature (relative to the melting temperature), and high confining pressure.

If the material shows marked creep prior to rupture, then both the compressive strength and the tensile strength are likely to increase significantly with increasing strain rate. The magnitude of the effect might be such that strength is proportional to strain rate raised to the power n , where n could be between $\frac{1}{2}$ and $\frac{1}{4}$. This means that strength changes by a factor of two as strain rate changes by roughly an order of magnitude. This kind of behavior can be expected in ice and ice-bonded soils for typical environmental temperatures and loading durations of a few seconds or more. Similar behavior could occur at higher temperatures and lower strain rates in some other rocks and minerals, for example rock salt or sulphur.

By contrast, if the material deforms elastically and fails by brittle fracture, then the dependence of strength on strain rate is likely to be much weaker. As long as the deformation is predominantly elastic, changes in strain rate of many orders of magnitude are not likely to alter the strength by more than 20 to 40%. At typical environmental temperatures, most of the common rocks and minerals are far below their melting temperatures, and under low confining pressures they show little evidence of creep over periods of minutes. Thus there is not likely to be much variation in penetration resistance as loading duration varies from 10 to 0.1 s, and this range could probably be extended by one or two orders of magnitude without much effect on the situation.

Effect of strain rate on the stress field under an indenter

Just as the inherent strength of a material is influenced by time-dependent deformation, or ductility, so is the stress field induced by an indenter. At strain rates or loading rates which are high enough to produce an elastic response, the resulting stress fields are of the kind predicted by elastic theory, as outlined in an earlier section. On the other hand, with extremely low strain rates in highly ductile material, the resulting stress fields will perhaps be more akin to those predicted by plasticity theory. In principle, a plastic yield zone has to form to permit penetration, whether the initial stress field is elastic or not. However, in reality it is quite likely that the pattern of yielding will be different for the two cases, with localized crushing and chipping occurring near stress concentrations in the elastic stress field.

Another consequence of change in ductility is a change in the form of the failure criterion. At the very low strain rates which allow a material to flow, it is likely that the deviatoric yield stress will be insensitive to changes of hydrostatic pressure; i.e. the failure criterion will be of the von Mises type. At the high strain rates which produce brittle fracture, nonmetallic solids are likely to show increase of the deviatoric yield stress with increasing bulk stress; i.e. the failure criterion is of the Mohr-Coulomb type.

These effects are probably not of major significance for typical rocks, and for the strain rates typical of tool operations. However, they could be important where there are wide variations of strain rate in ice, ice-bonded soils, rock salt, or other "creepy" materials.

Inertial effects, compressibility, and shock phenomena

In a material of low compressibility, where penetration occurs by displacement to the free surface, the elastic stress field, the crack patterns, and the slip line displacement field are all likely to be more or less unaffected by penetration speed as long as it stays above the limit for ductile response but well below the elastic wave velocity of the material. However, the displaced material does have to be accelerated and provided with kinetic energy, and consequently some increase of penetration resistance with penetration speed can be expected. The relative significance of this effect is likely to be greatest in weak material.

When penetration speed becomes greater than the elastic wave velocity of the target material, there is no chance for elastic stress fields, crack patterns, or slip fields to form ahead of the indenter. Instead, shock waves are created, and they interact to form a shock front. There is a very abrupt pressure increase across the shock front, and the pressure rise is determined by the compressibility of the material, the particle velocities, and the shock velocity, in conformance with the principles of mass and momentum conservation. Behind an intense shock, the behavior of the material is likely to be hydrodynamic. For finite penetration distance, the shock attenuates as it propagates, eventually decaying to an elastic stress wave which can continue to break material until its amplitude has been attenuated to something less than the material strength.

Since the elastic wave velocities of typical intact rocks are several kilometers per second, the shock situation is applicable more to high velocity free projectiles than to captive indenters, and it will not be considered any further here.

In highly compressible materials, such as very porous rocks and soils, something analogous to a shock wave can form at penetration velocities well below the elastic wave velocity of the material. The indenter compacts the adjacent material, propagating a relatively slow plastic compression wave and a fast elastic precursor. However, this phenomenon is only marginally relevant to the present consideration, since indentation tools are not normally used in weak crushable materials.

PRACTICAL INDENTATION MECHANISMS

Types of indenters

When a simple indenter such as a wedge or a cone is pushed at right angles into rock or concrete, it is rarely driven by static thrust against a reaction; the usual situation is for the indenter to be propelled inertially by percussion or by direct impact. Two kinds of inertial indenters can be distinguished: 1) percussion devices that remain in contact with the material while they are energized, and 2) free projectiles that strike the target material at high velocity, either burying themselves or rebounding. In both cases the indenter is given a certain amount of *energy*, and neither force nor penetration depth is controlled directly. The devices which drive indenters of these types will not be discussed in this report.

The most common mechanism that employs normal indentation and quasi-static thrust is the roller cutter. The simplest roller cutter is a sharp-edged wheel, exemplified on a small scale by the roller glass cutter. Wheels, or disc cutters, of this type are used on tunnel boring machines and raise borers that work in relatively weak rocks. For indentation cutting in very strong rocks, the simple disc cutter is modified by setting tungsten carbide studs into the rim, thus increasing the indentation stresses and improving the resistance to abrasion. In order to limit the number of individual cutters on the boring head of a large machine, several disc cutters may be formed from a single forging and set onto a common bearing. Alternatively, the roller cutter may be a frustum of a cone with hemispheric or conical studs set into the surface. For rotary drilling in hard rock, and for center cutters on tunneling machines, two or more cone cutters are mounted in a cluster with their axes of rotation radiating from the center of the hole. For work in rocks that are weak, ductile or compressible, roller cutters may be made with teeth like those of a gear wheel. Some of these gear-tooth cutters are capable of digging out cohesive fragments when the teeth are penetrating deeply into the work.

The remaining sections of this report deal entirely with the principles and the performance characteristics of roller cutters.

Dynamics of a simple disc cutter

Consider the simple disc shown in Figure 47. Its radius is R , and it has uniform thickness w , so that the perimeter has sharply squared edges. It is rolled along the surface of a material, and thrust into it to constant depth ℓ by application of an axle force that can be resolved into components H and V that are respectively parallel and normal to the surface of the material. These forces are assumed to be invariant with time (i.e. the cutting process is a continuous one, as distinct from a process of intermittent chip formation).

Since the depth of penetration ℓ is constant, the path traced out by any point on the rim of the disc is a regular cycloid (see Part II, p. 12-13). Thus, if an elementary segment of the rim is regarded as an indenter, it penetrates along a cycloidal path. At any stage of the penetration defined by the angle θ in Figure 47, the slope of the penetration path is given by the standard equation of the cycloid (eq 6 of Part II) as dy/dx :

$$\frac{dy}{dx} = \frac{dy}{d\phi} \cdot \frac{d\phi}{dx} = \frac{\sin \phi}{1 - \cos \phi} = \cot(\phi/2) \quad (86)$$

where ϕ is the conventional angular position used in the standard cycloid equation, such that $\phi = (2\pi - \theta)$. Thus,

$$dy/dx = \cot(\pi - \theta/2) = -\cot(\theta/2) \quad (87)$$

and the inclination from the normal direction is

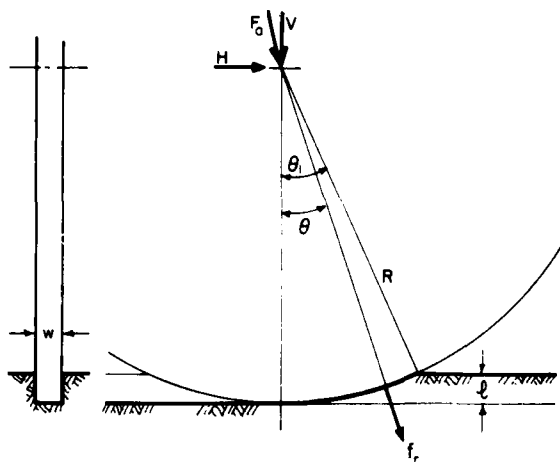


Figure 47. Rolling disc of uniform thickness.

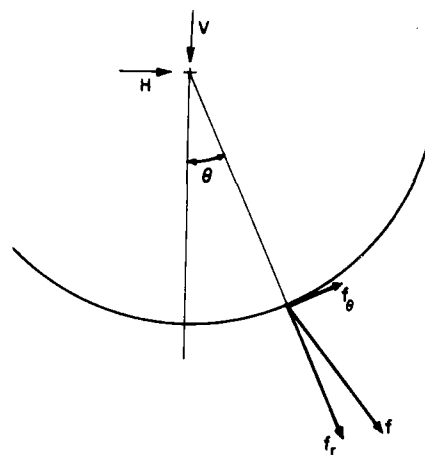


Figure 48. Force components on the rim of a simple disc cutter.

$$dx/dy = -\tan(\theta/2). \quad (88)$$

In other words, at any position defined by the angle θ , the penetration path is inclined at angle $(\theta/2)$ to the normal direction.

If s is distance measured along the cycloidal path

$$ds/d\phi = 2R \sin(\phi/2). \quad (89)$$

If the elementary indenter enters the material at a position defined by angle θ_1 , as indicated in Figure 47, the penetration distance along the cycloidal path s' is

$$s' = 4R [\cos(\theta/2) - \cos(\theta_1/2)] \quad (90)$$

$$= 4R \left(\pm \sqrt{\frac{1+\cos\theta}{2}} \mp \sqrt{\frac{1+\cos\theta_1}{2}} \right)$$

$$= 2\sqrt{2} R \left(\pm \sqrt{2 - \frac{l}{R} - \frac{\Delta l}{R}} \mp \sqrt{2 - \frac{l}{R}} \right). \quad (91)$$

Since $\Delta l/R$ is much smaller than $(2-l/R)$,

$$s' \approx \frac{\sqrt{2} \Delta l}{\sqrt{2-l/R}} \approx \frac{\Delta l}{\sqrt{1-(l/2R)}} \approx \frac{\Delta l}{\cos(\theta_1/2)}. \quad (92)$$

When l/R is very small, $s' \approx \Delta l$.

As each element of the rim penetrates, it applies and experiences a force f whose direction ought to be tangential to the cycloidal penetration path; it can be resolved into components f_r and f_θ that are respectively normal and tangential to the rim (Fig. 48). If the bearing of the disc is frictionless, the tangential components f_θ must sum to zero, since there can be no net moment about the center of the disc. Under these circumstances, the forces are purely radial. From resolution of forces parallel and normal to the material surface:

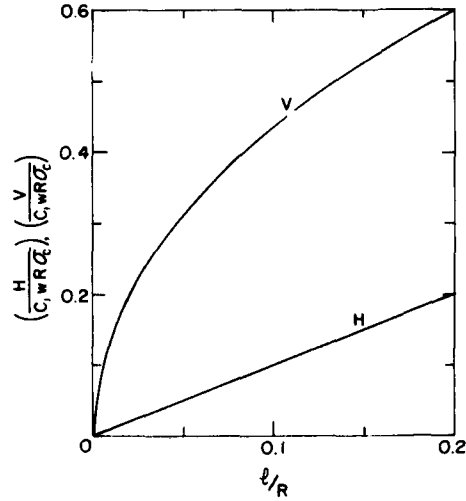


Figure 49. Variation of axle forces with penetration depth for a disc of uniform thickness.

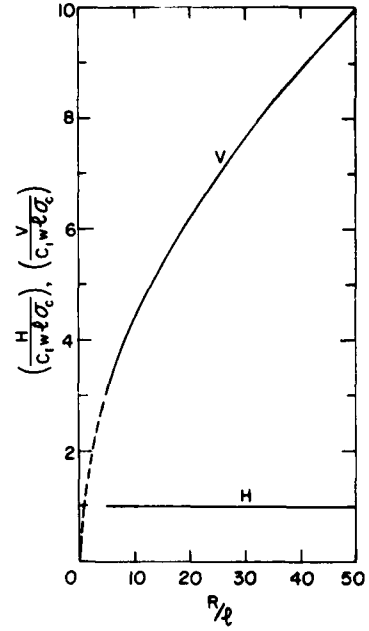


Figure 50. Variation of axle forces with disc radius for a disc of uniform thickness.

$$H = - \int_{\theta_1}^0 f_r \sin \theta \, d\theta \quad (93)$$

$$V = - \int_{\theta_1}^0 f_r \cos \theta \, d\theta. \quad (94)$$

According to simple theory, the penetration resistance is independent of penetration depth for an indenter of uniform width, in which case the force component f_r would be independent of θ :

$$f_r = C_1 w \sigma_c \quad (95)$$

where C_1 is a constant defined by the failure criterion of the material, w is the width of the disc, and σ_c is the uniaxial compressive strength of the material. Hence,

$$H = C_1 w R \sigma_c (1 - \cos \theta_1) = C_1 w l \sigma_c \quad (96)$$

$$V = C_1 w R \sigma_c \sin \theta_1 = C_1 w \sigma_c l \sqrt{(2R/l) - 1}. \quad (97)$$

These relationships* are shown graphically in Figures 49 and 50. When $2R/l \gg 1$,

$$V \approx C_1 w \sqrt{2Rl}. \quad (98)$$

* The analysis may also apply to the problem of a rigid towed wheel that sinks into "plastic" ground.

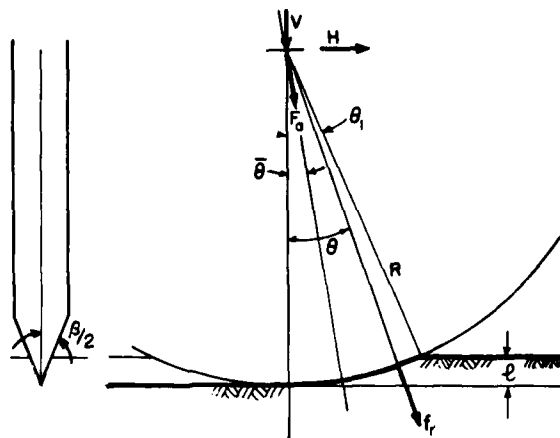


Figure 51. Rolling disc with a tapered rim.

The resultant force on the axle F_a is

$$F_a = \sqrt{H^2 + V^2} = 2 C_1 w R \sigma_c \sin(\theta_1/2) = C_1 w \sigma_c \sqrt{2lR} \quad (99)$$

and the inclination of F_a from the normal direction is given by

$$\frac{H}{V} = \frac{1 - \cos \theta_1}{\sin \theta_1} = \tan(\theta_1/2). \quad (100)$$

In summary, simple theoretical considerations for continuous cutting by a disc of uniform thickness lead to the expectation that: 1) H will be proportional to l and independent of R , 2) V will be approximately proportional to \sqrt{l} and to \sqrt{R} , 3) F_a will be proportional to \sqrt{l} and to \sqrt{R} , and 4) F_a will be inclined at angle $(\theta_1/2)$ from the normal direction.

Dynamics of a taper-edge disc cutter

The preceding item deals with continuous cutting by a disc of uniform width; the next step is to consider a disc which has its edge tapered in a wedge-shaped cross section, as shown in Figure 51. The half-angle of the edge is $\beta/2$, the radius to the tip is R , and the constant penetration depth is l . Position on the cutting section of the rim is defined by an angle θ from the normal direction, and the point of entry into the material is at angle θ_1 . The resultant axle force F_a is resolved into components H and V as before, and the bearing is again assumed to be frictionless. Thus there is only a radial component of force f_r exerted by each elementary segment of the rim. The penetration path is cycloidal, with distances and angles defined by eq 86-92 of the preceding article.

According to theories outlined earlier for simple indenters, penetration resistance for a two-dimensional wedge ought to increase linearly with the depth of penetration as a consequence of the increase of bearing area. Thus it might be postulated that the penetration resistance f_r for each elementary segment of the rim of a disc cutter is

$$f_r = C_2 h \sigma_c \quad (101)$$

where C_1 is a dimensionless constant determined by the wedge angle β and the failure criterion of the material, h is the effective penetration depth, and σ_c is the uniaxial compressive strength of the

material. If h is taken as approximately equal to distance along the cycloidal penetration path s' , then

$$h \approx 4R [\cos(\theta/2) - \cos(\theta_1/2)]. \quad (102)$$

Resolution parallel to the material surface gives

$$\begin{aligned} H &= - \int_{\theta_1}^0 f_r \sin \theta R d\theta \\ &= -4C_2 R^2 \sigma_c \int_{\theta_1}^0 \sin \theta [\cos(\theta/2) - \cos(\theta_1/2)] d\theta \\ &= -4C_2 R^2 \sigma_c \left[-\frac{4}{3} \cos^3(\theta/2) + \cos \theta \cos(\theta_1/2) \right]_{\theta_1}^0 \\ &= -4C_2 R^2 \sigma_c \left\{ -\frac{4}{3} + \frac{\ell}{R} \left(1 - \frac{\ell}{2R}\right)^{1/2} + \frac{4}{3} \left(1 - \frac{\ell}{2R}\right)^{1/2} \right\} \\ &\approx 2C_2 R^2 \sigma_c \left\{ \left(\frac{\ell}{2R}\right)^2 + \frac{1}{3} \left(\frac{\ell}{2R}\right)^3 \right\}. \end{aligned} \quad (103)$$

The approximation in the last line arises from the series expansion of the previous line with powers of $(\ell/2R)$ greater than the third neglected. Since $(\ell/2R)$ is likely to be very small for a practical disc cutter, it is probably sufficient to take the approximation

$$H \approx 2C_2 R^2 (\ell/2R)^2 \sigma_c \approx \frac{1}{2} C_2 \ell^2 \sigma_c \quad (104)$$

which assumes that $(\ell/6R) \ll 1$.

Resolution normal to the material surface gives

$$\begin{aligned} V &= - \int_{\theta_1}^0 f_r \cos \theta R d\theta \\ &= -4C_2 R^2 \sigma_c \int_{\theta_1}^0 \cos \theta [\cos(\theta/2) - \cos(\theta_1/2)] d\theta \\ &= -4C_2 R^2 \sigma_c \left[2 \sin(\theta/2) - \frac{4}{3} \sin^3(\theta/2) - \cos(\theta_1/2) \sin \theta \right]_{\theta_1}^0 \\ &= -4C_2 R^2 \sigma_c \left\{ -\frac{1}{3\sqrt{2}} (1 - \cos \theta_1)^{1/2} \right\} \\ &= -4C_2 R^2 \sigma_c \left\{ -\frac{1}{3\sqrt{2}} \left(\frac{\ell}{R}\right)^{1/2} \right\} \\ &= \frac{2\sqrt{2}}{3} C_2 \sigma_c R^{1/2} \ell^{1/2}. \end{aligned} \quad (105)$$

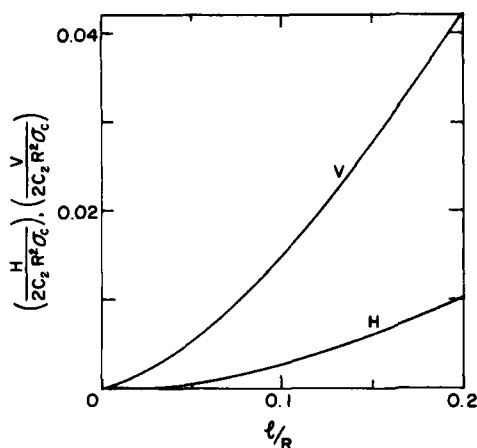


Figure 52. Variation of axle forces with penetration for a taper-edge disc.

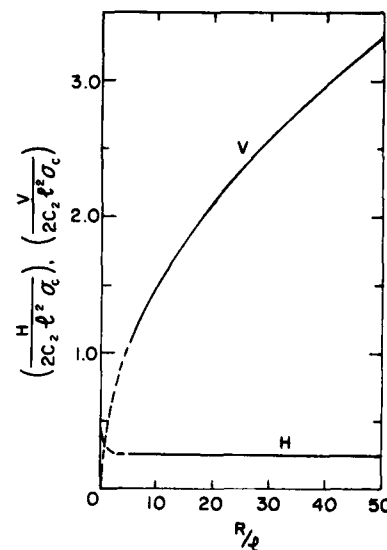


Figure 53. Variation of axle forces with disc radius for a taper-edge disc.

The relationships given by eq 103 and 105 are shown graphically in Figures 52 and 53.

The resultant force on the axle F_a is

$$F_a = \sqrt{H^2 + V^2} \approx \frac{2\sqrt{2}}{3} C_2 \sigma_c R^{1/2} l^{3/2} \left[1 + \frac{9}{16} \left(\frac{l}{R} \right) \right]^{1/2}. \quad (106)$$

For many practical purposes the second term of the radical can be neglected, in which case $F_a \approx V$.

The angle between the direction of F_a and the normal direction, $\bar{\theta}$, is given by $\tan^{-1}(H/V)$. Taking the approximation for H ,

$$\tan \bar{\theta} = \frac{H}{V} = \frac{3}{4} \left(\frac{l}{2R} \right)^{1/2} = \frac{3}{4} \sin(\theta_1/2). \quad (107)$$

In cases where the angle $(\theta/2)$ is very small, $\bar{\theta} \approx (3/8)\theta_1$.

Summing up these results, the indications are that: 1) H will be proportional to l^2 and independent of R , 2) V will be proportional to $l^{3/2}$ and to \sqrt{R} , 3) F_a will be approximately proportional to V , and 4) F_a will be inclined to the normal direction at an angle whose tangent is $(3/4) \sin(\theta_1/2)$.

Dynamics of a taper-edge disc with bearing friction

The preceding articles deal with disc cutters whose axle bearings are frictionless, so that the net tangential force at the rim is zero. When there is finite friction in the bearing, there must be a net tangential force at the rim in order to rotate the disc against the torque resistance of the bearing.

The system of forces acting on the axle of the disc can be expressed as a radial force F_a passing through the center, plus a moment M_B about the center of the axle (Fig. 54). F_a can be resolved into components H and V in directions parallel and normal to the material surface. The moment M_B is determined by the radial force F_a and the effective friction coefficient for the bearing μ_B . In the case of a journal bearing, μ_B is defined such that

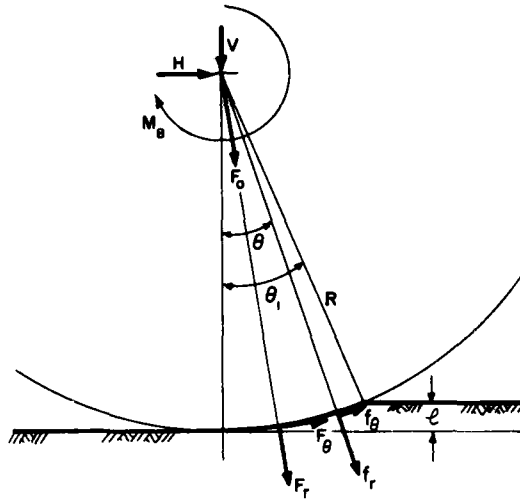


Figure 54. Taper-edge disc with bearing friction.

$$M_B = \mu_B F_a r \quad (108)$$

where r is the radius of the shaft or journal.

The cutting force applied to the material by an elementary segment of the rim can be resolved into a radial component f_r and a tangential component f_θ . When these are integrated with respect to θ between 0 and θ_1 , they give a resultant cutting force F_c which has radial and tangential components F_r and F_θ . Considering the equilibrium of the disc,

$$F_r = F_a \quad (109)$$

$$F_\theta = M_B/R = \mu_B F_a (r/R). \quad (110)$$

If the bearing friction is extremely high, the interfacial friction between the disc and the material it is cutting may be insufficient to give a high enough value of F_θ . Under these circumstances the disc will stop rolling and simply skid along, acting as a drag bit cutter with strong negative rake. If the interfacial friction coefficient between the disc and the material is μ_1 , a restriction is set by

$$F_\theta < \mu_1 F_r \quad (111)$$

or

$$\mu_B (r/R) < \mu_1. \quad (112)$$

When the tangential component of cutting force f_θ is included in the integrals that give H and V , following the general approach outlined for the frictionless cases, the results turn out to be relatively complicated. It is therefore worth considering whether bearing friction has any significant effect.

For good journal bearings, μ_B is commonly less than 0.01, and even with heavily loaded bearings, or bearings going through the start-up stage at low rotational speeds, it is not likely to be over 0.1. For typical disc cutters, the ratio (r/R) might be of the order of 0.1. Thus F_θ/F_r is not likely to exceed 0.01 with a bearing that is in good condition, and it could easily be an order of magnitude lower

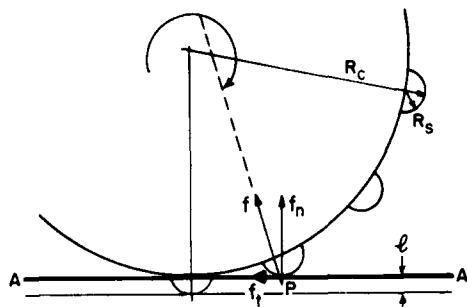


Figure 55. Rolling disc with peripheral studs.

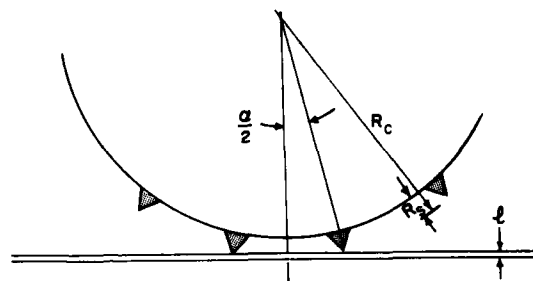


Figure 56. Minimum penetration for positive operation of a studded disc.

during normal operation at full rpm. Thus the effect of bearing friction can safely be neglected for analyses of design and operation parameters. Similarly, the condition for skidding of a disc, as given by eq 112, is not likely to be achieved unless there is complete failure of the bearing.

It seems reasonable to conclude that the foregoing analyses for frictionless bearings remain valid for frictional bearings of typical design.

Action of a studded disc

An alternative to the taper-edge disc is a disc whose rim is armed with hard studs, usually of tungsten carbide, or with wedge-shaped teeth. The studs are typically hemispheric projections or conical projections with rounded tips. As the disc is rolled along the surface of the material, studs or teeth descend successively with the action of three-dimensional indenters.

There are obviously some practical limits set by the size and spacing of studs. As was mentioned in an earlier report of this series (Part II, p. 30), the maximum penetration depth l cannot usefully exceed the length by which the stud projects from the rim of the disc; otherwise, the whole rim of the disc has to be thrust into the work. Another limit for a single disc is set by the necessity of having at least one stud always in the work.* Since this consideration was omitted from Part II, it will be included here.

Looking at the studded disc in Figure 55, it is clear that under some circumstances the force f developed between the stud and the material at the initial contact point P could tend to oppose the rolling motion unless there is a high coefficient of interfacial friction at P . In order for that stud to begin its penetration, it might well need tangential reaction from a stud that is already in the work. There obviously could be operating difficulties if two adjacent studs are able to lie above the line AA' at the same time, as shown in Figure 56. With N studs set at equal intervals around the rim of the disc, the angular spacing α between the studs is $2\pi/N$. If the disc is rigidly mounted for cutting to constant depth l , the condition to guarantee that at least one stud will always be below the surface level is

$$l > R_c(1 - \cos \alpha/2) \quad (113)$$

or

$$l > R_c[1 - \cos(\pi/N)] \quad (114)$$

where R_c is the radius to the tip of the stud. Conical studs[†] are considered here for simplicity of illustration—the geometry for hemispheric studs is more complicated. To provide a positive guarantee that there will always be at least one stud in the work and under stress, the relative stud spacing

* This restriction does not necessarily apply for multiple discs fixed on a common axle.

† The same geometry applies to gear-tooth cutters.

has to be *half* that given by eq 113-114, since a new stud has to be entering the work before the preceding one departs from the point of maximum penetration, i.e.

$$l > R_c(1 - \cos\alpha) \quad (115)$$

or

$$l > R_c[1 - \cos(2\pi/N)]. \quad (116)$$

In practice there are factors which allow a studded disc to operate even when the above conditions are not met. A rough rock surface will catch the studs and rotate the disc, the disc itself may have low enough bearing friction and high enough inertia to give it a flywheel effect, and the mounting of the disc may be compliant (i.e. "springy"). Nevertheless, it is probably prudent to design and operate so that: 1) the chipping depth is less than the projecting length of the stud, and 2) there is always at least one stud in the work and under load. This means that under normal operation conditions,

$$R_s > l > R_c[1 - \cos(2\pi/N)]. \quad (117)$$

The spacing of studs around the perimeter of a disc ought to be determined, at least in part, by the requirements for efficient indexing, i.e. by optimum interference effects between adjacent craters. However, this distance varies with the penetration depth l , and an upper limit to N may be set by the practical matter of putting studs into the rim and maintaining adequate structural support for them. For hemispheric buttons and 90° cones the base diameter is $2R_s$, while for sharp 60° cones it is R_s . In general, we can express the base diameter of the stud as $k_1 R_s$ and the spacing between studs as $k_2 R_s$, so that the number of studs N is the integer given by

$$N = \frac{2\pi(R_c - R_s)}{(k_1 + k_2)R_s} = \frac{2\pi}{(k_1 + k_2)} [(R_c/R_s) - 1]. \quad (118)$$

For typical studded rock-cutting discs, (R_c/R_s) is typically around 10 to 30, $k_1 \approx 2$, and k_2 might range from about 1.5 to 6. The final values of N might range from around 16 to more than 40. On typical milled-tooth cutters the projections are wedges, or truncated wedges. (R_c/R_s) is relatively small (3 to 6), $k_1 \approx 1$, $k_2 \approx 0$, and N is about 12 to 30.

From these considerations it can be seen that an ideal studded disc is not likely to have more than one stud in action at a time. For example, if $R_c/R_s = 15$ and $N = 18$, it is found from eq 117 that $l/R_s = 0.9$ for a minimum of one stud under load. Thus a realistic analysis of the action of a studded disc has to treat the case where there is only one stud at a time operating, with consequent fluctuation of axle forces in both magnitude and direction.

If the thrust capability is limited, to the extent that sharing of loads between two or more operative studs is undesirable, then there is an additional condition that tends to conflict with the foregoing ones:

$$l > R_c[1 - \cos(2\pi/N)]. \quad (119)$$

Thus it may be that the optimum operating condition for a single studded disc is

$$(l/R_c) \approx 1 - \cos(2\pi/N). \quad (120)$$

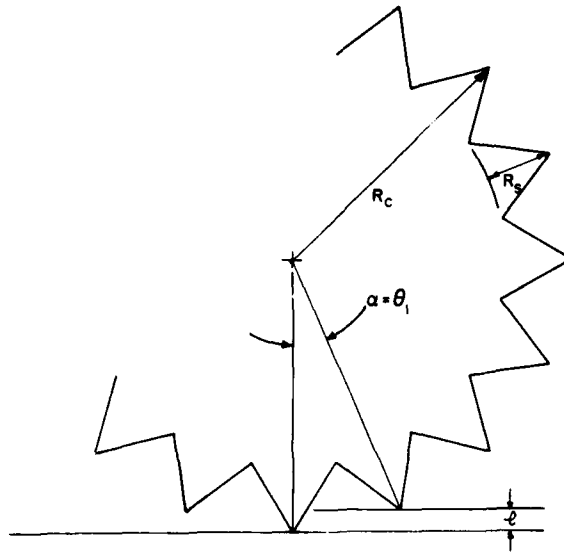


Figure 57. Geometry of a toothed cutter.

Because of the variability of rock properties, this may not be a realistic condition to impose. However, the problem tends to disappear when two or more discs are set on a single axle with their stud positions staggered. The main practical concern is to recognize what is going on, so that a machine is not operated inappropriately, either when there is a generous reserve of thrust available in soft rock, or when the machine is at the limit of its thrust capability in very hard rock.

Action of a toothed cutter

The diagrams for a disc with conical studs (Fig. 56 and 59) are not essentially different from the diagram for a cutter with wedge-shaped teeth (Fig. 57). Thus the limiting penetration for independent action by one tooth at a time has already been given by eq 115 and 116, i.e.

$$(\ell/R_c)_* = 1 - \cos \alpha = 1 - \cos(2\pi/N). \quad (121)$$

This condition differs from the one derived by Teale (1964) and endorsed by Roxborough and Rispin (1972, 1973). The Teale equation, which can be written in the symbols used here as

$$\begin{aligned} (\ell/R_c)_* &= \cos(\alpha/2) - \cos(3\alpha/2) \\ &= \cos(\pi/N) - \cos(3\pi/N), \end{aligned} \quad (122)$$

is not strictly correct for a rigidly mounted roller cutter, since it implies that the axle of the cutter will move up and down relative to the work piece.

The significance of the limiting penetration for operation of one tooth at a time is that the normal force is likely to increase disproportionately when more than one tooth is acting at any given time.

Another consideration is that the cutting teeth should not "bottom out," as they would with $\ell > R_s$ (Fig. 58 and 59). In reality, cutter teeth can become clogged with fragmented material at

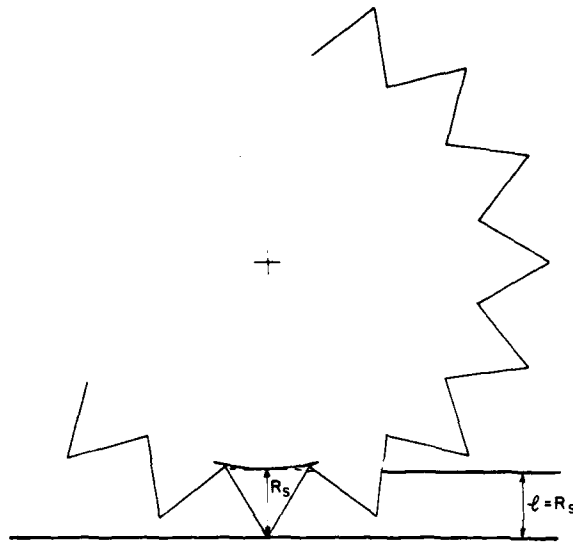


Figure 58. Maximum penetration of a toothed cutter before "bottoming-out" occurs.

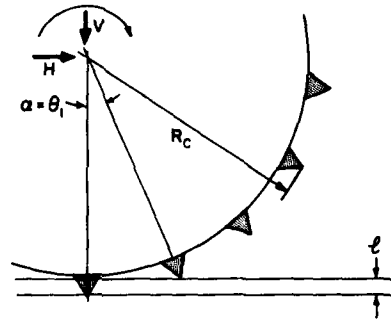


Figure 59. Forces on a studded disc.

penetrations significantly less than R_c in some kinds of rock. When this happens, normal force on the cutter axle can be expected to increase abruptly.

Forces on a studded disc

In theory, a smooth-rim disc is capable of constant-force operation (ignoring intermittent formation of chips in brittle material). By contrast, a disc with studs on its rim necessarily experiences force fluctuations as the separate studs penetrate and disengage. For a typical stud, penetration resistance ought to increase as penetration distance increases, reaching a maximum as it passes under the lowest point of the disc. If a second stud enters the work while the preceding one is still operating, there should be an immediate jump in the axle force of the disc.

Since a studded rock-cutting disc is quite likely to have only one stud at a time under high load, the forces developed by a single cycle of stud indentation are of direct significance. If more than one stud is working at a given time, the forces on the wheel can be obtained by appropriate summation if the material is ductile, or if the studs are widely spaced ($R_c \alpha$ significantly greater than l).

Consider the cutter shown in Figure 59. The studs are shown as sharp cones to simplify the geometry of the problem. Each stud enters the work at a position defined by the angle θ_1 , which for the case shown equals the angular space between studs α . As the disc rotates, the tip of the stud descends to depth l along a cycloidal path whose geometry was described earlier. As the stud descends, it also rotates, turning through angle θ_1 in descending to depth l .

Plastic penetration of a cone along a curved path is difficult to analyze rigorously, especially when interfacial friction is taken into account. However, for present purposes it is probably permissible to assume that penetration resistance develops a force which acts radially through the stud and the disc, since there is no indication that a cutter would cease to work with a frictionless axle bearing. This assumption implies that the pattern of plastic yielding is able to equilibrate the stresses so as to produce a radial resultant force.

According to the theory for plastic indentation, the penetration resistance for a cone ought to increase in proportion to the square of the penetration depth:

$$F_r = C_3 h^2 \sigma_c \quad (123)$$

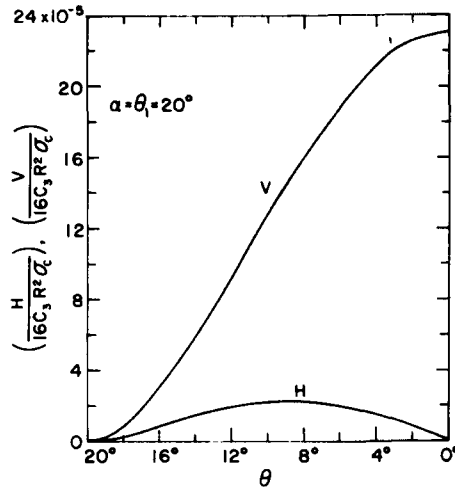


Figure 60. Illustration of variation of axle forces on a studed disc when the action is limited to penetration of one stud at a time.

where F_r is penetration resistance, h is penetration depth, σ_c is the uniaxial compressive strength of the material, and C_3 is a dimensionless constant determined by the cone angle, the failure criterion of the material, and the interfacial friction. If h is taken as approximately equal to s' , as in eq 102, then F_r is

$$F_r = 16 C_3 R_c^2 [\cos(\theta/2) - \cos(\theta_1/2)]^2 \sigma_c. \quad (124)$$

With only one stud operating at a given time, the axle force is simply F_r , and its components H and V are:

$$H = F_r \sin \theta = 16 C_3 R_c^2 \sigma_c \sin \theta [\cos(\theta/2) - \cos(\theta_1/2)]^2 \quad (125)$$

$$V = F_r \cos \theta = 16 C_3 R_c^2 \sigma_c \cos \theta [\cos(\theta/2) - \cos(\theta_1/2)]^2. \quad (126)$$

In Figure 60 the variation of H and V with θ is illustrated for one cycle of stud indentation when $\theta_1 = \alpha = 20^\circ$. The horizontal force H increases from zero at the stud's entry to a maximum at a point roughly halfway through the working stroke; it then declines back to zero at the point of maximum penetration. The vertical force V increases throughout the working stroke, from zero at the stud's point of entry to a maximum at the point of deepest penetration. The resultant axle force F_r is almost identical to V in magnitude (in Fig. 60, the curve for F_r lies fractionally above the curve for V , but the separation is too small to distinguish at the scale of Fig. 60).

The maximum depth of penetration normal to the surface ℓ is reached when $\theta = 0$ and the relation between ℓ and θ is

$$\ell = R_c (1 - \cos \theta_1) = 2 R_c [1 - \cos^2(\theta_1/2)]. \quad (127)$$

Thus,

$$\cos(\theta_1/2) = \pm (1 - \ell/2R_c)^{1/2} \quad (128)$$

and since $\ell/2R_c \ll 1$

$$\cos(\theta_1/2) \approx \pm(1 - \ell/4R_c) \quad (129)$$

and the positive root is the required value (the same result is obtained by substituting $\theta = 0$ in eq 102).

The maximum value of F_r is reached when $\theta = 0$, i.e. when the stud has penetrated to depth ℓ :

$$(F_r)_{\max} = 16C_3R_c^2\sigma_c[1 - \cos(\theta_1/2)]^2 \quad (130)$$

or, substituting for $\cos(\theta_1/2)$ from eq 129,

$$\begin{aligned} (F_r)_{\max} &= 16C_3R_c^2\sigma_c[1 - (1 - \ell/4R_c)]^2 \\ &= C_3\sigma_c\ell^2 \end{aligned} \quad (131)$$

which is also the maximum value of the normal force component V . In other words, the maximum value of V is proportional to ℓ^2 , and independent of R_c .

Forces on a wheel with wedge-shaped teeth

A simple analysis for the penetration of a single tooth on a gear-type cutter can be made along the same lines as the foregoing stud analysis, provided that maximum penetration depth is less than the projecting length of the tooth.

The penetration resistance of a two-dimensional wedge in a plastic material ought to be directly proportional to the penetration depth h . Neglecting end-effect complications, the normal force F_r for a "wide" wedge of width b ($h \ll b$) might therefore be written as

$$F_r = C_4hb\sigma_c \quad (132)$$

where C_4 is a dimensionless constant determined by the wedge angle, the failure criterion of the material, and the interface friction. Following the procedure adopted in the previous section for the derivation of eq 124, i.e. assuming $h \approx s'$ as in eq 102, then the force F_r for a cutter at position θ after entry at θ_1 is

$$F_r = 4C_4R_cb\sigma_c[\cos(\theta/2) - \cos(\theta_1/2)]. \quad (133)$$

With only one tooth operating at any time, the total axle force is F_r , which resolves into the horizontal and normal components H and V as:

$$H = F_r \sin \theta = 4C_4R_cb\sigma_c \sin \theta [\cos(\theta/2) - \cos(\theta_1/2)] \quad (134)$$

$$V = F_r \cos \theta = 4C_4R_cb\sigma_c \cos \theta [\cos(\theta/2) - \cos(\theta_1/2)]. \quad (135)$$

In Figure 61 the variation of H and V with θ is illustrated for one cycle of tooth indentation when $\theta_1 = 20^\circ$. This permits a direct comparison with the calculated behavior of a studded disc, shown in Figure 60. The overall trend is not very much different, although the toothed cutter has a more rapid initial buildup of force.

A rough idea of force fluctuations for multiple tooth operation can be gained by appropriate superposition of graphs like Figure 61, but in reality the situation is complicated by tooth interactions in brittle material. When the cutter has a large number of teeth, the behavior ought to tend towards that of a simple disc cutter with uniform width (Fig. 47).

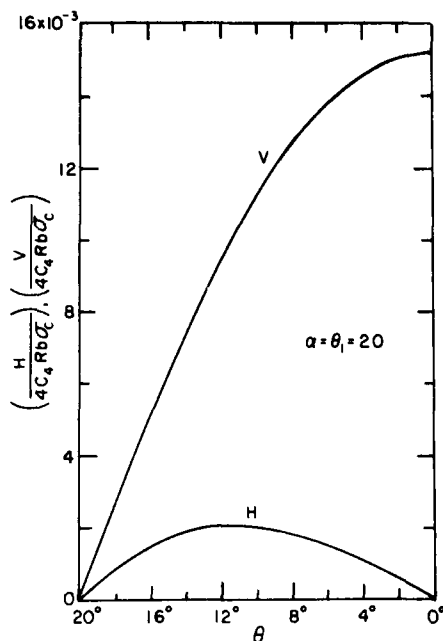


Figure 61. Illustration of variation of axle forces on a cutter with wedge-shaped teeth when the action is limited to penetration of one tooth at a time (cf. Fig. 60).

The maximum value of F_r , reached when θ is zero and the tooth has penetrated to depth ℓ , is

$$(F_r)_{\max} = 4C_4 R_c b \sigma_c [1 - \cos(\theta_1/2)] \quad (136)$$

or, substituting for $\cos(\theta_1/2)$ from eq 129,

$$\begin{aligned} (F_r)_{\max} &= 4C_4 R_c b \sigma_c \left[1 - \left[1 - (\ell/4R_c) \right] \right] \\ &= C_4 b \sigma_c \ell = V_{\max}. \end{aligned} \quad (137)$$

Thus with single-tooth operation the maximum value of F_r , or V , is directly proportional to ℓ , independent of R_c , and proportional to the tooth width b .

Energetics of disc cutters

If a disc cutter is operating with constant depth of penetration ℓ , the force component V does not move through any finite distance, and therefore the work done in moving the cutter a distance X is determined solely by the horizontal force component H and the distance X . If H does not vary with time and distance and there is negligible friction in the bearing, then the work done W_X is

$$W_X = \int_0^X H dx = HX. \quad (138)$$

The power P_c needed to operate the cutter at constant horizontal speed U is

$$P_c = HU. \quad (139)$$

The volume of material that is broken by the cutter in traveling a distance X is the average cross-sectional area of the groove multiplied by X . If the cross section of the groove is approximated as a triangle with constant depth ℓ , the cross-sectional area A_g is

$$A_g = \ell^2 \tan \phi \quad (140)$$

where ϕ is the apex half-angle of the triangular groove. If the cutter has a tapered edge of half-angle β , the minimum value for ϕ in eq 140 is β . If the groove has an apex half-angle greater than β , that angle is sometimes referred to as the "overbreak angle" ϕ_r (see Parts I and II).

The specific energy E_s for a disc cutter is the work W needed to break a volume V , or alternatively the power P_c needed to break material at a volumetric rate \dot{V} . With the assumptions made here,

$$E_s = \frac{W}{V} = \frac{P_c}{\dot{V}} = \frac{H}{A_g} = \frac{H}{\ell^2 \tan \phi} \quad (141)$$

Taking the approximate value of H for a taper-edge cutter, as given by eq 104, the specific energy becomes

$$E_s \approx \frac{C_2 \sigma_c}{2 \tan \phi} \quad (142)$$

In this expression, C_2 is a dimensionless constant determined by the cutter angle β and by the failure criterion of the material (see eq 101). Following the ideas outlined during the discussion of cutting principles, C_2 can also be expressed in the form $C_2 = 2A \tan \beta$, where the constant A covers only secondary effects brought on by the wedge angle β (plus effects of the failure criterion). The approximation in eq 142 is taken to be acceptable for the condition $(\ell/6R) \ll 1$.

Inspection of eq 142 shows that there is no *explicit* dependence of E_s upon ℓ or R . In other words it appears to predict that specific energy will not vary with cutting depth or cutter radius. However, this interpretation makes no allowance for implicit dependencies, i.e. for variations of σ_c and ϕ with ℓ . In general, σ_c can be expected to decrease as the volume of stressed material increases. Furthermore, the size of the "crushing zone" under the tip of the cutter is not likely to increase in proportion to ℓ , and ϕ may vary systematically with ℓ .

Energetics of a studded disc

The penetration force of a conical indenter was taken earlier (eq 123) as

$$F = C_3 h^2 \sigma_c \quad (143)$$

where h is the penetration depth, C_3 is a constant for a given material and a given type of indenter, and σ_c is the uniaxial compressive strength of the material. With penetration resistance of this form, the work done in thrusting to depth ℓ is

$$\begin{aligned} W &= \int_0^\ell C_3 h^2 \sigma_c dh \\ &= \frac{1}{3} C_3 \sigma_c \ell^3 \end{aligned} \quad (144)$$

or, since

$$F_{\max} = C_3 \sigma_c \ell^2 \quad (145)$$

$$W = \frac{1}{3} F_{\max} \ell. \quad (146)$$

If the conical indenter is a stud on a disc whose radius is large relative to ℓ , then the work done for indentation of one stud to depth ℓ should be approximately the same, i.e.

$$W_1 \approx \frac{1}{3} (F_r)_{\max} \ell \approx \frac{1}{3} V_{\max} \ell. \quad (147)$$

However, energy is usually supplied to a studded disc by doing work parallel to the indentation surface, i.e. by moving the axle force H through a distance x . Thus the work required for complete indentation of one stud is

$$W_1 = \int_0^{x=R_c \theta_1} H dx \quad (148)$$

where R_c is the radius to the stud tip and θ_1 is the entry angle (Fig. 59). Substituting for H from eq 125 and integrating with respect to θ instead of x

$$\begin{aligned} W_1 &= - \int_{\theta_1}^0 H R_c d\theta \\ &= 16 C_3 R_c^3 \sigma_c \int_0^{\theta_1} \sin \theta [\cos(\theta/2) - \cos(\theta_1/2)]^2 d\theta \\ &= 16 C_3 R_c^3 \sigma_c [-\cos^4(\theta/2) + \frac{8}{3} \cos(\theta_1/2) \cos^3(\theta/2) - 2 \cos^2(\theta_1/2) \cos^2(\theta/2)]_0^{\theta_1} \\ &= 16 C_3 R_c^3 \sigma_c \left[-\frac{1}{3} \cos^4(\theta_1/2) + 2 \cos^2(\theta_1/2) - \frac{8}{3} \cos(\theta_1/2) + 1 \right]. \end{aligned} \quad (149)$$

Making the substitution $\cos(\theta_1/2) \approx [1 - (\ell/4R_c)]$ from eq 129:

$$W_1 = 16 C_3 R_c^3 \sigma_c \left[\frac{4}{3} (\ell/4R_c)^3 - \frac{1}{3} (\ell/4R_c)^4 \right] \quad (150)$$

and neglecting the second term because $(\ell/4R_c) \ll 1$:

$$\begin{aligned} W_1 &\approx \frac{1}{3} C_3 \sigma_c \ell^3 \\ &\approx \frac{1}{3} V_{\max} \ell \end{aligned} \quad (151)$$

which is the same result obtained earlier in eq 144 and 147.

The stud makes a crater that is roughly conical, and if it is assumed that the crater shape keeps the same form when penetration depth ℓ increases (geometric similarity), then the crater volume V_c can be written as

$$V_c = K \ell^3 \quad (152)$$

where K is a constant or a "shape factor."

The specific energy E_s for indentation by a single stud is the work input divided by the volume of material broken, i.e.

$$E_s = \frac{W_1}{V_c} = \frac{1/3 C_3 \sigma_c \ell^3}{K \ell^3} = A \quad (153)$$

where A is a constant for a given material and a given type of indenter. In other words, this simple argument predicts that E_s will not vary with penetration depth.

Energetics of a tooth cutter

For the indentation of a single tooth to a penetration depth ℓ , the work done W_1 is given approximately by the work needed to thrust a wedge to depth ℓ . If the force on the wedge is of the form given in eq 132, i.e.

$$F = C_4 h b \sigma_c \quad (154)$$

then the work done to drive to a total depth of $h = \ell$ is

$$W_1 = \int_0^\ell C_4 h b \sigma_c dh = \frac{1}{2} C_4 b \sigma_c \ell^2 \quad (155)$$

or, since

$$F_{\max} = C_4 b \sigma_c \ell \quad (156)$$

$$W_1 = \frac{1}{2} F_{\max} \ell. \quad (157)$$

When the same wedge is a tooth on a roller, the external work is usually performed by moving the horizontal component of axle force through a distance $R_c \theta_1$, where R_c is the radius to the tooth tip and θ_1 is the entry angle measured "backwards" from the normal (Fig. 57). Thus

$$W_1 = \int_0^{x=R_c \theta_1} H dx \quad (158)$$

or, since $dx = -R_c d\theta$,

$$W_1 = - \int_{\theta_1}^0 H R_c d\theta. \quad (159)$$

Taking H as a function of θ from eq 134

$$\begin{aligned} W_1 &= 4 C_4 R_c^2 b \sigma_c \int_0^{\theta_1} \sin \theta [\cos(\theta/2) - \cos(\theta_1/2)] d\theta \\ &= 4 C_4 R_c^2 b \sigma_c \left[-\frac{4}{3} \cos^3(\theta/2) + \cos(\theta_1/2) \cos \theta \right]_0^{\theta_1} \\ &= 4 C_4 R_c^2 b \sigma_c \left[\frac{2}{3} \cos^3(\theta_1/2) - 2 \cos(\theta_1/2) + \frac{4}{3} \right]. \end{aligned} \quad (160)$$

Substituting for $\cos(\theta_1/2)$ from eq 129 and expanding the \cos^3 term:

$$\begin{aligned} W_1 &= 4C_4 R_c^2 b \sigma_c \left[\frac{2}{3} \left[1 - \frac{3\ell}{4R_c} + 3\left(\frac{\ell}{4R_c}\right)^2 - \left(\frac{\ell}{4R_c}\right)^3 - 2\left(1 - \frac{\ell}{4R_c} + \frac{4}{3}\right) \right] \right] \\ &= 4C_4 R_c^2 b \sigma_c \left[2\left(\frac{\ell}{4R_c}\right)^2 - \frac{2}{3}\left(\frac{\ell}{4R_c}\right)^3 \right]. \end{aligned} \quad (161)$$

Since $\ell/4R_c$ is small, eq 161 can be approximated by dropping the second term, so that

$$W_1 = \frac{1}{2} C_4 b \sigma_c \ell^2 \quad (162)$$

or

$$W_1 = \frac{1}{2} V_{\max} \ell = \frac{1}{2} (F_r)_{\max} \ell. \quad (163)$$

This is the same result as eq 157, obtained from consideration of work in the vertical direction.

The volume of material broken by penetration of a wedge-shaped tooth can be assumed to be that of a wedge-shaped crater, which in general will be bigger than the volume of the indenter itself. If the indentation craters are geometrically similar as ℓ varies, then the crater volume V_c can be expressed as

$$V_c = K b \ell^2 \quad (164)$$

where K is a constant, or "shape factor," b is the tooth width, and ℓ is the penetration depth.

The specific energy of the indentation process E_s is thus

$$E_s = \frac{W_1}{V_c} = \frac{\frac{1}{2} C_4 b \sigma_c \ell^2}{K b \ell^2} = A \quad (165)$$

where A is a constant for a given type of material and for given wedge dimensions. This implies that E_s is unaffected by penetration depth.

EXPERIMENTAL DATA FOR DISC CUTTERS

Experimental Investigations

It seems that there are relatively few sources of experimental data for disc cutters and comparable free-rolling devices. In the experiments that have been done, the main objectives have been to determine relationships between cutter forces and rock penetration, and hence to derive data for specific energy and working rates. Experimental variables have included such things as cutter diameter, rim angle, cutting speed, the spacing between adjacent cutting grooves, and the rock type.

Two approaches to experimental design have been adopted by investigators. One involves rolling a cutter along a plane rock surface and measuring the forces and the width of groove. The other attempts to roll the cutter along a plane rock surface with the normal force component held constant, while the depth and width of the groove and the tangential force component are measured. The former is the approach that was used by the Newcastle group directed by Roxborough, while the latter is the approach followed by the U.S. Bureau of Mines group at Minneapolis.

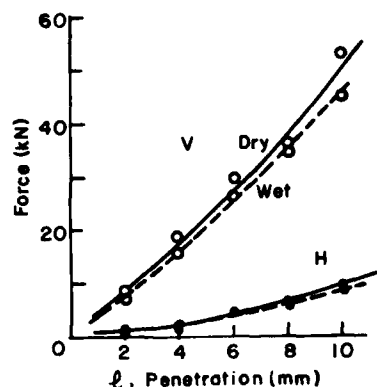


Figure 62. Force components as functions of penetration depth for a disc cutter operating in wet and dry sandstone (Roxborough and Phillips 1975a).

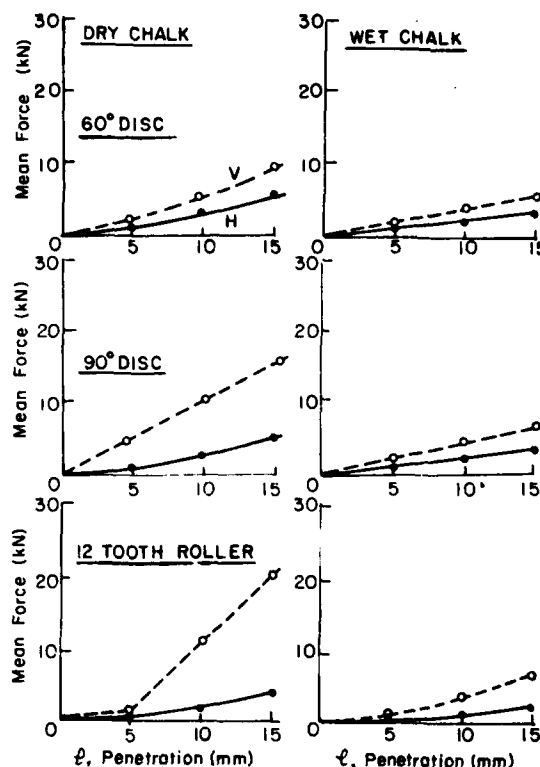


Figure 63. Force components as functions of penetration depth for disc cutters and a tooth cutter operating in wet and dry chalk (Roxborough and Rispin 1973).

When examining experimental data it is well to keep in mind some of the experimental difficulties that exist. First of all, the laboratory equipment used so far has lacked the size, strength and stiffness to handle very big cutters. Secondly, the cutter runs have been fairly short; the cutter travels in a straight line or a circular arc over a fairly small distance, starting from rest and being brought to a stop at the end of the travel. Finally, there are inevitably problems of stiffness and compliance in both the loading mechanism and the force measuring devices. The last point is particularly relevant to tests which attempt to maintain constant force.

Relationships between normal force and penetration

Figures 62 through 68 give data for the relationship between the normal force component V and the penetration ℓ for various rocks and cutter designs. Note that in one group of experiments the imposed variable is mean normal force, while in the other group the penetration is set and held constant; the graphs follow the usual convention of dependent variable plotted as ordinate, so that the two sets of data are plotted differently.

The simple theory outlined in the previous section predicts that V will be proportional to $\ell^{2/3}$ for a taper-edge disc (see eq 20). The trend of some of the experimental results (Fig. 62, 63, 65 and possibly 67) gives qualitative support to this idea. Other results (Fig. 66) are somewhat contradictory, suggesting that V is proportional to ℓ^n , where n is slightly less than unity. Yet other results (Fig. 63, 65) appear to show direct proportionality between V and ℓ . The lines given (without data points) by Phillips and Bilgin (1977) are hard to accept at face value, as they imply finite penetration with zero force.

In view of the uncertainties that attend the interpretation of experimental results, an interim conclusion might be that normal force and penetration are approximately proportional, although the predictions of the simple theory still seem reasonable.

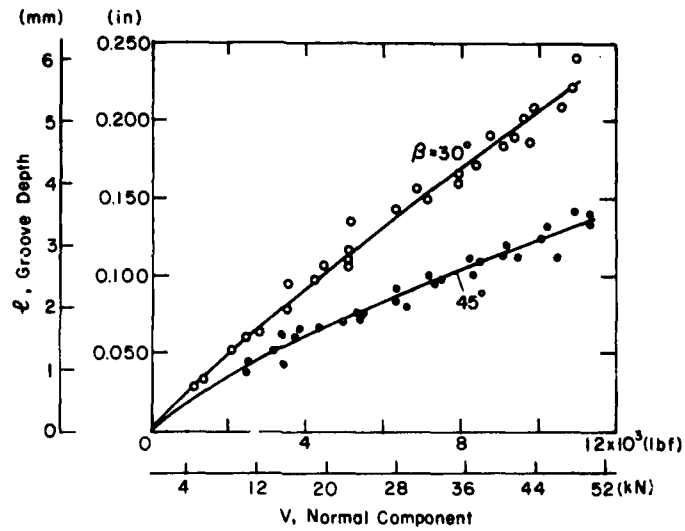


Figure 64. Penetration depth as a function of the normal force component for disc cutters operating in marble (Morrell et al. 1970).

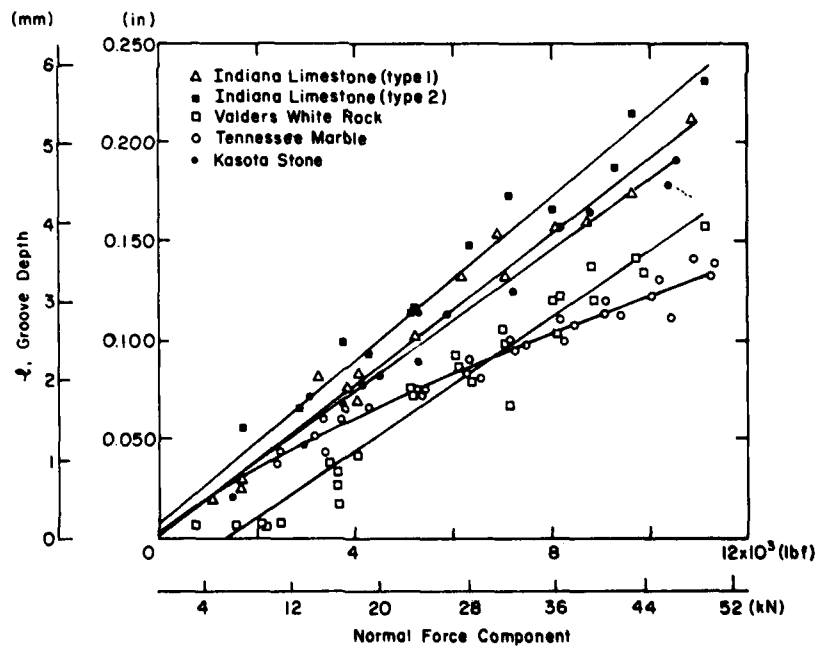


Figure 65. Penetration depth as a function of the normal force component for a disc cutter operating on a variety of rock types (Morrell et al. 1970).

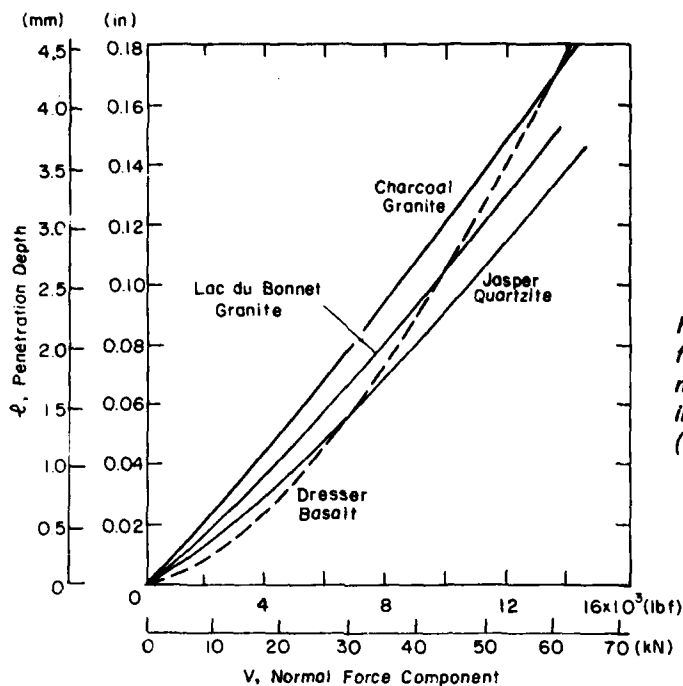


Figure 66. Penetration depth as a function of normal force component for a disc cutter operating in various types of hard rock (Morrell and Larson 1974).

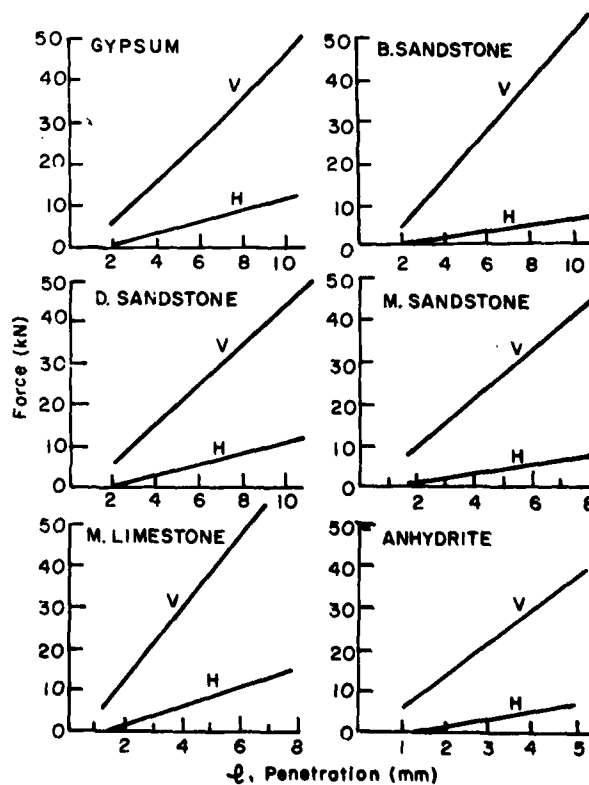


Figure 67. Force components as a function of penetration depth for a disc cutter (150-mm-diam, $\beta = 40^\circ$) operating in different types of rock (Phillips and Bilgin 1977).

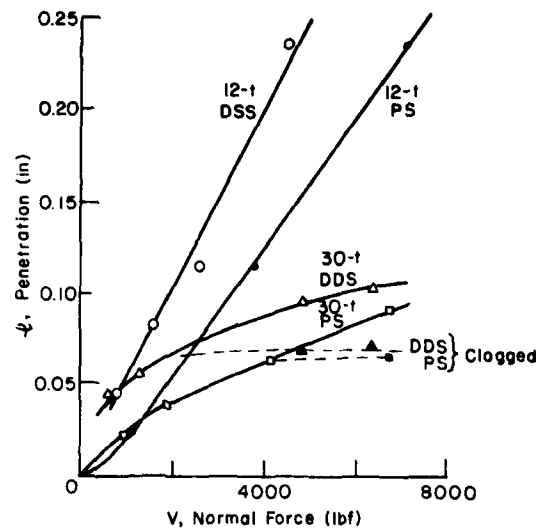


Figure 68. Relationship between normal force and penetration depth for toothed cutters in sandstone (DDS = Darley Dale sandstone, PS = Pennant sandstone) (Teale 1964).

Relationships between tangential force and penetration

The simple theory developed here for taper-edge discs predicts that the tangential force component H will be approximately proportional to ℓ^2 . Some of the experimental results tend to give qualitative support to this idea (Fig. 62, 63 and possibly 67), while others suggest that the relation is not far from linear (Fig. 63). Results by Phillips and Bilgin (1977) do not show data points, but a power relation would seem more reasonable than the straight lines with penetration intercepts that they draw. The Bureau of Mines results (Morrell et al. 1970, Morrell and Larson 1974) do not give H as a function of ℓ directly, but relationships between H and V are developed. These show $H \propto V^n$, where n ranges from 1.7 to 2.1 (Morrell and Larson 1974; see also Fig. 69-71). In other

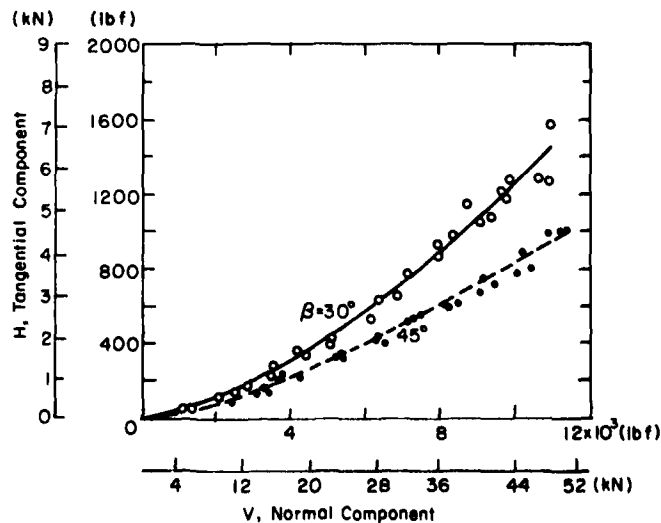


Figure 69. Relationship between tangential and normal force components for disc cutters operating in marble (Morrell et al. 1970).

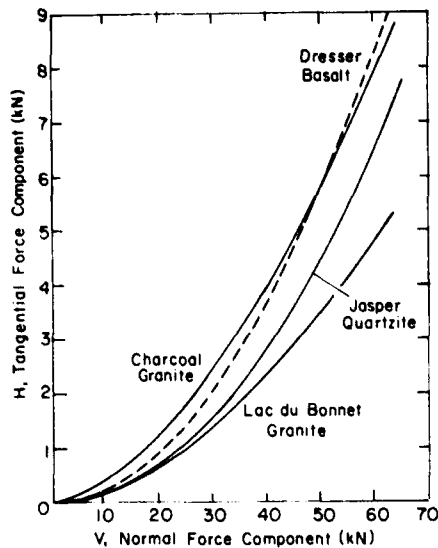


Figure 70. Relationship between tangential and normal force components for a disc cutter operating in different types of rock (Morrell and Larson 1974).

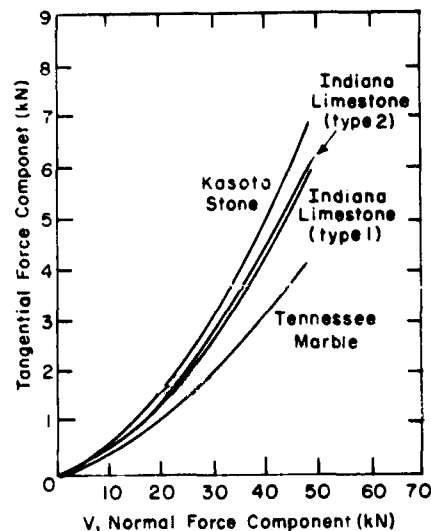


Figure 71. Relationship between tangential and normal force components for a disc cutter operating in various types of rock (Morrell and Larson 1974).

words, according to the Bureau of Mines results, H is approximately proportional to V^2 and, since V itself is approximately proportional to ℓ , this means that H is approximately proportional to ℓ^2 .

The general conclusion here might be that simple theory and existing experimental data are in reasonable accord, showing H proportional to ℓ^2 .

Relationship between force and penetration for tooth cutters

Figures 63 and 68 give force/penetration data for roller cutters with wedge-shaped teeth. The first question is what the data actually mean, since for small penetrations (one tooth at a time in operation) either force or penetration has to fluctuate with time. In the experiments by Teale (1964), an initial normal load was applied by a hydraulic jack, and during the cutting run the signals from the load cell measuring normal force were integrated so as to give a time-averaged value. In the work by Roxborough and Rispin (1972), both mean and peak values of the force components were recorded for fixed penetration depth, but there was surprisingly little difference between the two. However, the smallest penetration depth used for the experiments (5 mm) was only a little less than the "single tooth" critical depth for a perfectly stiff system, as given by eq 121 (7.4 mm), while the highest imposed penetration (18 mm) was more than twice as great as the calculated critical depth for single-tooth operation. The maximum penetration depths reached in this work were comparable with the tooth width (25.4 mm), so that edge effects on the wedge-shaped teeth probably became significant.

In Figure 68 the results for the 12-tooth wheel were all obtained with single-tooth operation, the deepest penetration being about 60% of the critical depth. The data show the time-average value of the normal component V to be directly proportional to the penetration depth ℓ . The simple theory developed earlier (eq 137) predicts proportionality between ℓ and the *maximum* value of V . If there is approximate proportionality between the maximum value of V and the time-averaged value of V , then the experimental data provide some confirmation of the simple theory.

In Teale's (1964) tests with a 30-tooth wheel (Fig. 68), penetrations exceeded the critical depth, so that at least two teeth were operating at the same time. The data for an unclogged wheel show a disproportionately rapid increase of V with ℓ , thus confirming the qualitative expectations. When the same wheel became clogged with cuttings, there were large increases in V without any corresponding increase in ℓ . The data for dry chalk in Figure 63 also show a disproportionate increase in V with more than one tooth in operation, but the effect is not strongly marked in the results for wet chalk.

Effect of cutter radius on cutting forces

The simple theory that is developed here for taper-edge discs predicts that, within the limits of R/ℓ for which the analysis is considered valid, the normal force V will be proportional to the square root of cutter radius R , and the tangential force H will be independent of cutter radius.

The only available data bearing on this point are the results of Roxborough and Phillips (1975a, b) shown in Figure 72, although straight-line representations of data (Fig. 73) are given by Phillips and Bilgin (1977). The theoretical prediction for H is borne out fully, while the data for V could conceivably suggest a relation of the form $V \propto R^n$, where n is less than unity.

The conclusion might be that the simple theory gives useful guidance that will suffice until more complete experimental results become available.

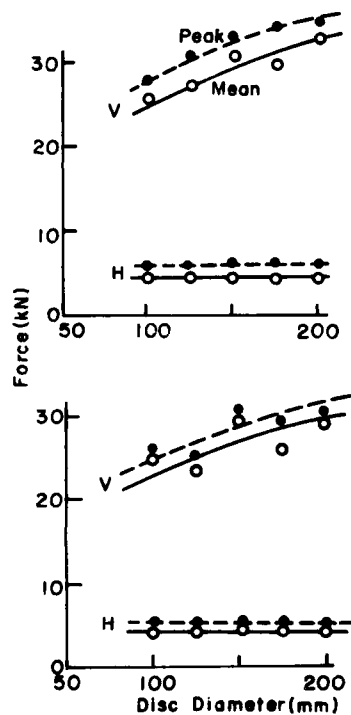


Figure 72. Force components as functions of diameter for disc cutters operating in wet and dry sandstone (Roxborough and Phillips 1975a). V = vertical; H = horizontal.

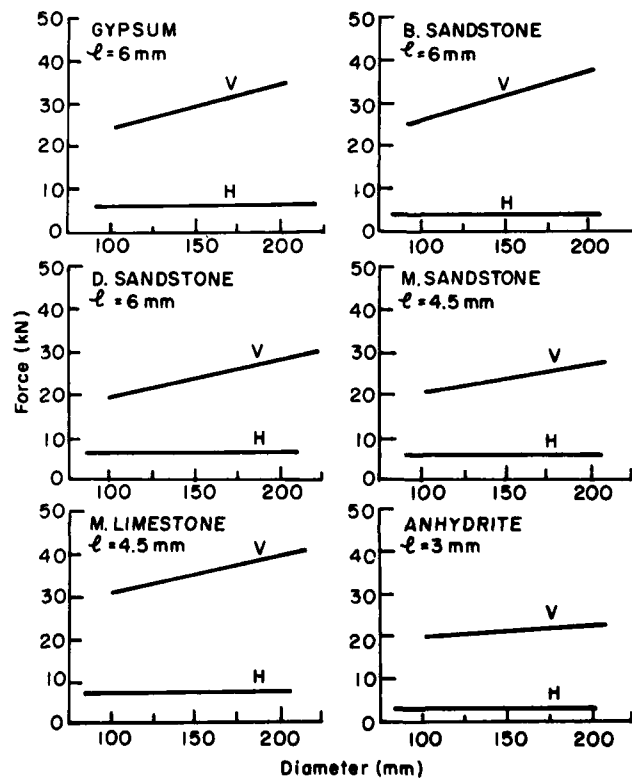


Figure 73. Force components as functions of diameter for disc cutters ($\beta = 40^\circ$) operating in various types of rock (Phillips and Bilgin 1977).

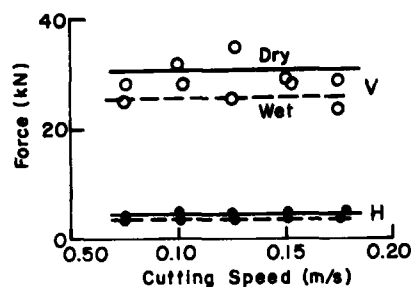


Figure 74. Force components plotted against cutter speed for a disc operating in wet and dry sandstone (Roxborough and Phillips 1975a).

Effect of cutting speed on cutting forces

Roxborough and Phillips (1975a and b) investigated the effect of cutter travel speed on the cutting forces and found no discernible variation (Fig. 74). Cutter speeds used in this experiment were 10 times smaller than typical design speeds for cutters on drilling and tunneling machines, but it is quite likely that insensitivity to cutting speed would be sustained for speeds up to two or three meters per second.

Influence of edge angle on cutting forces for a taper-edge disc

In the theory that was outlined earlier, effects of edge angle β for a taper-edge disc are described by the factor C_2 (see eq 101, 103, 105). Following the ideas developed in the section on cutting principles in connection with wedge penetration, C_2 might be rewritten as $C_2 = 2A \tan \beta$. In this expression, $\tan \beta$ accounts for the increase of nominal bearing area as the wedge angle increases, and A is a dimensionless factor that covers any secondary effects of angle, as illustrated in Figures 24, 26, 29, 31 and 32.

The most systematic experimental results that have been found for taper-edge discs are the data of Roxborough and Phillips (1975a, b) shown in Figure 75 and the graphs of Phillips and Bilgin (1977) shown in Figure 76. Roxborough and Phillips considered that H and V were directly proportional to β , with no secondary angle effects, and their experimental data were in fair agreement with this idea. The relationship they proposed implies that $A = 4$, irrespective of the value of β , which is more or less in accord with the experimental findings of Hustrulid (1968) for wedge indentation (see Fig. 43). The graphs of Phillips and Bilgin (1977) indicate that V is proportional to $\tan \beta$ in most cases; i.e. A is invariant with β . The scale of the graphs for H is not really suitable for analysis.

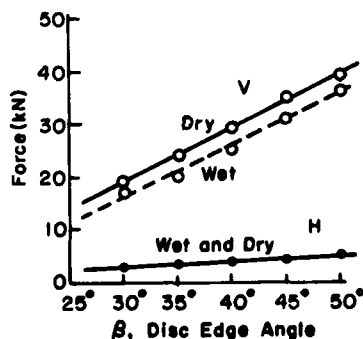


Figure 75. Force components as functions of edge angle for disc cutters operating in wet and dry sandstone (Roxborough and Phillips 1975a).

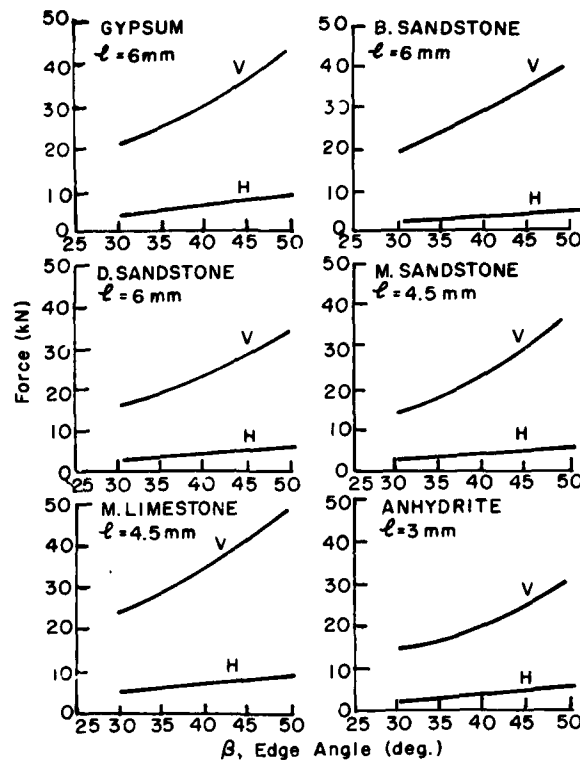


Figure 76. Force components as functions of edge angle for disc cutters (150-mm-diam) operating in various types of rock (Phillip and Bilgin 1977).

Shape of groove cross section

In a ductile material like lead or wet clay, the groove formed by a rolling indenter will take the cross section shape of the roller itself. By contrast, in a material that behaves in a brittle manner, chips will break out and the groove will very often be wider than the cutter that formed it. The shape of a typical groove is irregular, but it is always wider at the top than at the bottom, and it is commonly idealized as having a triangular cross section.

Morrell and Larson (1974) measured the average width of cutting grooves (presumably measured in the surface plane) and related it to the average depth for a certain length of groove. The results for a variety of rock types (Fig. 77-79) showed a linear relationship between width and depth for the range of dimensions that was investigated. This implies that geometric similarity was probably maintained as grooves became deeper. If the groove cross section is idealized as a triangle for the taper edge cutter, the "overbreak angle" ϕ was approximately 70° to 72° for very hard rocks, and about 76° for weaker rocks.

Roxborough and Rispin (1972) obtained effective values of ϕ for chalk; average values were 73° for wet chalk and 76.5° for dry chalk.

Rad and Olson (1974) related groove width to the uniaxial compressive strength of the rock (Fig. 80), finding that width decreased somewhat as rock strength increased. In other words, for a triangular groove ϕ would decrease as rock strength increased.

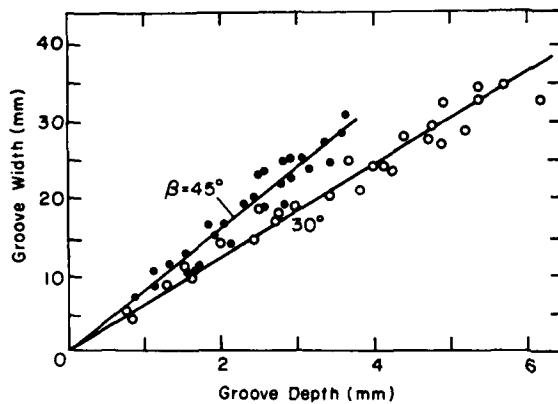


Figure 77. Relation between width and depth for grooves made in marble by disc cutters (adapted from Morrell 1970).

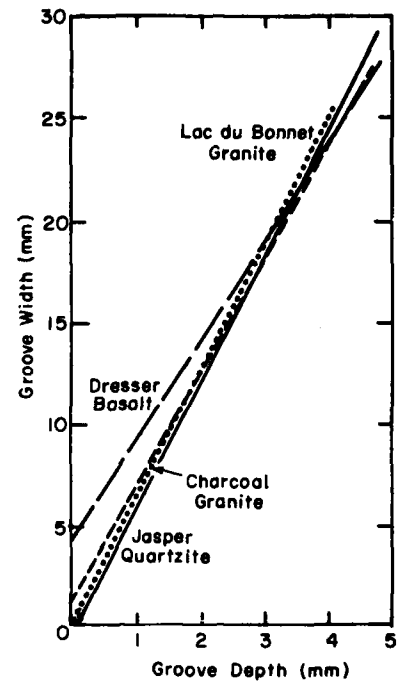


Figure 78. Relation between width and depth for grooves excavated by a disc cutter in various types of hard rock (Morrell and Larson 1974).

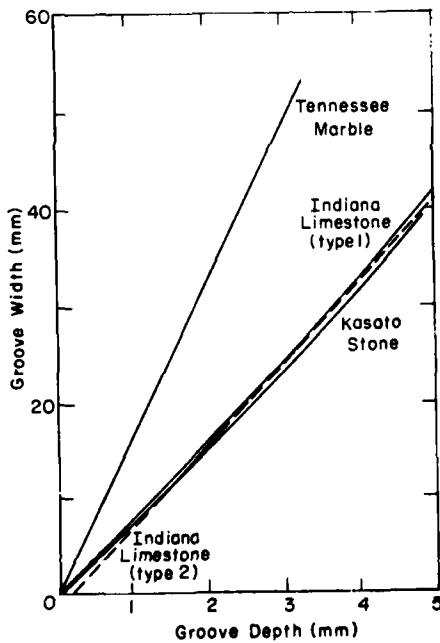


Figure 79. Relation between width and depth for grooves excavated by a disc cutter in various types of rock (Morrell and Larson 1974).

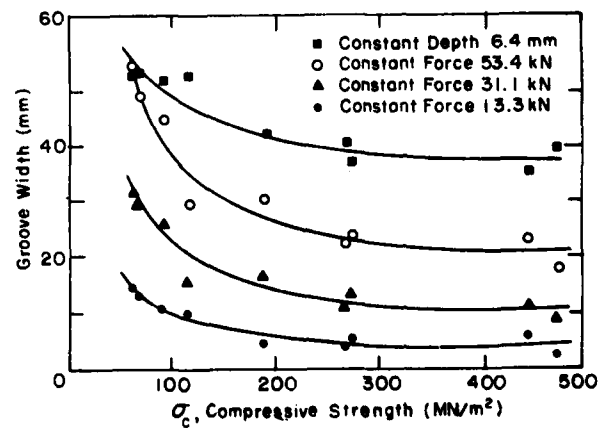


Figure 80. Width of the groove excavated by a disc cutter plotted against uniaxial compressive strength for various rocks (Rad and Olson 1974).

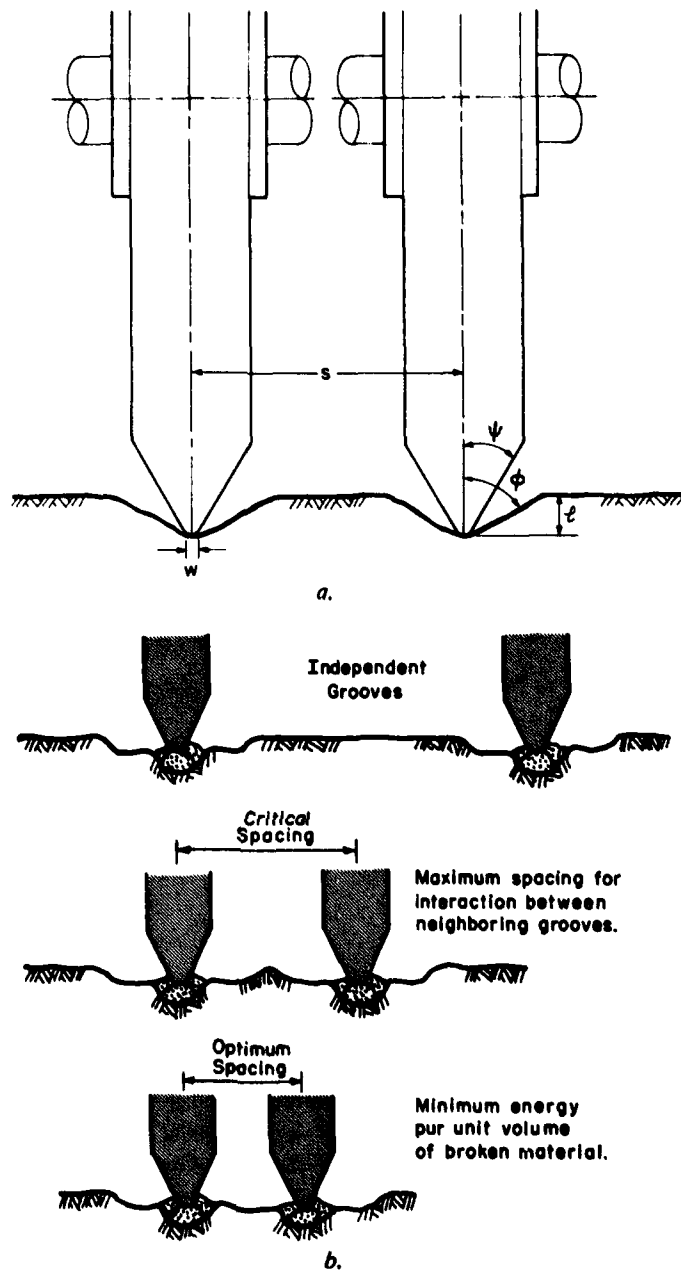


Figure 81. Effect of lateral spacing between parallel cutting grooves.

Force reduction by interaction between adjacent cutting tracks

The experiments discussed so far have involved a single cutter running along a plane surface that is sufficiently wide for it to be regarded as the undisturbed surface of a semi-infinite medium. In practice, cutters do not work in isolation, and there is often useful interaction between adjacent parallel kerfs, or grooves (Fig. 81). Experiments have been carried out in order to determine the optimum spacing of grooves for minimizing specific energy consumption and reducing cutting forces.

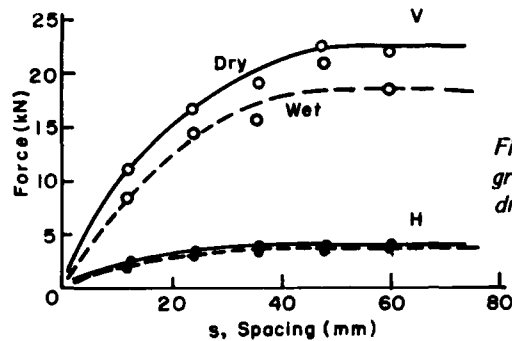


Figure 82. Variation of force components with groove spacing for disc cutters operating in wet and dry sandstone (Roxborough and Phillips 1975a).

For constant depth of penetration ℓ , the force components H and V ought to tend to zero as the center-to-center spacing of adjacent grooves s tends to zero. As the spacing s becomes large, the values of H and V must attain the values that apply for independent cutting. The limit of interaction is likely to be reached when the edges of adjacent grooves just begin to touch. For a triangular groove of half-angle ϕ , this limit would be given by

$$s/\ell = 2 \tan \phi.$$

With ϕ ranging from 70° to 76° , as mentioned in the previous item, the limit for s/ℓ would be in the range 5.5 to 8.

Roxborough and Phillips (1975a, b) measured cutting forces as a function of s (Fig. 82), confirming the expected trend and finding a limit for groove interaction somewhere in the range $6.5 < s/\ell < 8.5$ for the relatively weak sandstone used in the experiments.

Groove interaction is usually discussed in connection with optimization of specific energy, and this topic will be taken up later.

Calculation of specific energy

In experimental work, specific energy is usually calculated as the ratio of energy input for a finite length of cut to the volume of material broken out from the resulting groove. In the Bureau of Mines studies, energy input was calculated as the average tangential force H multiplied by the length of run *plus* the average normal force V multiplied by the average groove depth. The second term, i.e. the "vertical work," was apparently then disregarded since it was small compared to the "horizontal work." In the work done at Newcastle-upon-Tyne, it is not clear exactly how the energy input was calculated, but it seems that a small "vertical work" term was included. Actually, the vertical force component in a constant penetration experiment probably ought to be ignored completely; the product $V\ell$ will become increasingly insignificant as the length of run increases.

Specific energy as a function of penetration depth

Results for taper-edge disc cutters working in chalk (Roxborough and Rispin 1972, 1973) and in sandstone (Roxborough and Phillips 1975a, b) show specific energy E_s decreasing as penetration ℓ increases (Fig. 83, 84) with a constant value of R . Rad (1974) shows data obtained by Wang (1972) which also indicate a decrease of E_s with increase of ℓ (Fig. 85). Studies sponsored by the U.S. Bureau of Mines (Morrell et al. 1970, Morrell and Larson 1974) do not give E_s as a function of ℓ directly, but graphical relations between energy and volume are given. The 1970 work shows direct proportionality between input energy and crater volume for all rocks tested (Fig. 86, 87), and the 1974 work shows direct proportionality for the weaker rocks; these results imply that E_s does not vary with ℓ . By contrast, the 1974 work on very strong rocks (Fig. 88) shows input energy

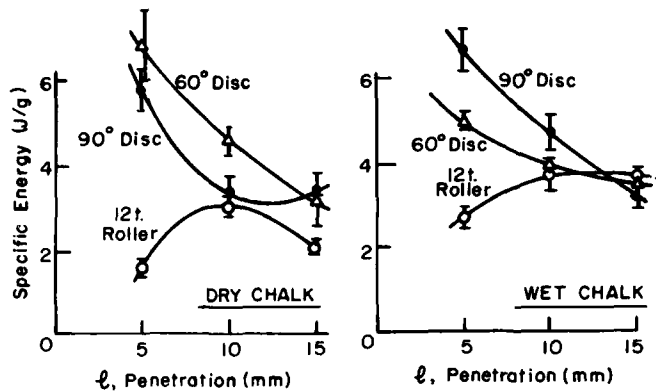


Figure 83. Specific energy plotted against penetration depth for roller cutters working in chalk (Roxborough and Rispin 1973).

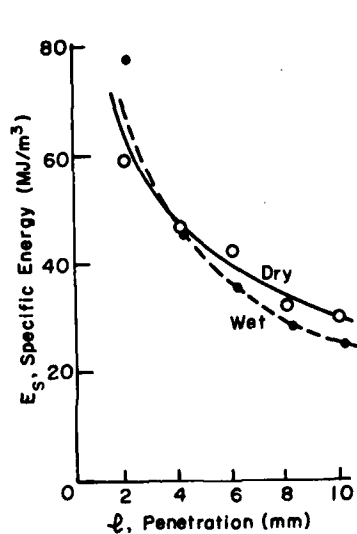


Figure 84. Specific energy as a function of penetration depth for a disc cutter operating in wet and dry sandstone (Roxborough and Phillips 1975a).

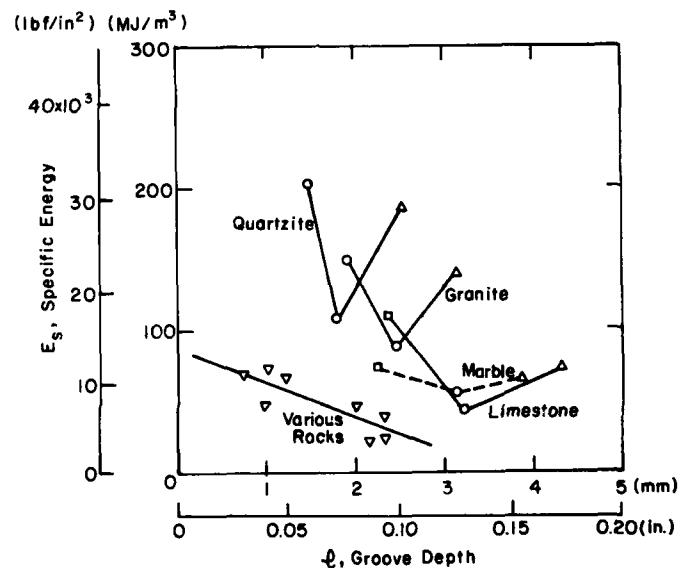


Figure 85. Specific energy as a function of penetration depth for disc cutters operating in different kinds of rocks (Rod 1974, using data from Rad and Olson 1974, and from Wang 1972).

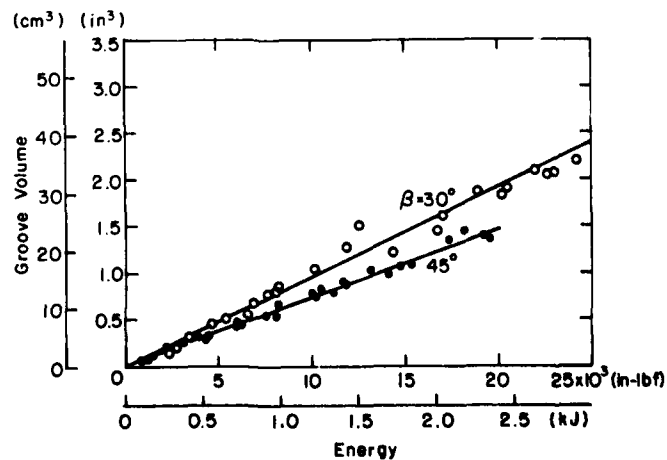


Figure 86. Volume of the excavated groove plotted against energy input for a disc cutter operating in marble (Morrell et al. 1970).

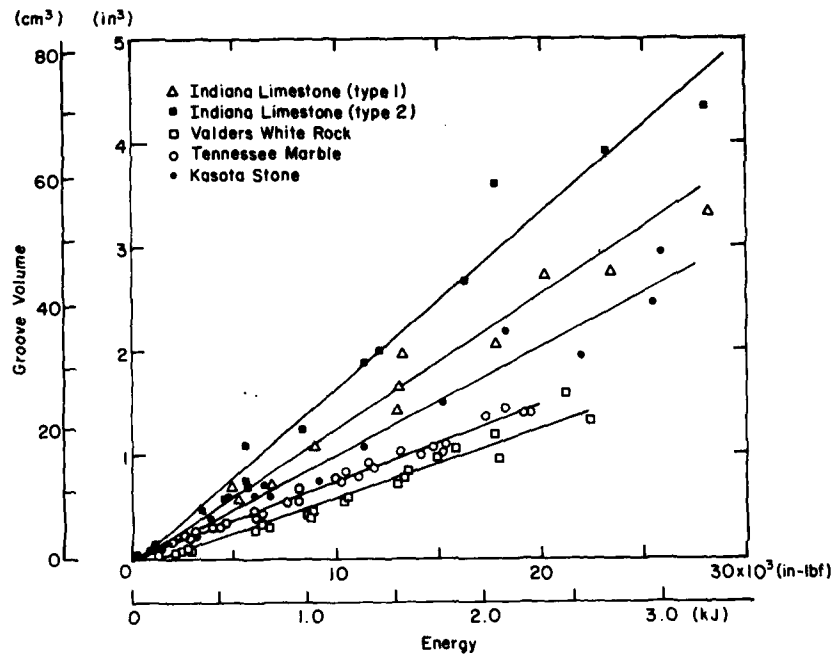


Figure 87. Groove volume as a function of Input energy for a disc cutter operating in a variety of rock types (Morrell et al. 1970).

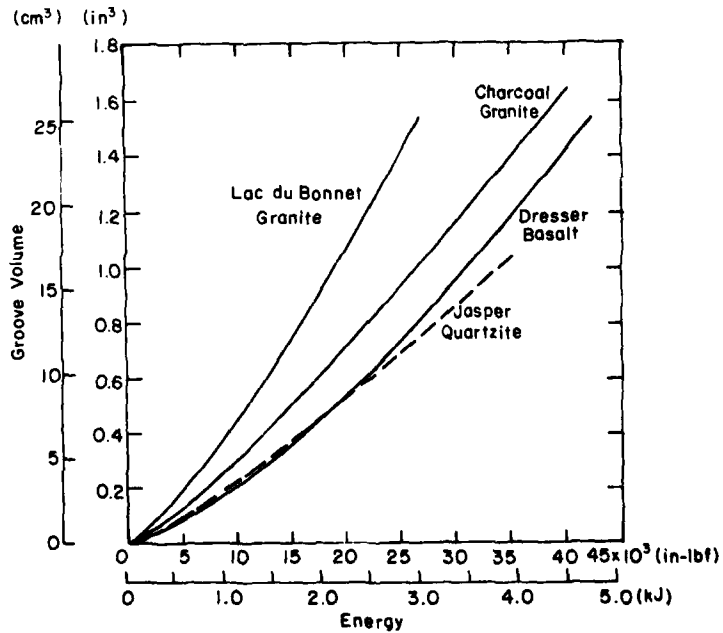


Figure 88. Groove volume as a function of Input energy for a disc cutter operating in various types of rock (Morrell and Larson 1974).

proportional to groove volume raised to a power of n (where $1/n = 1.2$ to 1.4). This means that E_s is proportional to groove volume raised to the power $(n-1)$, and if volume is proportional to ℓ^2 (as required by geometric similarity), then E_s should be proportional to $\ell^{2(n-1)}$. Inserting the values of n , E_s becomes inversely proportional to ℓ raised to powers from 0.33 to 0.57.

The simple theory developed in the previous section showed no explicit dependence of E_s upon ℓ , and most of the results from the studies by the Bureau of Mines agree with this indication. However, it was pointed out that there might be implicit dependency arising from changes in stressed volume and possible breakdown of geometric similitude in the zone of extreme stress; such things might explain the results of Roxborough et al. (1970) and the Morrell and Larson (1974) results for hard rocks.

The simple analysis for a tooth-type cutter also predicts that E_s should be independent of ℓ . The limited data (Fig. 83) show E_s changing with ℓ in chalk, but the trends are neither strong nor consistent.

Effect of cutter radius on specific energy

The simple theory of the previous section shows E_s independent of cutter radius R , at least as far as explicit relationships go. Roxborough and Phillips (1975) made tests on sandstone with disc cutters ranging in diameter from 100 to 200 mm, the depth of penetration ℓ being kept constant at 6 mm. They fitted the data (Fig. 89) by straight lines of zero slope, which would be in accordance with the simple theoretical prediction. However, the data seem to show a slight increase of E_s with R , which is what might be expected if E_s decreases as ℓ/R increases.

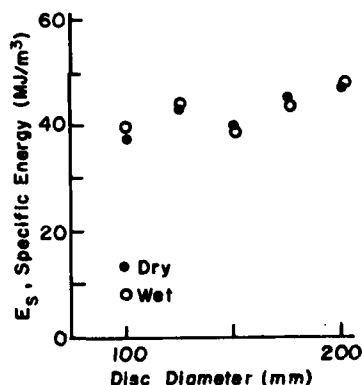


Figure 89. Specific energy plotted against diameter for disc cutters operating in wet and dry sandstone (Roxborough and Phillips 1975a).

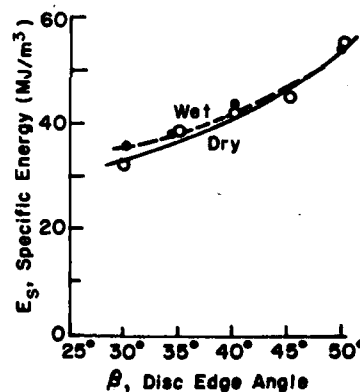


Figure 90. Specific energy as a function of edge angle for disc cutters operating in wet and dry sandstone (Roxborough and Phillips 1975a).

Effect of edge angle on specific energy

Measurements on chalk by Roxborough and Rispin (1973) failed to show a systematic difference of specific energy for discs with $\beta = 30^\circ$ and $\beta = 45^\circ$ (Fig. 83). In dry chalk the sharper disc seemed less efficient overall, but in wet chalk the situation was reversed. At the largest depth of cut (15 mm) there was no significant difference between the two discs. Tests on sandstone by Roxborough and Phillips (1975a, b) gave a different picture, with E_s increasing steadily as β was increased from 30° to 45° (Fig. 90). Morrell et al. (1970) used two different cutters in their experiments on a

range of rock types, one with $\beta = 30^\circ$ and the other with $\beta = 45^\circ$. In all cases the sharper disc ($\beta = 30^\circ$) was the more efficient. Specific energy values for the disc with $\beta = 45^\circ$ were higher by factors ranging from 1.25 to 1.56.

The simple theory suggests that E_s will increase in proportion to $\tan\beta$, and that there will be a further dependence on β that is more or less indeterminate at this stage. The proportionality with $\tan\beta$ implies that E_s for $\beta = 45^\circ$ should be higher than E_s for $\beta = 30^\circ$ by a factor of 1.73. The results of Morrell et al. (1970) give corresponding factors from 1.25 to 1.56, and the results of Roxborough and Phillips (1975a, b) give corresponding factors of 1.72 and 1.53.

Variation of specific energy with cutting speed

Roxborough and Phillips (1975a, b) measured specific energy as a function of cutter speed over the range 0.075 to 0.175 m/s and concluded that there was no significant variation (Fig. 91), although there is some indication of a rising trend in the results for wet sandstone.

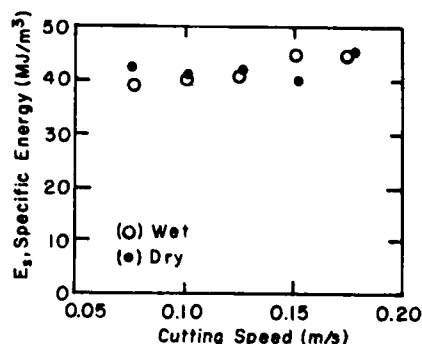


Figure 91. Specific energy plotted against cutting speed for a disc operating in wet and dry sandstone (Roxborough and Phillips 1975a).

Effect of groove spacing on specific energy

The way in which specific energy E_s is likely to vary with groove spacing s is less easy to deduce than the variation of cutting force with s . This is because both the input energy and the volume of broken material both tend to zero for small spacings. For constant depth of penetration, Roxborough and Rispin (1973) and Roxborough and Phillips (1975) conclude that the graphical relation between E_s and s is a U-shaped curve for the range of s where groove interaction occurs. The data for chalk (Fig. 92) provide only partial support for this idea, but the results for various cutters working in sandstone (Fig. 93) are more convincing. The limit of interaction indicated by specific energy data appears to be around $s/l \approx 10$ for chalk, and s/l somewhere between 10 and 20 for sandstone. The latter is surprisingly high. The optimum spacing s/l for minimum specific energy was considered to be about 3 to 5 for chalk, and about 6 to 8 for sandstone. Superficial inspection of the data for sandstone (Fig. 93) seems to allow acceptance of a lower optimum spacing, say $s/l \approx 5$.

Groove spacing studies by Rad and Olson (1974) are less easy to interpret because penetration l can vary as the spacing s varies, and the original report does not express spacing data in the dimensionless units of s/l [the potential for confusion is brought out by Tarkoy's (1976) discussion of Rad's (1975) paper]. The Rad and Olson (1974) test results for constant force show the same general trend as the results of Roxborough and Phillips, i.e. a U-shaped graphical relation between E_s and s for the range of s where interaction occurs (they look different in the original report because s is plotted on a logarithmic scale). Rad and Olson also give plots of l against $\log s$, and these can be used to express their optimum and critical groove spacings in terms of s/l . The resulting approximate values of s/l for optimum spacing are 6.9 for marble, 7.8 for limestone, 6.7 for granite, and

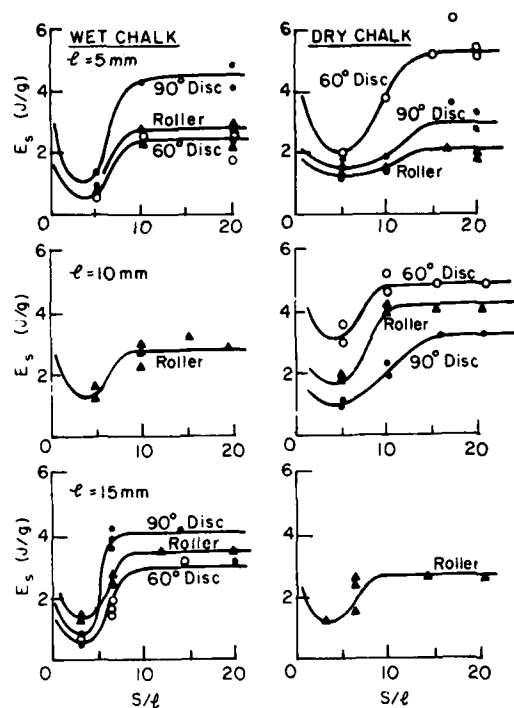


Figure 92. Variations of specific energy with groove spacing for discs and toothed rollers operating in wet and dry chalk (Roxborough and Rispin 1973).

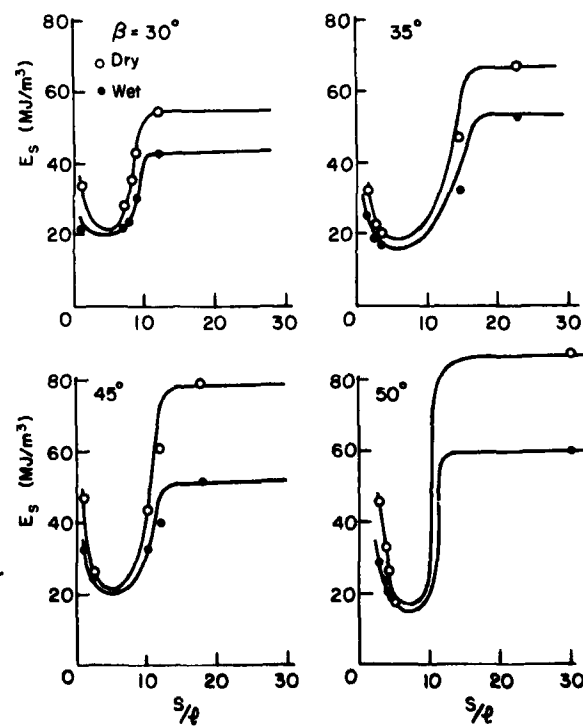


Figure 93. Variation of specific energy with groove spacing for disc cutters operating in wet and dry sandstone (Roxborough and Phillips 1975a).

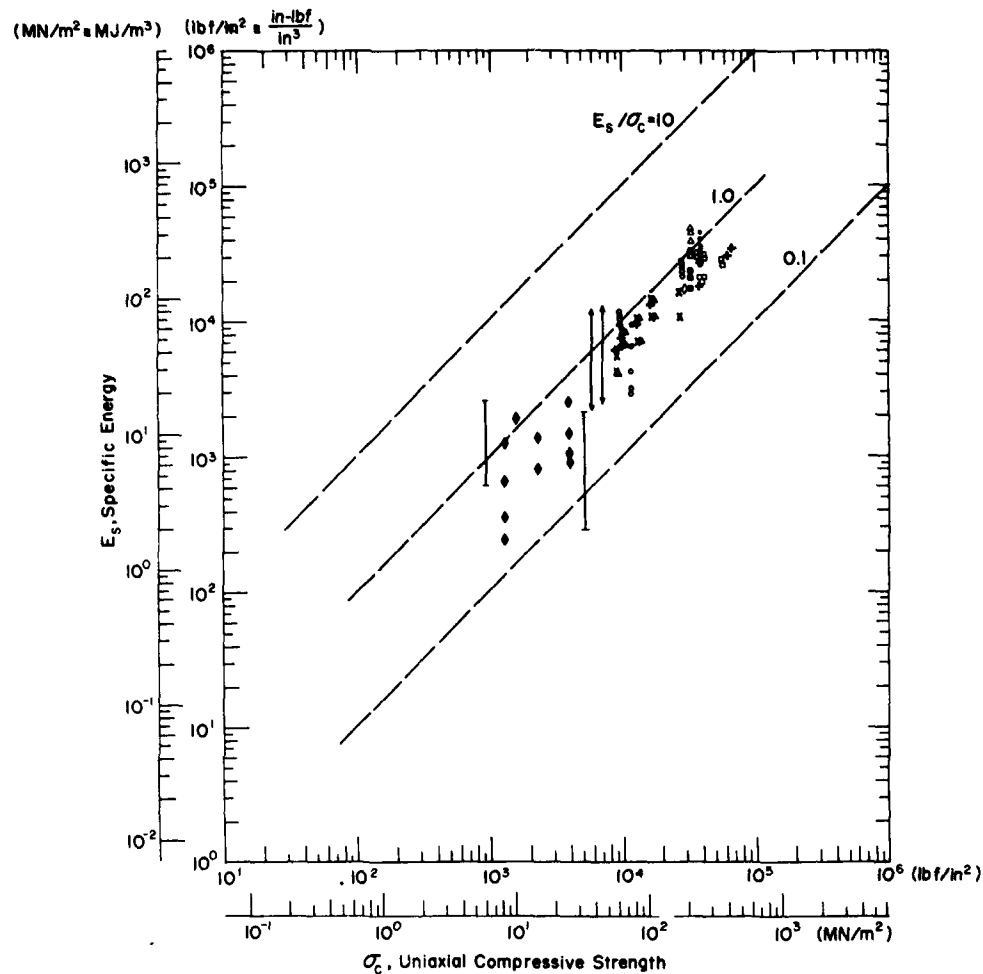


Figure 94. Specific energy as a function of uniaxial compressive strength for normal indentation devices.

- ◇ Hawkes and Mellor, unpub. (indenter in granite)
- Lundquist (indenters)
- Miller and Sikarskie (indenters)
- Lundquist (indenters)
- ◆ Bailey 1967 (indenters in ice and frozen soil)
- △ Rad (discs)
- ▲ Bruce and Morrell (discs)
- Rad (interacting discs)
- ┌ Roxborough and Rispin 1972 (disc cutters in chalk)
- ↑ Roxborough and Phillips 1975a (disc cutters in sandstone)
- + Morrell and Larson 1974 (disc cutters in various rocks)

7.5 for quartzite. For the limits of groove interaction, the approximate values of s/l are 16.4 for marble, 19.2 for limestone, 9.4 for granite and 13.8 for quartzite.

A general conclusion might be that, for grooves cut into a plane surface, optimum spacing in typical rocks is somewhere in the range $3 < s/l < 8$. The limit for groove interaction is higher than might be expected from data on *average* groove width; it lies somewhere in the range $10 < s/l < 20$.

The complications in applying these findings to practical machine design are easy to see. The cutting discs of a rotary boring machine track repeatedly along the same groove paths, and the surface they cut is not a plane surface. Furthermore, s will usually be a fixed dimension determined by the cutter positions, while l is variable depending on the advance rate and the rotary head speed.

Variation of specific energy with rock strength

All of the cutting theories consider that cutting forces and specific energy values are directly proportional to the strength of the rock. This question has not been addressed by direct systematic experiments, and it is difficult to use existing data because the numerous other variables are not held constant. An alternative approach is to look for a correlation between specific energy and rock strength when all of the available data are plotted.

Figure 94 compiles specific energy data from a wide range of laboratory experiments. It includes results for rotary cutting by discs and other rollers, and also results for indentation by spheres, cones and wedges. The data are plotted on logarithmic scales, so that the lines drawn represent direct proportionality for different values of E_s/σ_c . Scatter of the data can be expected because 1) there is a variation of E_s with indenter geometry, penetration and spacing, and 2) the values accepted for σ_c are to some extent arbitrary, depending on test technique and specimen size.

For the strong brittle rocks, with σ_c greater than 50 MN/m², there appears to be a reasonable linear correlation between E_s and σ_c . However, the data for materials that are weak, and perhaps somewhat ductile, do not fit the correlation quite so well. For example, the experiments on wet and dry chalk gave specific energy values in much the same range for both materials, although their measured strengths differed by a factor of 5.5 (possibly because tests were made at low rates). Data for ice and frozen soils are not easy to plot with confidence, largely because σ_c is so sensitive to strain rate for these materials. In Figure 94 the values of E_s for ice and frozen soils are "high rate" values taken from Bailey (1967), while the values of σ_c are high rate strength values taken from various sources.

In spite of the data scatter in Figure 94 there appears to be a reasonable linear correlation between E_s and σ_c , and there is no strong reason to doubt the broad validity of the usual theoretical assumptions.

The results that represent indentation under reasonably favorable conditions lie mostly in the band $1.0 > E_s/\sigma_c > 0.5$, and only the data for disc cutters in chalk reach as low as $E_s/\sigma_c \approx 0.1$. By contrast, corresponding test results for drag bits (Fig. 88 of Part IV) show E_s/σ_c typically of order 0.1, with most of the data below 0.5. However, it should be kept in mind that most of the test data for indentation were obtained with devices appreciably smaller than the roller cutters used on tunneling machines and raise borers.

LITERATURE CITED

- Bailey, J.J. (1967) A laboratory study of the specific energy of disengagement of frozen soils. Conducted by CREARE, Inc. for CRREL. CRREL Internal Report 99 (unpublished).
- Benjumea, R. and D.L. Sikarskie (1969) A note on the penetration of a rigid wedge into a nonisotropic brittle material. *International Journal of Rock Mechanics and Mining Sciences*, vol. 6, p. 343-352.
- Cheatham, J.B. (1958) An analytical study of rock penetration by a single tooth bit. *Proceedings Eighth Drilling and Blasting Symposium*, University of Minnesota.
- Cheatham, J.B. (1964) Indentation analysis for rock having a parabolic yield envelope. *International Journal of Rock Mechanics and Mining Sciences*, vol. 1, p. 431-440.
- Cheatham, J.B. and P.F. Gnirk (1967) The mechanics of rock failure associated with drilling at depth. *Eighth Symposium on Rock Mechanics*, American Institute of Mining, Metallurgical and Petroleum Engineers, p. 410-439.
- Dalziel, J.A. and E. Davies (1964) Initiation of cracks in coal specimens by blunted wedges. *The Engineer*, vol. 217, p. 217.
- Dollinger, G.L. (1977) Choosing cutters for the best boreability. *Compressed Air Magazine*, September 1977, p. 15-19.
- Dutta, P.K. (1972) A theory of percussive drill bit penetration. *International Journal of Rock Mechanics and Mining Sciences*, vol. 9, p. 543-567.
- Evans, I. and C.D. Pomeroy (1973) The strength, fracture and workability of coal. Published by the authors (obtainable from Mining Research and Development Establishment, National Coal Board, England).

- Galín, L.A. (1961) Kontakn'e Zadachi Teorri Uprugosti (Contact Problems in the Theory of Elasticity). North Carolina State College Applied Mathematics Research Group, translator H. Moss.
- Gnirk, P.F. (1966) An experimental study of indexed single bit tooth penetration into dry rock at confining pressures of 0 to 7500 psi. *Proceedings of the First Congress of the International Society of Rock Mechanics* (Lisbon), p. 121-129.
- Hawkes, I. and M. Mellor (1970) Uniaxial testing in rock mechanics laboratories. *Engineering Geology*, vol. 4, no. 3, p. 177-285.
- Hill, R. (1950) *The mathematical theory of plasticity*. Oxford Engineering Science Series. Oxford: Oxford University Press.
- Hustrulid, W.A. (1968) A theoretical and experimental study of percussive drilling of rock. Ph.D. Thesis, University of Minnesota (unpublished).
- Hustrulid, W.A. and C. Fairhurst (1971) A theoretical and experimental study of the percussive drilling of rock. Part I: Theory of percussive drilling. *International Journal of Rock Mechanics and Mining Sciences*, vol. 8, p. 311-333.
- Lundberg, B. (1974) Penetration of rock by conical indenters. *International Journal of Rock Mechanics and Mining Sciences*, vol. 11, p. 209-214.
- Lundquist, R.G. (1968) Rock drilling characteristics of hemispherical insert bits. M.Sc. Thesis, University of Minnesota (unpublished).
- Miller, M.H. and D.L. Sikarskie (1968) On the penetration of rock by three-dimensional indenters. *International Journal of Rock Mechanics and Mining Sciences*, vol. 5, p. 375-398.
- Morrell, R.J., W.E. Bruce and D.A. Larson (1970) Tunnel boring technology: disk cutter experiments in sedimentary and metamorphic rocks. U.S. Bureau of Mines Report of Investigations 7410.
- Morrell, R.J. and D.A. Larson (1974) Tunnel boring technology: disk cutter experiments in metamorphic and igneous rocks. U.S. Bureau of Mines Report of Investigations 7961.
- Paone, J. and S. Tandanand (1966) Inelastic deformation of rock under a hemispherical drill bit. U.S. Bureau of Mines Report of Investigations 6838. (Also in *Transactions of Society of Mining Engineers*, AIME, vol. 235, p. 113-123.)
- Pariseau, W.G. and C. Fairhurst (1967) The force-penetration characteristic for wedge penetration into rock. *International Journal of Rock Mechanics and Mining Sciences*, vol. 4, p. 165-180.
- Paul, B. and D.L. Sikarskie (1965) A preliminary theory of static penetration by a rigid wedge into a brittle material. *Transactions of the Society of Mining Engineers*, AIME, December, p. 372-383.
- Phillips, H.R. and N. Bilgin (1977) Correlation of rock properties with the measured performance of disc cutters. *Proceedings of Conference on Rock Engineering*, University of Newcastle-Upon-Tyne, p. 181-196.
- Prager, W. and P.G. Hodge (1951) *Theory of perfectly plastic solids*. New York: John Wiley.
- Rad, P.F. (1974) Correlation of laboratory cutting data with tunnel boring machine performance. U.S. Bureau of Mines Report of Investigations 7883.
- Rad, P.F. (1975) Importance of groove spacing in tunnel boring machine operations. *Journal of the Geotechnical Engineering Division, ASCE*, vol. 101, no. GT9, p. 949-962.
- Rad, P.F. and R.C. Olson (1974) Tunneling machine research: Interaction between disk-cutter grooves in rocks. U.S. Bureau of Mines Report of Investigations 7881.
- Roxborough, F.F. and H.R. Phillips (1975a) The mechanical properties and cutting characteristics of the Bunter sandstone. Report by Department of Mining Engineering, University of Newcastle-Upon-Tyne for Transport and Road Research Laboratory, Department of the Environment, England.
- Roxborough, F.F. and H.R. Phillips (1975b) Rock excavation by disc cutter. *International Journal of Rock Mechanics and Mining Sciences*, vol. 12, p. 361-366.
- Roxborough, F.F. and A. Rispin (1972) The mechanical cutting characteristics of the Lower Chalk. Report by Department of Mining Engineering, University of Newcastle-Upon-Tyne for Transport and Road Research Laboratory, Department of the Environment, England.
- Roxborough, F.F. and A. Rispin (1973) The mechanical cutting characteristics of the Lower Chalk. *Tunnels and Tunneling*, Jan/Feb.
- Smith, L.L. and J.B. Cheatham (1975) Plasticity of ice and sand-ice systems. *Journal of Engineering for Industry*, ASME, vol. 97, series B, no. 2, p. 479-484.
- Stephenson, B.R. (1963) Measurement of dynamic force-penetration characteristics in Indiana limestone. M.Sc. Thesis, University of Minnesota (unpublished).
- Tabor, D. (1970) The hardness of solids. *Physics in Technology*, vol. 1, no. 3, p. 145-179.
- Tarkoy, P.J. (1976) Discussion of paper by P.F. Rad (1975) on importance of groove spacing in tunnel boring machine operations. *Journal of the Geotechnical Engineering Division, Proceedings of ASCE*, GT10, p. 1122-1124.
- Teale, R. (1964) The mechanical excavation of rock—experiments with roller cutter. *International Journal of Rock Mechanics and Mining Sciences*, vol. 1, no. 1, p. 63-78.
- Timoshenko, S. and J.N. Goodier (1951) *Theory of elasticity*. New York: McGraw-Hill.
- Vanzant, B.W. (1963) Dynamic rock penetration tests at atmospheric pressure. *Proceedings of the Fifth Symposium on Rock Mechanics*. New York: Pergamon Press, p. 61-91.
- Wang, F.D. (1972) A theoretical and experimental study of tunnel boring by machine with an emphasis on boreability predictions and machine design. Colorado School of Mines Contract Report for U.S. Bureau of Mines (Contract H0210043).

A facsimile catalog card in Library of Congress MARC format is reproduced below.

Mellor, Malcolm

Mechanics of cutting and boring; Part 5: Dynamics and energetics of indentation tools / by Malcolm Mellor. Hanover, N.H.: U.S. Cold Regions Research and Engineering Laboratory; Springfield, Va.: available from National Technical Information Service, 1980.

x, 97 p., illus.; 28 cm. (CRREL Report 80-21.)

Prepared for Directorate of Military Programs, Office of the Chief of Engineers, by Corps of Engineers, U.S. Army Cold Regions Research and Engineering Laboratory under DA Project 4A762730AT42.

Bibliography: p. 81.

Mellor, Malcolm

Mechanics of cutting and...

Card 2
1980

1. Boring machines. 2. Excavating machines.
3. Excavation. 4. Ice cutting. 5. Machine design.
6. Permafrost excavation. 7. Rock cutting.
I. United States. Army. Corps of Engineers.
II. Cold Regions Research and Engineering Laboratory, Hanover, N.H. III. Series: CRREL Report 80-21.

DATE
FILMED
- 8